Optimization of nickel oxide-based electrochromic thin films

Dae-Hoon Park

N° d'ordre : 4031

THÈSE

PRÉSENTÉE A

L'UNIVERSITÉ BORDEAUX 1

ÉCOLE DOCTORALE DES SCIENCES CHIMIQUES

Par PARK, Dae Hoon

POUR OBTENIR LE GRADE DE

DOCTEUR

SPÉCIALITÉ : PHYSICO-CHIMIE DE LA MATIERE CONDENSEE

OPTIMIZATION OF NICKEL OXIDE-BASED ELECTROCHROMIC THIN FILMS

Thèse dirigée par : CAMPET, Guy et ROUGIER, Aline

Soutenue le 8 Juin 2010

Après l'avis favorable de MM. :

M. H. S. HILAL, Professeur, An-Najah N. University
M. M. SUBRAMANIAN, Professeur, Oregon State Univeristy — Rapporteurs

Devant la commission d'examen formée de :

M. DELMAS Claude, Directeur de Recherche, ICMCB-CNRS, Université Bordeaux 1 — Président-Rapporteur
M. HWANG Seong-Ju, Professeur, Ewha Womans University, Seoul — Examinateurs
M. TOUPANCE Thierry, Professeur, ISM-CNRS, Université Bordeaux 1
Mme. DELVILLE M. Hélène, Directrice de Recherche, ICMCB-CNRS, Université Bordeaux 1
Mme ROUGIER Aline, Directrice de Recherche, LRCS-CNRS, Université de Picardie Jules Verne
M. CAMPET Guy, Directeur de Recherche, ICMCB-CNRS, Université Bordeaux 1

This thesis is dedicated

To my wife Jung-Eun

To my Son and Daughter, Whui-Ho and Hyo-Youn

To my family (Parents, Parents-in-law, Brother and Sisters)

Acknowledgments

First of all, I would like to express my sincere gratitude to **Dr. *Claude DELMAS***, Director of ICMCB-CNRS, for welcoming me at ICMCB and also providing a great scientific environment.

I am very grateful to president ***Goo-Jae HAN*** and vice president ***Dr. Seung-Wook HAN*** of DANSUK Co., Ltd. for their great human support and financial help.

Many thanks to my supervisors **Dr. *Aline ROUGIER*** and **Dr. *Guy CAMPET*** for their wonderful guidance. There is no doubt that they did teach me based on not only their great scientific knowledge but also their sincere care and love.

I would like also to express my gratitude to the distinguish **Prof. *Jin-Ho CHOI***, **Prof. *Seong-Ju HWANG*** in Ewha Womans University, Korea, **Prof. *Thierry TOUPANCE*** in ISM-CNRS, **Dr. *Hansang KWON*** in EMPA, Switzerland for their effective discussion on my research work. Also, another many thanks to Prof. *Thierry TOUPANCE*, for allowing me intensively to use his laboratory. Also I would like to thank all the jury members for their efforts to review and judge this work.

I would like to thank very much French government (Bourses Blaise Pascal) and KWANJEONG educational foundation (Scholarship for studying abroad). Part of the research was supported by the FP7 INNOSHADE project.

My deep gratitude to **Prof. *Jong-Ho JUN***, **Prof. *No-Seung MYUNG***, **Prof. *Hwan-Gi KIM***, **Prof. *Jae-Jun LEE***, and **Prof. *Young-Soo YOON*** for their encouragements during my whole Ph.D. period.

I would like to thank the following people from outside the ICMCB, ***Elisabeth SELLIER***, **Dr. *Bong-Gi MIN***, ***In-Young KIM***, ***TAE-Woo KIM***, ***Jung Eun KIM***, ***Odile BABOT***, ***Laurent THOMAS***, **Dr. *Eric LAURCHESE*** for the effective collaboration on sample measurements concerning structural, morphological, thermal analyses, etc.

I am thankful to all the following people from the ICMCB for the help, experiments they did or the effective discussions: ***Eric LEBRAUD***, **Dr.** ***Marie-Helene DELVILLE***, ***Laëtitia ETIENNE***, ***Christine LABRUGERE***, and **Dr.** ***Patrick ROSA***. I am also thankful to my friends at the ICMCB for the encouragements, help and support: **Dr.** ***Nicola PENIN***, **Prof.** ***Iyad SADDEDIN***, **Dr.** ***Sandrine DULUARD***, ***Lydia RAISON***, ***Sonia PINHO***, ***Agnieszka MILEWSKA***, ***David MESGUICH***, ***Ie-Rang JEON***, ***Hakim MOULKI***, ***Hong Feng WANG***, **Dr.** ***Cong Ling YIN***, ***Olivia WAHYUDI***, ***Qiang LIU***, ***Laeëtitia VAURIOT***, **Dr.** ***U-Chan CHUNG SEU***, **Dr.** ***Véronique JUBERA***, **Dr.** ***Grigoris MOUNTRICHAS***, **Dr.** ***Virginia MARTIN TORRES***, ***Romain EPHERRE***, ***David MESGUICH, Manuel ARVEUX***, ***Anand Theerthan RAMANATHA DAYALU***.

My deep gratitude to my dear friends from outside the ICMCB for the support and encouragements listed hereafter: Prof. ***Hyun JUNG***, ***Su-Gil HUR***, ***Seung-Tae KIM***, ***Tae-Woo KIM***, ***In-Young KIM***, ***Yong-Suk LEE***, ***Jung-Hyuk LIM***, ***Young-Jun YU***, ***Byung-Gil LIM***, ***Eun-Hwa KOWN***. ***Dong-Hun LEE***.

I will take this opportunity to express my profound gratitude to my beloved family in Korea and America (***my parents, my parents-in-law, my brother, my sisters, my brother-in-laws, and my sister-in-law***) for the continuous support and encouragement.

Finally, I strongly express my profound gratitude to my dearly loved wife ***Jung-Eun***, my son ***Whui-Ho*** and my daughter ***Hyo-Youn*** for the moral support and patience during my study.

List of abbreviations

A : absorbance

AFM : atomic force microscopy

CA : chronoamperometry

CE : coloration efficiency

CR : contrast ratio

CV : cyclic voltammogram

DC : dip coating

dmaeH : N,N-dimethylaminoethanol

DOE : department of energy

EC : electrochromic

ECD : electrochromic device

ECM : electrochromic material

ECW : electrochromic window

EDS : energy dispersive spectroscopy

EXAFS : extended X-ray absorption fine structure

FE-SEM : field emission–scanning electron microscopy

FTO : fluorine doped tin oxide

FWHM : Full Width at Half Maximum

g : gravity

h : film thickness

hcp : hexagonal close packed

HVAC : heating, ventilation and air conditioning

ICP : inductively coupled plasma

ITO : indium doped tin oxide

JCPDS : joint committee on powder diffraction standards

LCD : liquid crystal display

OCLI : optical coating laboratory incorporated

PLD : pulsed laser deposition

PVD : physical vapor deposition

Ra : roughness (average)

Rmax : roughness (maximum)

R_x : reflected light intensity in bleached state

R_o : reflected light intensity in colored state

SAED : selected area electron diffraction

SC : spin coating

SHGC : solar heat gain coefficient

SPD : suspended particle device

T : transmittance

T_b : transmittance in bleached state

T_c : transmittance in colored state

TG-DTA : thermogravimetry-differential thermal analyses

TEM : transmission electron microscopy

TEOS : tetraethyl orthosilicate

TnP : titanium *iso*-propoxide

UV : ultraviolet

v : withdrawal speed

XRD : X-ray diffraction

YBCO : yttrium barium copper oxide

η : coloration efficiency

η_v : viscosity

ρ : liquid density

λ : wavelength

γ_{LV} : liquid-vapor surface tension

Δ OD : change in optical density

Abstract

Aiming at enhancing the electrochromic properties of NiO thin films, deposited on FTO substrates, we have employed three different approaches. They deal with: 1) lithium doping of NiO, the corresponding thin film-deposition method is PLD (Pulsed Laser Deposition); 2) NiO nanoparticles embedded into zinc doped amorphous titanium oxide matrix, a solution method is used to deposit the corresponding thin films ; 3) Carbon-doped NiO thin films deposited using, a specific sol-gel method.

Owing to lithium doping of NiO, we could induce film amorphization, thereby enhancing the film electrochemical-capacity. Most importantly, the adhesion between the film and the FTO substrate was improved leading to enhanced electrochemical cyclability in aqueous KOH electrolyte.

We could enhance the electrochromic performances of TiO_2/NiO composite thin films by doping TiO_2 with Zn^{2+}, forming to a new composite thin film $Ti_{1-x}Zn_xO_{2-x}\square_x$-NiO.

Finally we have successfully stabilized the electrochromic properties (durability and optical property) of NiO thin films in aqueous KOH electrolyte, owing to the development of a specific sol-gel method leading to carbon-doped NiO nanoparticles. For the first time 25000 cycles were successfully achieved without significant decrease of the electrochromic performances.

Keywords: *Thin films; Pulsed Laser Deposition (PLD); Sol-gel; NiO; Lithium doping;* $Ti_{1-x}Zn_xO_{2-x}\square_x$*/NiO; Carbon-addition.*

Résumé

Dans la perspective du développement de vitrages électrochromes « en milieu protonique », des films minces électrochromes à coloration anodique, à base d'oxyde de nickel, ont été synthétisés et caractérisés. Afin d'améliorer la durabilité des films minces à base de NiO, trois approches ont été envisagées.

(i) Des films d'oxyde de nickel et d'oxyde mixte nickel/lithium, déposés par PLD (Pulsed Laser Deposition). Nous avons étudié l'influence du lithium sur les propriétés physico-chimiques ('amorphisation..), et les caractéristiques électrochromes (électrochimique-optique) en milieu aqueux KOH 1M.

(ii) Des films composites, préparés par voie chimique (solution), constitués d'une phase amorphe (en diffraction des Rayons X), de composition $Ti_{1-x}Zn_xO_{2-x}\square_x$, englobant des cristallites de NiO de ~ 5 nm de diamètre. Les courbes voltampérométriques révèlent que seule la phase NiO est électrochimiquement active, mais la phase amorphe, grâce aux lacunes anioniques neutres, $\square_x$, renforce la tenue mécanique des films déposés sur les substrats FTO/verre. Il s'ensuit que ces films composites sont plus stables au cyclage, en milieu aqueux KOH 1M, que leurs homologues TiO_2/NiO.

(iii) Des films minces d'oxyde de nickel dopés par du carbone, préparés par une voie sol-gel originale, présentant une remarquable tenue en cyclage (> 25000 cycles en milieu aqueux KOH 1M), jamais observée jusqu'ici pour NiO.

Mots-clefs: *Films minces ; Ablation laser (PLD) ; Sol gel ; NiO ; $Ti_{1-x}Zn_xO_{2-x}\square_x$/NiO ; NiO dopé Li ; NiO dopé C*

Table of contents

Chapter II: Electrochromic properties of undoped and lithium-doped nickel oxide thin films prepared by Pulsed Laser Deposition (PLD) 37

Presentation of the topic:

Over the last decades, there has been tremendous research on electrochromic materials because of their wide range of applications such as smart windows, displays, rearview mirrors, and so forth [1-14]. Over all, the glazing in building is the most discussed issue due to the fact that it is strongly related to energy saving [10-14]. For electrochromic materials, molybdenum oxide, niobium oxide, tungsten oxide, etc. are regarded as cathodic colored materials (i.e. colored in the reduced state) whereas iridium oxide, cobalt oxide, nickel oxide, and ruthenium oxide are classified as anodic colored materials (i.e. colored in the oxidized state). Among the cathodic colored materials, tungsten oxide, showing a blue color in the reduced state, has been mostly investigated due to its high coloration efficiency and cycling durability, resulting in commercialized electrochromic windows (ECWs) [15,16]. However, there has been an increasing demand of electrochromic devices, including ECWs, which show a neutral-grey coloration. Therefore, 'NiO' has been selected in this study, due to its brownish color in its oxidized state which is complementary to the blue color of the reduced 'WO_3'. However, despite previous research efforts [17-23], it still remains as a challenging issue to stabilize the electrochromic performances of NiO thin films upon cycling.

In this work, we aimed at enhancing the electrochromic durability of 'NiO' thin films, deposited on FTO (Fluorine-doped Tin dioxide)/glass substrates. We have employed three different approaches. They deal with: 1) lithium doped NiO thin films deposited by PLD (Pulsed Layer Deposition); 2) NiO nanoparticles embedded into an amorphous zinc doped titanium oxide matrix where a solution/dip coating method is used to deposit the corresponding thin films and 3) Carbon-doped NiO thin films deposited using a specific sol-gel/spin coating method.

The strategies supporting these three approaches will be presented in Chapters II, III, and IV, respectively, following a general review (Chapter I).

References

[1] C.G. Granqvist, *Handbook of Inorganic Electrochromic Materials*, Elsevier, Amsterdam (1995).

[2] K.C. Ho, C.B. Greenberg, D.M. Macarthur, *Electrochem. Soc. Proc.*, Electrochromic Materials and their Applications III PV (1996) 96.

[3] C.G. Granqvist, E. Avendano, A. Azens, *Thin Solid Films* **442** (2003) 210.

[4] A. Azens, G.G. Granqvist, *J. Appl. Electrochem.* **7** (2003) 64.

[5] C.G. Granqvist, E. Avendaño, A. Azens, *Thin Solid Films* **442** (2003) 201.

[6] F. Michalak, K. von Rottkay, T. Richardson, J. Slack, M. Rubin, *Electrochim. Acta* **44** (1999) 3085..

[7] E. Avendaño, A. Azens, G.A. Niklasson, C.G. Granqvist, *Sol. Energy Mater. Sol. Cells* **84** (2004) 337.

[8] S.-J. Wen, J. Kerr, M. Rubin, J. Slack, K. von Rottkay, *Energy Mater. Sol. Cells* **56** (1999) 299.

[9] M. Martini, G.E.S. Brito, M.C.A. Fantini, A.F. Craievich, A. Gorenstein, *Electrochim. Acta* **46** (2001) 2275.

[10] S.J. You, Y.E. Sung, *News & Information for Chemical Engineers* **26** (2008) 518.

[11] A.W. Czanderna, D.K. Benson, J.-Z. Zhang, C.E. Tracy, S.K. Deb, *Overview of criteria for assessing the durability of electrochromic windows for buildings applications, 2nd Int. Meeting on Electrochromism (IME-2)*, San Diego, 1996.

[12] M. Green, *US patent* 5598293, 1997.

[13] M. Wigginton, *Glass in Architecture, Phaidon*, London, 1966.

[14] A. Campagno, *Intelligente Galsfassaden/Intelligent Galss FaÇades, 4th Edition, birkhäuser*, Basel, 1999.

[15] http://www.econtrol-glas.de/ (Date accessed: 13 Apr. 2010)

[16] http://www.sage-ec.com/ (Date accessed: 13 Apr. 2010)

[17] Y. Ushio, A. Ishikawa, T. Niwa, *Thin Soild Films* **280** (1996) 233.

[18] A. Fukazawa, M. Chihiro, *European Patent* EPXXDW EP 1434083, 2004.

[19] I. Bouessay, A. Rougier, P. Poizot, J. Moscovici, A. Michalowicz, J.-M. Tarascon, *Electrochim. Acta* **50** (2005) 3737.

[20] I. Bouessay, A. Rougier, J.-M. Tarascon, *J. Electrochem. Soc.* **151** (2004) H145.

[21] C.M. Lampert, R.C. Popowich, *Optical Materials Technology for Energy Efficiency and Solar Energy Conversion VIII*, SPIE, (1989) 1149**.**

[22] A. Pennisi, C.M. Lampert, *SPIE*, **1061** (1988) 131.

[23] S. Passerini and B. Scrosati, A. Gorenstein, A.M. Andersson, C.G. Granqvist, *J. Electrochem. Soc.* **136** (1989) 3394.

Chapter I

General review

1. Chromism

In chemistry, chromism is a process that induces a reversible change in the optical properties of compounds [1]. In most cases, chromism is based on a change in the electron states of molecules, especially the π- or d-electron state. This phenomenon is induced by various external stimuli which can alter the electron density of substances. So, chromism can be classified according to the kinds of used stimuli. The major kinds of chromisms are,

- **Thermochromism** is chromism that is induced by heat, i.e. temperature change.
- **Photochromism** is induced by light irradiation. This phenomenon is based on formation of light-induced color centers in crystals, precipitation of metal particles in a glass, or other reversible mechanisms… [1].
- **Electrochromism** is induced by gain and loss of electrons. This phenomenon occurs in compounds with redox active sites.
- **Solvatochromism** depends on the polarity of the solvent.

Table 1 exhibits a number of different chromic systems. In all these systems, chromism is operated by different sources of stimuli.

Technology	Electrochormic	Solvatochromic		Photochromic	Thermochromic
		Liquid crystal display	Suspended particle display		
Principle	Charge transfer	Polarization molecular orientation	Polarization molecular orientation	Photoabsorption	Phase transition
Representative materials	WO_3/electrolyte /PB organic materials	Liquid crystal+ eventually colored dye	Polarized particles	AgCl, precipitation of metal particles in a glass	Mo doped VO_{2-x}
Operating voltage	1~3V	0~100V	0~100V	Light (UV)	Heat ~40 °C
Response time (900 cm^2)	~1 min	10 msec	100 msec	~ 5 min	~ 3 min
Average transmittance of sun light (%)	5 ~ 85	40 ~ 70	5 ~ 70	60 ~ 85	10 ~ 50

Table 1: Several chromogenic technologies and their characteristics [1].

The transmittance of photochromic and thermochromic devices cannot be optionally controlled. Contrary to this, transmittance of Electrochromic Devices (ECDs), Suspended Particle Devices (SPDs), and Liquid Crystal Devices (LCDs) can be controlled by means of applied voltage, the later being advantageously much lower for ECDs. If the transparency in the bleached state is high for ECDs, both the SPDs and LCDs experience haze phenomenon. From now on, we will uniquely consider electrochromism which constitutes the topic of the present work.

2. Electrochromism

2-1. Design and operation of electrochromic devices (ECDs) and their applications as electrochromic windows (ECWs)

2-1-a. Design and operation of ECDs

Electrochromic materials (ECMs) modulate their optical properties depending on charge (electrons and ions) insertion/extraction [2,3]. In fact standard* electrochromic devices (ECDs) behave as thin film batteries which change their optical properties depending on insertion rate in the ECM films (*see § 2-3 below where the different types of ECDs are listed). However, in such ECDs the electrical contact is insured by a transparent conducting layer (Fig. 1).

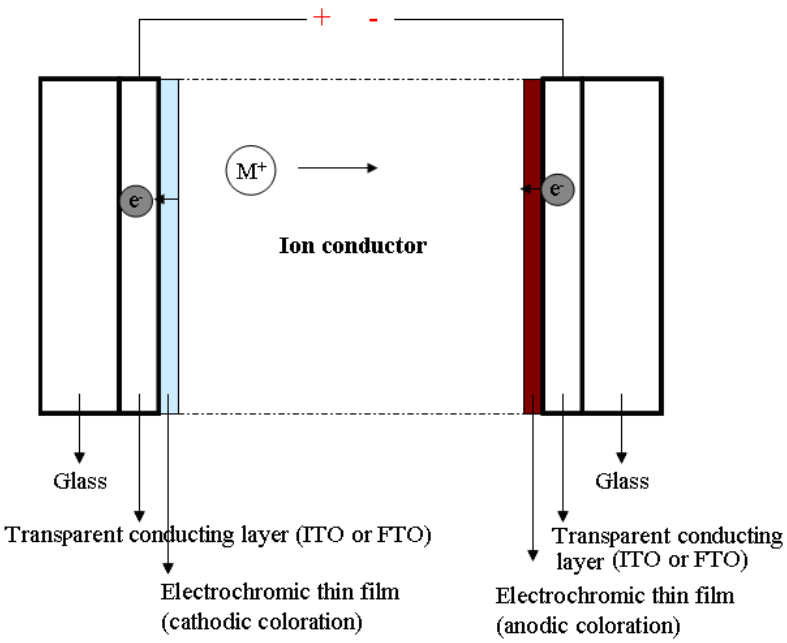

Fig. 1: Movement of ions under an applied voltage leading to the bleaching of an initially colored ECD. A reverse voltage will color the device.

In terms of optical and electrical properties, the most efficient transparent conducting layers are based on Sn-doped In_2O_3 (referred to ITO) and F-doped SnO_2 (referred to FTO) [4,5]. FTO has the advantage of being less costly than ITO but required generally high temperature deposition ($T \geq 350\ ^oC$). The central three-layer design in Fig. 1 embodies a M^+ ion conductor (M^+ can be H^+ or Li^+), in film form, that can be organic (an adhesive polymer for instance) or inorganic. The ion conductor is in direct contact with an electrochromic thin film (tungsten oxide being a typical example). On the other side of the ion conductor is a film serving as ion storage, ideally with complementary electrochromic properties (nickel oxide being a typical example). Cathodic and anodic materials color when they are reduced and oxidized, respectively.

When a voltage of the order of a few volts is applied between the transparent electrical conductors, ions are shuttled between the ion storage film and the EC film and simultaneously the electrons are injected (extracted) from the transparent conductors. The

optical properties of the electrochromic thin films, and therefore of the electrochromic devices (ECDs) are thus modified. The coloration can be controlled at any intermediate level, and the device exhibits open-circuit memory (like a battery).

2-1-b. Application of ECDs as electrochromic windows (ECWs)

An ECW is illustrated in Fig. 2. It operates as shown in Fig. 1. Visible light and part* of solar heat energy (* FTO or ITO films reflect infrared radiations) penetrate the ECW into indoors when the electrochromic window is in off-state (bleached state). The transmitted visible light and solar heat energy (from exterior to interior of buildings) can be minimized when the electrochromic window is in on-state (colored state).

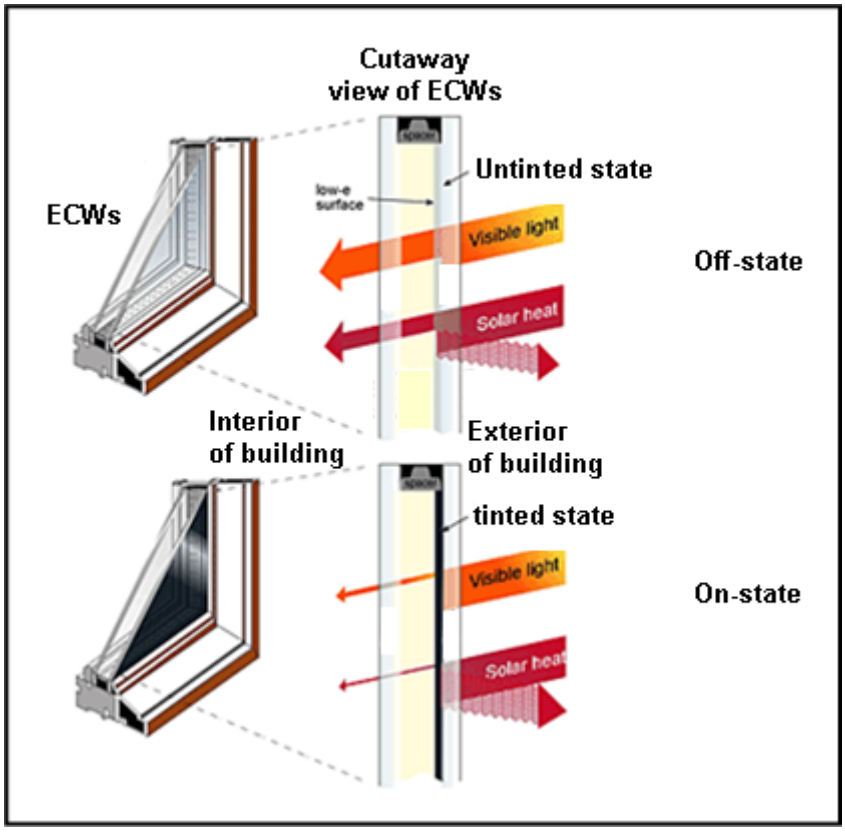

Fig. 2: Electrochromic windows, ECWs, with illustration of visible light and solar heat energy during operation.

Fig. 3 shows the evolution of the Solar Heat Gain Coefficient (SHGC) versus the light transmission of the electrochromic windows produced by the three main companies:, SAGE, Econtrol, and Gesimat [6]. (In case of Saint Gobain, a pro-type factory line is expected to be completed in the middle of 2010.) The SHGC is a fraction of the heat from the sun that enters through a window [7]. SHGC is expressed as a number between 0 and 1. The lower a window's SHGC, the less solar heat it transmits. We see in Fig. 3 that Gesimat's electrochromic windows [6] are the most efficient at the moment.

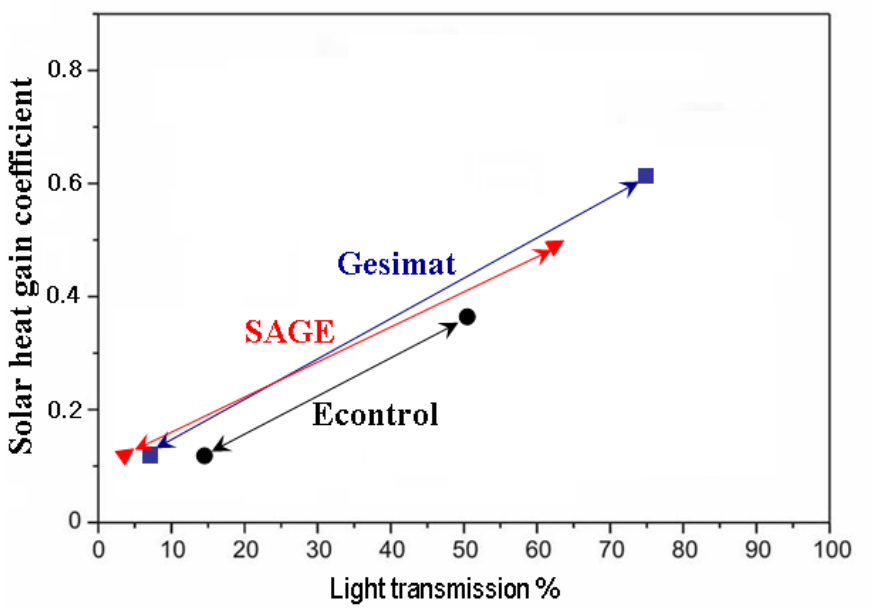

Fig. 3: The values of solar heat gain coefficient, SHGC, and % of light transmission of the electrochromic windows developed by the different companies, SAGE, Econtrol, and Gesimat [6].

In § 2.5, we will present additional benefits offered by the electrochromic windows.

2-1-c. Various applications of electrochromic devices (ECDs)

In addition to electrochromic windows (ECWs) for buildings, Fig. 4 gathers other practical applications using electrochromic devices (ECDs) such as smart sunroofs, filters, rear-view mirrors, smart glass wears, helmets, and displays.

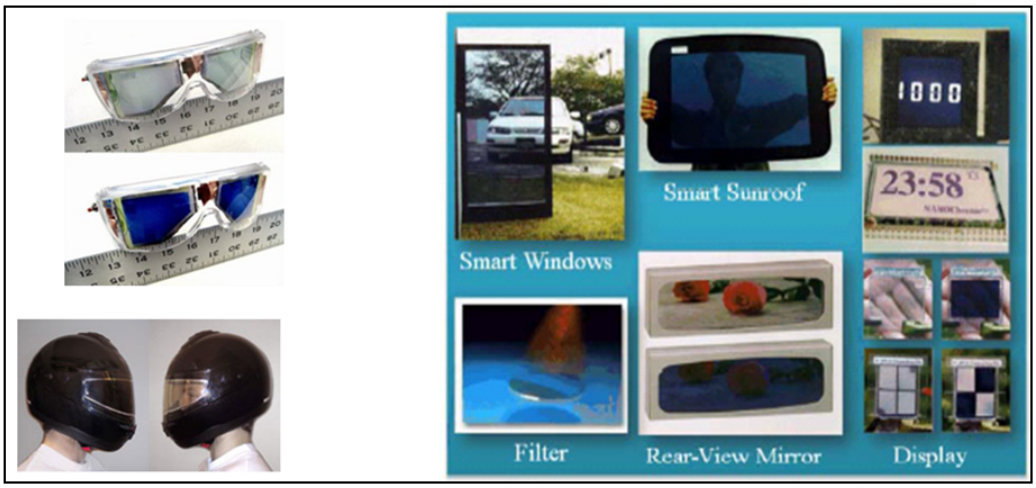

Fig. 4: Various ECD applications [8].

2-2. Materials in electrochromic devices (ECDs)

Electrochromic devices cover a wide range of materials from conductive substrates to electrolytes and to electrochromic materials [9].

2-2-a. Conductive substrates

For transmissive ECDs, current collectors in addition to being electronic conductors, must be also as transparent (> 80 %) and as colorless as possible in the visible wavelength domain. Several kinds of systems have been studied including metal grids or conductive polymers. However, the most used by far are the Transparent Conductive Oxides (TCO) [9,10]. n-type TCO thin films are generally based on In_2O_3:Sn (ITO) and SnO_2:F (FTO) using commonly deposition techniques of PVD and CVD, respectively. Recent investigations report resistivities as low as 7-8 10^{-5} Ωcm for ITO films. Films of ZnO:Al (or ZnO based) are currently attracting much attention as a consequence of the rising prices of In. A recent, of much potential interest, discovered alternative to ITO is TiO_2:Nb. One of the biggest challenges for all TCOs is their fabrication on plastic substrate for which low temperature deposition is required.

2-2-b. Electrolytes

The electrolyte, as pure ion conductor and electronic insulator, can be either organic or inorganic, liquid or solid. The ions should be small in order to be mobile, proton (H^+) or lithium ions (Li^+) are generally preferred. Proton conductors are commonly associated with higher ionic conductivity whereas lithium-based electrolytes show higher stability in a larger electrochemical active window and limited film dissolution partially linked to the absence of water or H_2 or/and O_2 formation. Solid-ion conducting electrolytes for use in ECDs are listed in Table 2. Inorganic electrolytes are often based on oxide thin films and in particular hydrated Ta_2O_5 generally evaporated or sputtered. Organic electrolytes fall in two categories, polyelectrolytes and polymer electrolytes.

Electrolytes	
Inorganic electrolytes	Organic polymers
$LiAlF_4$	Nafion™
$LiNbO_3$	Poly(acrylic acid)
Sb_2O_5 (inc. $HSbO_3$)	Poly(AMPS)
$HSbO_3$ based polymer	Poly(methyl methacrylate)
Ta_2O_5 (including « TaO_x »)	PMMA (« Perspex »)
TiO_2 (including « TiO_x »)	Poly(2-hydroxyethyl methacrylate)
$H_3UO_3(PO_4).3H_2O$ (« HUP »)	Poly(ethylene oxide), PEO
ZrO_2	Poly(vinyl chloride), PVC

Table 2: Solid ion-conducting electrolytes for use in ECDs [**11**]

2-2-c. Electrochromic materials (ECMs)

There are many types of ECMs, such as inorganic, organic, and metal organic complexes.

- Organic materials

A large number of electrochromic organic dyes and derivatives are known. They include bipyridinium systems, carbazoles, methoxybiphenyl, quinines, diphenylamine, pyrazolines [12]. The properties of the most studied organic materials are gathered in Table 3a. Extensive literature reports on bipyridinium compounds and particularly on 1,1'-

dimethyl -4,4'-bipyridinium, also called methyl viologen [13]. They can be either used as such by solubilising in the electrolytic solution or as solid films after polymerisation or grafting onto an appropriate substrate. Organic materials also include conductive polymers. The properties of the most utilized are gathered in Table 3b.

As opposed to inorganic ECMs, organic ECMs usually take advantage of very high colouration efficiencies (hundred of cm^2/C), fast switching time and wide colour ranges. They can be either anodically or cathodically coloured.

Organic compound	Col.	Oxidized	Reduced		Ref.
Viologens: Bipyridilium (bipm)	C	**$bipm^{2+}$**	**$bipm^{+\bullet}$**	**bipm**	**[14-16]**
R = alkyl	C	**Colourless**	Blue/ Violet	Weak colour	
R = aryl	C	**Colourless**	Green	Weak colour	
Diphenylamine p-phenylene diamine	C	**Colourless**	Highly coloured		**[17]**
Tetracyanoquinodimethane (TCNQ)	C	**Colourless**	Blue		**[18]**
Carbazole	A	**$Carbazole^{+\bullet}$**	**Carbazole**		**[19]**
R = H	A	Dark green	**Colourless**		
R = ethyl	A	Green	**Colourless**		
R = phenyl	A	Iridescent	**Colourless**		
Violene: Methoxybiphenyl	A	Blue or Green	**Colourless**		**[20]**
Quinones types	A	RQ **≈ colourless**	$RQ^{\bullet}$ Blue, Pink, Yellow, Red		**[21-24]**
Pyrazoline compounds	A	Green or Red	Yellow		**[25]**

(a)

Electrochromic polymers	Colouration Cathodic (C) or Anodic (A)	Oxidized	Reduced	Ref.
Poly(thiophene):				
R1=R2=H	C/A	Blue	Red	**[26]**
R1=CH3	C/A	Deep Blue	Red	
R1=R2=CH3	C/A	Dark Blue	Pale Brown	
R1=Ph	C/A	Green Blue	Yellow	
R1=R2=Ph	C/A	Blue/Grey	Yellow	
PEDOT (polyethylenedioxi -thiophene	C	Pale Blue	Dark Blue	
Poly(aniline)	A	Blue/Dark Yellow/Green	**Colourless**	**[26]**
Poly(pyrolle)	A	Blue/Violet	Yellow/Green	**[26]**

(b)

Table 3: (a) Properties of organic ECMs and (b) polymeric ECMs.

- Inorganic materials

The electrochromic materials used in electrochromic windows are generally inorganic materials owing to their thermal stability. Till the mid 90's, most of the inorganic electrochromic materials were transition metal oxides. Most of them known so far have structures built from MeO_6 octahedra with a Me transition metal at the center, arranged in different corner-sharing and edge-sharing configurations [8]. As discussed below, in 1996 Philips in collaboration with the group of R. Griessen [27] demonstrated spectacular optical changes upon hydrogenation for metal hydrides, opening a new family of inorganic electrochromic materials. In addition, among inorganic non-oxides, hexacyanometallates compounds of the general type $M_k[M'(CN)_6]^l$, where M and M' are transition metal ions with different vacancies can exhibit pronounced anodic coloration. One of the best examples is the case of Prussian Blue, PB [28]. Electrodeposited PB may be partially oxidized to Prussian Green (PG) and completely oxidized as Prussian Brown.

$$[Fe^{III}Fe^{II}(CN)_6]^- \rightarrow [Fe^{III}Fe^{III}(CN)_6] + e^-$$

(PB) (PX)

Reduction of PB yields Prussian white (PW) also known as Everitt's salt which appears colourless as a thin film.

$$[Fe^{III}Fe^{II}(CN)_6]^- + e^- \rightarrow [Fe^{II}Fe^{II}(CN)_6]^{2-}$$

(PB) (PW)

Interestingly, the coloration efficiency of PB is in the same range of the most efficient oxides (88 mC/cm^2).

A non exhaustive list of inorganic electrochromic materials is reported in Table 4**.** As for any electrochromic material, metal oxides can be generally divided into two groups: cathodic colouring materials (coloured in the reduced state) and anodic colouring materials (coloured in the oxidized state).

Oxide	Colouration Cathodic (C) or Anodic (A)	Oxidized	Reduced	Colouration efficiency : η (cm^2/C)	Ref.
WO_3	C	**Colourless**	Blue	42 (650 nm) to 115 (633 nm)	**[29,30]**
TiO_2	C	**Colourless**	Blue	5	**[31]**
Li_xCoO_2	A	Deep Blue	**Blue**	-10	**[32]**
MoO_3	C	**Colourless**	Blue	77 (700 nm)	**[33]**
V_2O_5	C	**Pale Yellow**	Pale Blue	-15 (600 nm)	**[34]**
'IrO_x'	A	Blue/Grey	**Colourless**	-30	**[35]**
Nb_2O_5	C	**Colourless**	Brown	<12	**[36]**
'NiO'	A	Brown/Black	**Colourless**	-36 (640 nm)	**[37]**
'$Li_{0.5}Ni_{0.5}O$'	A	Brown	**Pale Brown**	-40 (650 nm)	**[38]**
InO_2:Sn	C	**Colourless**	Brown	Irreversible	**[39]**

Table 4: Properties of the most studied electrochromic inorganic materials. The colouration efficiency values are highly dependent on the measurement conditions; they are given here as approximate indicators.

All of electrochromic materials exist in different phases and have crystalline, polycrystalline or amorphous structure associated with different coloured/bleached mechanisms. Among the ECMs in Table 4, WO_3 and 'NiO' are typical examples of cathodic and anodic ECMs respectively. In fact, nowadays precisely, interest is becoming more focused on electrochromic devices based on WO_3 and 'NiO' thin films due to their complementary coloration (blue for reduced 'WO_3' and brown for oxidized 'NiO') [40-79]. Intensive work has been first reported on rigid (glass-based) devices [40–53], then on flexible (polyester film-based) devices [54,55].

If NiO thin films experience strong electrochromic effect in KOH electrolyte, they show, unfortunately, low cycling durability in such electrolyte [65-79].

2-3. Different types of electrochromic devices (ECDs)

ECDs can be classified in three types, solution, hybrid, and battery-like types, as shown in Fig. 5. For solution and hybrid type ECDs, at least one electrode should be solution or gel-type electrolyte. The ECDs are self-erased under open circuit potential (meaning no memory effect). On the other hand, battery-like devices have a good memory effect under open circuit potential (like a battery in fact). Coloration of the two electrodes,

in battery-like devices, complements one another, thus showing their electrochromic superiority to the solution and hybrid types [9].

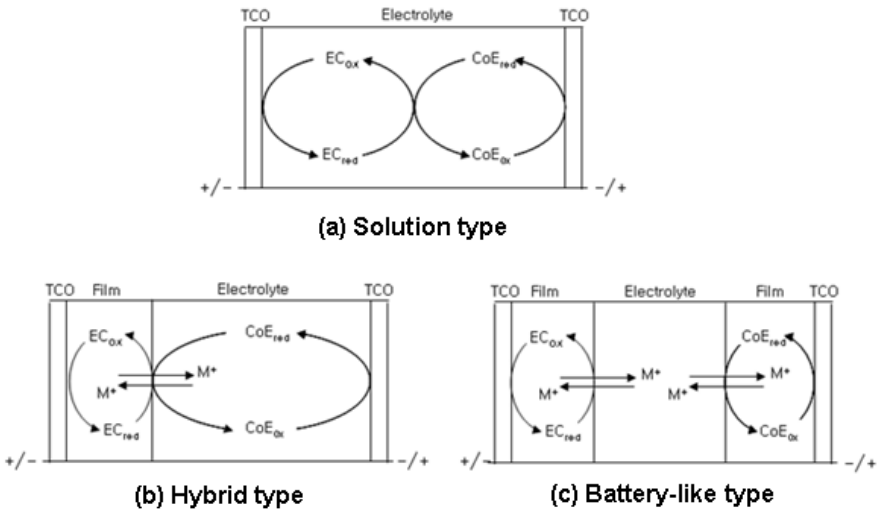

Fig. 5: Three different types of electrochromic devices (ECDs)**:**
(a) solution type, (b) hybrid type, and (c) battery-like type.
(TCO stands for Transparent Conducting Oxides).

2-4. Electrochromic device (ECD) features

Color change in the visible light is one important feature of electrochromic devices. Equation (1.1) expresses the contrast ratio (CR):

$$CR = Ro / R_x \tag{1.1}$$

Here, R_x and R_0 represent reflected light intensity in bleached and coloured states, respectively. Higher value of CR indicates larger difference in transmittance. Therefore, we could evaluate a given electrochromic device with its CR, together with its absorbance, A

Absorbance, A, is equal to change of optical density ΔOD (λ),

$$A = \Delta OD\ (\lambda) = \log T_b/T_c \tag{1.2}$$

when reflectivity is negligible compared to absorption. T_b and T_c designate transmitted light intensity in bleached and coloured states, respectively.

$\Delta OD\ (\lambda)$ is also expressed as [80],

$$\Delta OD\ (\lambda) = \eta Q = CE \cdot Q \tag{1.3}$$

Q is the injected electronic charge per unit area needed to switch the electrochromic thin film material from bleached to coloured state. η indicates the coloration efficiency, which is also expressed in the literature as CE (cm^2/C). Therefore, CE is proportional to ΔOD and inversely proportional to the quantity of electric charge per unit area.

An electrochromic device with high coloration efficiency provides big difference in transmittance with small amount of electric charge. The most representative inorganic thin film electrochromic materials such as WO_3 and NiO have a coloration efficiency (CE) of ~ 40 cm^2 / C and organic electrochromic thin films, such as PEDOT, show more than 100 cm^2 / C in CE [9].

Electrochromic devices are also evaluated based on response time. Generally we measure the time needed to reach 90 % of bleached/coloured state. Electrochromic devices show lower response time than that of liquid crystal displays (LCDs), (Table 1). However, the lower response time is not limiting for building applications according to tests organized by SAGE, Gesimat, and Econtrol-glas companies. Long cycling life is also required for ECDs.

2-5. Benefits with electrochromic windows (ECWs)

The ECWs deliver the following benefits [81,82];

- Block solar heat
- Always keep a view and connection to the outdoors

- Block glare
- Dramatically reduce fading

2-5-a. Solar heat blocking

The U.S. Department of Energy (DOE) estimates that electrically switchable ECWs are capable of providing up to 40 % savings on energy bills [7, 81].

2-5-b. Keeping a view and connection to the outdoors

Many studies point out to the importance of natural daylight and outdoor views to people's happiness and well-being. Because ECWs and skylights can eliminate most of the negative aspects of sunlight, buildings can be designed with vision area in spaces and elevations where it was not possible to do so before. ECWs give those who design buildings, whether commercial or residential, a new tool for creating spaces that takes full advantage of available daylight. And this is important because research shows that providing people with daylight and a connection to the outdoors can increase retail sales, improve children's scholastic achievement, reduce absenteeism and boost productivity in the workplace.

2-5-c. Glare Blocking

ECWs can be tinted to allow in only 3.5% visible light in summer season [81]. By comparison, commercial buildings typically have windows that transmit about 45 % of visible light [81]. In human factors evaluations carried out by the Lawrence Berkeley National Laboratory, Berkeley, California, people greatly preferred to be in the room with ECWs versus the room with regular static glass and blinds because of the level of comfort it brought to the space.

2-5-d. Dramatically reduce fading

It is also expected that ECWs greatly reduce interior fading by protecting furniture, artwork, and carpet. In case of fading and damage, UV rays are the primary culprit. However, there is also a part of the visible spectrum that causes fading, up to 700 nanometers. When glass manufacturers say their product reduces the radiation that causes fading, they typically mean the UV portion only. Electrochromic windows block not only nearly 100% of the UV radiation, but also the portion of visible light that causes fading.

2-6. Current R&D in electrochromic technology

The International Energy Agency (IEA), Department of Energy (DOE), and National Renewable Energy Laboratory (NREL), in US, have focused on the development of a process for testing electrochromic windows, ECWs. DOE is actually testing the ECWs of the four companies, Donelly Corp., OCLI (Santa Rosa, California), EIC Labs (Norwood. Miami), and Anderson Windows (St. Paul, Minnesota).

Moreover, St. Paul and SAGE Electrochromics, Inc., Minnesota have received, from NIST in US, a huge fund, aimed at developing large area electrochromic devices on plastic substrates. SAGE Electrochromics, Inc. announced more than $100 million in DOE loan guarantees and government tax credits, spurred on by the Department of Energy's Loan Guarantee Program, which was established under the Energy Policy Act of 2005.

Lawrence Berkeley national laboratory (LBNL) aimed at developing large area electrochromic polymer layers (PEDOT) working with lithium ions. Pilkington PLC (UK) has carried out multi electrochromic glazing under program of Joule 11. Flachglas (Germany), Davionics AS (Denmark), Oxford Brookes University, University of Southampton and others, are involved in this project. Flachglas and Saint-Gobain are producing sunroofs for cars in size of 46 $\times$ 78 cm^2 which transmit 14 % of the visible light

in the coloured state. Asahi Glass has steadily developed ECWs based on Li_xWO_3/inorganic lithium ion conductor/NiO_x under Sunshine Project funded by the Japanese government. Asahi Glass applied about 200 pieces of their prototype products into Seto Bridge Meseum (Kojima, Okayama-Pref., Japan).

Owing to the mentioned global activities above, EControl-glass successfully commercialized smart electrochromic windows for buildings for the first time in 2006; the electrochromic thin films were deposited by sputtering. EControl-glass established a mass production line with vertical typed sputtering machines in Plauen (Germany) in 2009. In 2008 SAGE Electrochromics, Inc. started the commercialization in North America of large area ECWs (100 × 150 cm^2) with 3~5 min of switching time [81]. They used the monolithic technology to construct their Li-based ECWs. Saint-Gobain is starting the commercialization of proton-based ECWs for buildings with relatively short switching response time. In 2010, Gesimat produces the world's most energy-efficient window glass as illustrated in Fig. 3.

3. Background on nickel compounds

3-1. Nickel and nickel compounds [83]

Nickel is a hard, malleable, silvery white, ferromagnetic metallic element. Nickel is a Group VIIIB element, with atomic number 28 and atomic mass 58.69 g/mol. The melting point for nickel is ~1,453 °C and the boiling point is ~2,732 °C. Nickel has different oxidation states (0, 1+, 2+, 3+, and 4+). The electronic configuration for nickel is $[Ar]4s^23d^8$. Magnetic and chemical properties of nickel resemble those of iron and cobalt. So, it easily forms a number of alloys such as nickel-iron, nickel-copper, nickel-chromium, nickel-zinc and others. Nickel compounds mostly have blue or green colors. Nickel could

be combined with many other elements, including chlorine, sulfur and oxygen. Many nickel compounds dissolve readily in water forming characteristic green or blue colors. Nickel compounds are used in electrochromic device, coloring ceramics, batteries and chemical reaction catalysts.

3-2. Nickel(II) Oxide, NiO

The mineralogical form of NiO bunsenite, is rare. Therefore, it must be synthesized. There are many kinds of routes to synthesize NiO. Among those, the most well known route is a pyrolysis of Ni^{2+} compounds such as hydroxide, nitrate and carbonate, which yield a light green powder. Heating in oxygen or air atmosphere leads to black 'NiO' powder which indicates nonstoichiometry [84]. NiO belongs to NaCl structure, so-called rock salt structure. The space group of NaCl structured NiO is Fm3m with lattice parameters a = 4.1769 Å (JCPDS, 47-1049). 'NiO' is often non-stoichiometric. The non-stoichiometry is accompanied by a color change from green to black due to the existence of Ni^{3+} resulting from Ni vacancies [85]. This leads to p-type conductivity.

In order to explain optical absorption gap in NiO, there are two main theories, which deal respectively with p → d transitions from oxygen to nickel (charge transfer) and cationic d → d transitions [86].

NiO and NiO-derived materials have been used in many applications such as fuel cells, secondary ion batteries, dielectric materials and others, which accounts for the ~ 4000 ton annual production of NiO [87]. With regard to toxicity, long term inhalation of NiO causes health risks such as lung cancers [88].

3-3. Nickel hydroxide, $Ni(OH)_2$

There are mainly two phases of nickel (II) hydroxide [$Ni(OH)_2$] which are α and β types. The two different phases are illustrated in Fig. 8. β-$Ni(OH)_2$ crystallizes in the

hexagonal system which is described as a hexagonal close-packed (hcp) structure of hydroxyl ions (AB oxygen packing) with Ni(II) occupying half the octahedral interstices. This structure is in fact a layered structure. Each layer consists of hexagonal planar arrangement of Ni(II) ions with an octahedral coordinated oxygen. The layers are stacked along the c-axis with the distance between layers of 4.6 Å.

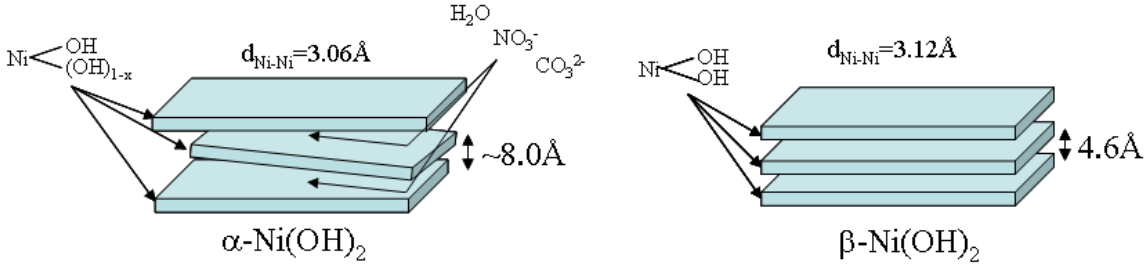

Fig. 6: Illustration of α-$Ni(OH)_2$ and β-$Ni(OH)_2$ phases [89].

The α-$Ni(OH)_2$ structure is a hydrated form of the β-$Ni(OH)_2$ phase. As illustrated in the left panel of Fig. 6, some guests such as water, NO_3^-, and CO_3^{2-} are intercalated in the $Ni(OH)_2$ slabs resulting in higher distance between them (~ 8.0 Å). A great variety of α-type hydroxides can be obtained depending on the degree of hydrated turbostratic hydroxide. The variety occurs between a highly turbostratic α-$Ni(OH)_2$ and the well stacked β-$Ni(OH)_2$, as proposed by Le Bihan *et al.* [90]. Fortunately, both types of $Ni(OH)_2$ are transparent in their thin film form.

. 3-4. Nickel oxyhydroxide, NiOOH

There still remain controversies about the structural characterization of layered 'NiOOH' phases obtained via either chemical or electrochemical oxidation reactions; the compounds have high degree of division and disordered sheet stackings, which results in a wide range of diffraction patterns. However, there are two basic types of layered nickel oxyhydroxide, NiOOH, which are β [91] and γ-NiOOH [92]. As shown in Fig. 7, β-NiOOH is considered as a relatively well defined material compared to γ-NiOOH. 'γ-

NiOOH' can be written as $A_xH_y(H_2O)_zNiO_2$ as a general formula. Water and alkali ions (mostly K^+ and Na^+) are intercalated in the 'NiO_2' layers. The range of oxidation state of nickel in 'γ-NiOOH' is between 3 and 3.75. Nevertheless, β- and 'γ-NiOOH' have distinct inter-sheet distances which are 4.7 and 7.0 Å, respectively (Fig. 7). Both types of NiOOH are brownish in thin film form which is very practical in the application of electrochromic devices as an active counter electrode.

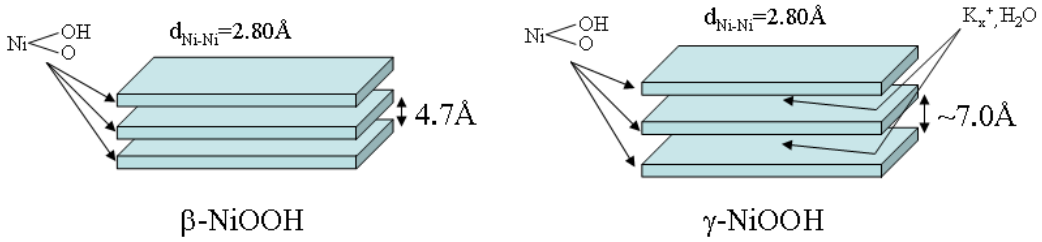

Fig. 7: Illustration of β-NiOOH and γ-NiOOH phases [89].

3-5. Redox mechanism and electrochromic properties of nickel oxide-based thin films.

Chemical and electrochemical properties of nickel oxide-based thin films have been mainly investigated in alkaline electrolyte, mostly aqueous KOH electrolyte. The surface of NiO particles is converted into $Ni(OH)_2$ when immersed in KOH electrolyte. Fig. 8 represents the general oxidation/reduction reaction scheme for hydrated NiO electrode in aqueous KOH electrolyte as proposed by Bode *et al*. [93].

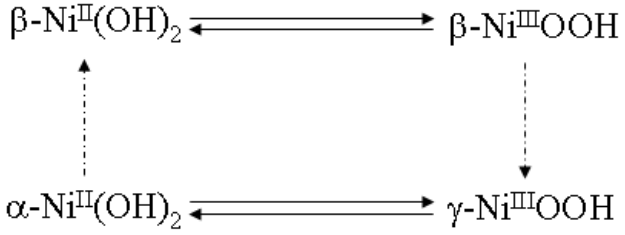

Fig. 8: The general reaction scheme proposed by Bode *et al*. [93].

The Bode scheme represents the transition between Ni(II) and Ni(III) as a main feature. Fig. 8 shows the two main oxidation/reduction reactions which are the α-$Ni(OH)_2$/ γ-NiOOH (α/γ) and β-$Ni(OH)_2$/ β-NiOOH (β^{II}/β^{III}) transformations [89]. β-$Ni(OH)_2$ and β-NiOOH phases are observed during cycling [94-96]. However, one can also observe the formations of the γ phase [91] and other intermediate phases [92,97]. The transformation from β-NiOOH to γ-NiOOH, which is irreversible, results from an overcharge of β-NiOOH.

The other reduction/oxidation chemical reaction deals with α/γ transformation where at least 1.3 electrons may be transferred [91,98-100].

Among all mechanisms proposed so far for nickel oxide thin films in aqueous basic electrolytes [66,89,101-114], equations (1.4) and (1.5) illustrate the generally accepted electrochromic mechanisms [89].

$$Ni(OH)_2 \rightleftharpoons NiOOH + H^+ + e^- \quad (1.4)$$

$$Ni(OH)_2 + OH^- \rightleftharpoons NiOOH + H_2O + e^- \quad (1.5)$$

bleached state *colored state*

4. Employed deposition methods of 'NiO' thin films in this work

In this work, NiO thin films have been prepared using:

- Physical vapor deposition method by pulsed layer deposition (PLD), (Chapter 2)
- Solution method by dip-coating, (Chapter 3)
- Sol-gel method by spin-coating, (Chapter 4).

4-1. Pulsed Laser Deposition (PLD)

PLD is a physical vapor deposition (PVD) technique for film deposition [115,116]. A high power pulsed laser beam is focused inside a vacuum chamber to hit a target.

Material is vaporized from the target inducing a plasma plume. This plasma plume reaches the substrate (SnO_2:F (FTO) or SnO_2:In (ITO)) followed by the film growth. Film deposition process may occur under high vacuum or a background gas atmosphere.

A typical configuration of a PLD deposition chamber is illustrated in Fig. 9.

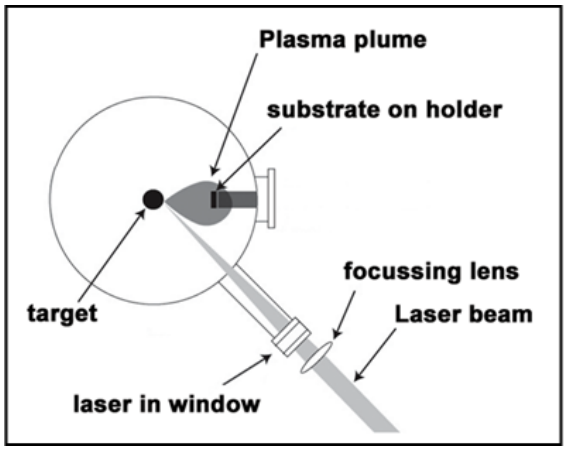

Fig. 9: A typical configuration of a PLD deposition chamber.

The PLD technique has several significant benefits over other film deposition methods such as: fast film deposition, easy control of film thickness, film deposition of complex materials like YBCO and others [117]. The PLD is also regarded as a quite practical film deposition technique for laboratory scale research works.

The main factors that influence deposition thickness are a) the target material (composition, density), b) the laser energy, c) the laser frequency d) the distance from target to substrate and e) the gas nature and pressure inside the chamber (Oxygen, Argon, etc.).

4-2. Dip Coating (DC)

Dip coating is a technique which is practical and economic for thin film deposition at industrial scale [118-124]. Fig. 10 represents dipping, wet layer formation, and solvent evaporation which belong to a typical dip-coating process.

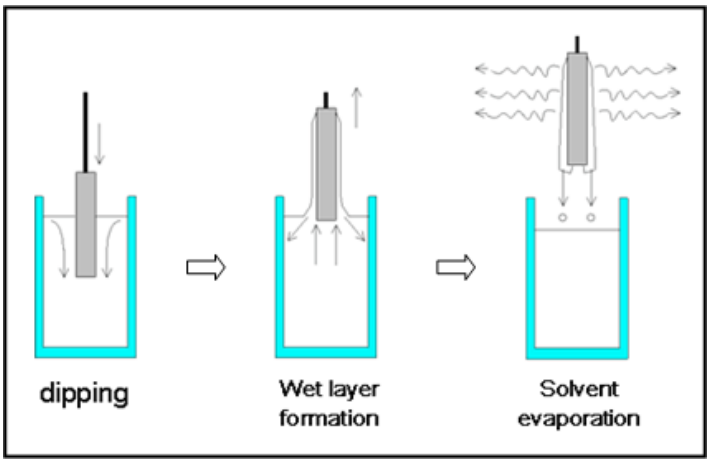

Fig. 10: Stages of the dip coating process: dipping of the substrate into the coating solution, wet layer formation by withdrawing the substrate and gelation of the layer by solvent evaporation.

The substrate is first immersed in the coating solution at constant speed. The substrate is then aged inside the solution and then pulled up. The thin film grows on the substrate during pulling up the substrate at constant speed. Finally the pulled-up substrate is aged in the air to evaporate the solvent from the liquid, forming thin film. The film thickness (h), which depends on the withdrawal speed (v) and the viscosity of the coating solution (η), can be determined using the Landau-Levich equation (1.6) [125],

$$h = 0.94 \cdot \frac{(\eta \cdot v)^{2/3}}{\gamma_{LV}^{1/6} (\rho \cdot g)^{1/2}} \tag{1.6}$$

where γ_{LV} = liquid-vapor surface tension, ρ = liquid density and g = gravity.

4-3. Spin Coating (SC)

The solution is placed on the substrate and then the substrate is rotated in order to spread the solution by centrifugal force. At this stage, gas blowing toward the substrate during rotation can be used. The film thickness can be controlled by varying rotation speed, rotation time and coating solution viscosity. The used solvent is usually volatile and

simultaneously evaporates. The machine used for spin coating is called a spin coater or spinner. A coating process using spin coater or spinner is illustrated in Fig. 11.

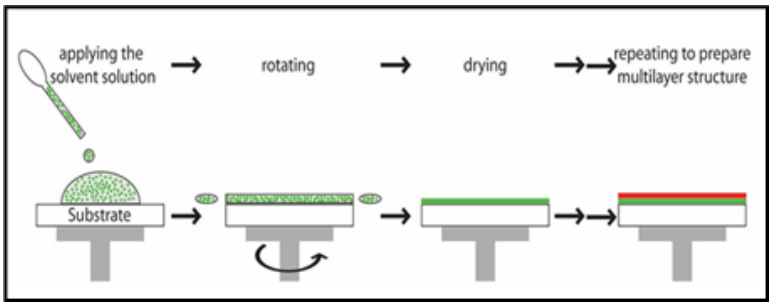

Fig. 11: A spin coating process: applying the solution onto the substrate, rotating the substrate and drying. Repeating this process leads to multilayer structure.

4-4. Sol-gel process

The meaning of "sol-gel" originated from "sol" indicating the evolution of inorganic networks through the formation of a colloidal suspension and "gel" corresponding to the gelation of the sol to form a network in a continuous liquid phase.

Sol-gel method is widely employed to deposit thin films, to synthesize nanomaterials and ceramics. The typical steps involved in sol-gel processing are shown in the schematic diagram below (Fig. 12) [126].

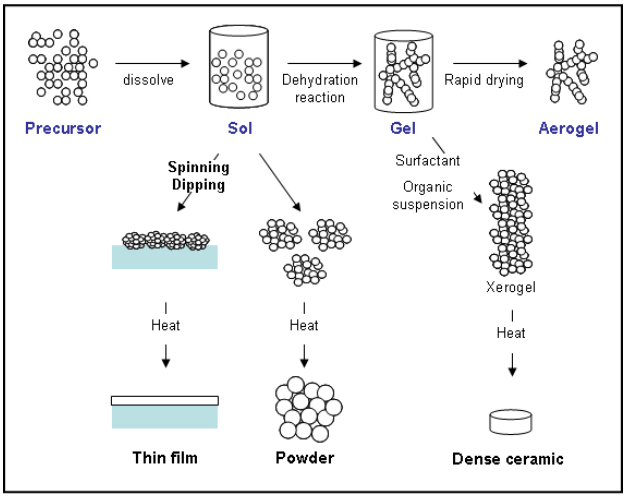

Fig. 12: Schematic representation of sol-gel process to synthesize thin films, nanomaterials and ceramics.

5. References

[1] P.M.S. Monk, S.P. Akhtar, J. Boutevin, J.R. Duffield, *Electrochim. Acta* **46** (2001) 2091.

[2] P.M.S. Monk, R.J. Mortimer, D.R. Rosseinsky, *Electrochromism: Fundamentals and Applications*. *Weinheim, VCH*, 1995.

[3] I. Hamberg, C.G. Granqvist, *J. Appl. Phys.* **60** (1986) R123.

[4] C.G. Granqvist, A. Hultåker, *Thin Solid Films* **411** (2002) 1.

[5] *http://www.econtrol-glas.de/* (Date accessed: 13 April 2010).

[6] Private communication with IP Bewertungs AG (IPB) company in Germany which evaluates recent technologies.

[7] US department of energy (DOE) – Building Energy Codes Program (http://resourcecenter.pnl.gov).

[8] C.G. Granqvist, *Handbook of Inorganic Electrochromic Materials, Elsevier, Amsterdam*, 1995, Reprinted 2002. See also http://www.goodmodo.com/page/11/ (Date accessed: 13 April 2010).

[9] A. Rougier, "Basic concepts on electrochromic materials and devices" *Galerne 2009, Materiaux pour l'énergie, Amiens 26-30 Octobre 2009*, LRCS-CNRS, Université de Picardie Jules Verne, Aimens (FRANCE). See also C.G. Granqvist, *Solar Energy Materials and Solar Cells* **91** (2007) 1529.

[10] G.J. Exarkhos, X.-D. Zhou, *Thin Solid Films* **515** (2007) 7025.

[11] All references in P.M.S. Monk, R.J. Mortimer, D.R. Rosseinsky, *"Electrochromism and Electrochromic Devices"*, Cambridge University Press (2007) p 421.

[12] R.J. Mortimer, *Electrochimica Acta*, **44** (1999) 2971.

[13] A. Samat, R. Guglielmetti, *Kirk-Othmer Encyclopedia of Chemical Technology (5th Edition)*, John Wiley & Sons, **6** (2004) 571.

[14] L.A. Summers, *Adv. Hetero. Chem.* **35** (1984) 281.

[15] A.J. Bard, A. Ledwith, H.J. Shine, *Adv. Phys. Org. Chem.* **13** (1976) 155.

[16] C.L. Bird, A.T. Kuhn, *Chem. Soc. Rev.*, **10** (1981) 49.

[17] A. Watanabe, K. Mori, Y. Iwasaki, Y. Nakamura, S. Niizuma, *Macromol*. **20** (1987) 1793.

[18] G. Inzelt, R.W. Day, J.F. Chambers, *J. Electroanal. Chem.* **161** (1984) 147.

[19] J.E. Dubois, F. Garnier, G. Tourillon, M. Gazard, *J. Elctroanal. Chem.* **129** (1981) 229.

[20] B. Grant, N.J. Clecak, M. Oxsen, A. Jaffe, G.S. Keller, *J. Org. Chem.*, **45** (1980) 702.

[21] A. Desbène-Monvernay, P.C. Lacaze, A. Cherigui, *J. Electroanal. Chem.*, **260** (1989) 75.

[22] J.E. Dubois, A. Desbène-Monvernay, A. Cherigui, P.C. Lacaze., *J. Electroanal. Chem.*, **169** (1984) 157.

[23] M. Yashiro, K. Sato, *Jpn. J. Appl. Phys.*, **20** (1981) 1319.

[24] V.K. Gater, M.D. Liu, M.D. Love, C.R. Leidner, *J. Electroanal. Chem.*, **101** (1979) 547.

[25] F.B. Kaufman, E.M. Engler, *J. Am. Chem. Soc.*, **101** (1979) 547.

[26] J. Dyer, L. Aubrey, J.R. Reynolds, *Electrochromism of conjugated conducting polymers, Handbook of Conducting Polymers (3th Edition)*, **1** (2007) 20.

[27] J.N. Huiberts, R. Griessen, J.H. Rector, R.J. Wijngaarden, J.P. Dekker, D.G. de Groot, N.J. Koeman, *Nature*, (1996), **380**, 231.

[28] R.J. Mortimer, D.R. Rosseinsky, *J. Chem. Soc., Dalton Trans.*, **9** (1984) 2059.

[29] M.L. Hitchmann, *J. Electrocanal. Chem.*, **85** (1977) 135.

[30] B.W. Faughnan, R.S. Crandall, P.M. Heyman, *RCA Rev.*, **36** (1975)177.

[31] P. Baudry, A.C.M. Rodriguez, M.A. Aegerter, L.O. Bulhões, *J. Non-Cryst. Solids*, **121** (1990) 319.

[32] M. Rubin, K. Von Rottkay, S.J. Wen, N. Özer, J. Slack, *Sol. Energy Mater. Sol. Cells* **54** (1998) 49.

[33] R.J. Colten, A.M. Guzman, J.W. Rabalais, *J. Appl. Phys.*, **49** (1978) 1734.

[34] A.I. Gavrilyuk. F.A. Chudnovski, *Sov. Tech. Lett.*, **3** (1977) 69.

[35] W.C. Dautremont-Smith, *Displays*, **3** (1982) 67.

[36] S.F. Cogan, R.H. Rauh, *Solid State Ionics*, **28-30** (1988) 1717.

[37] M. Kitao, S. Yamada, *Proc. of the Inter, Seminar on Soild State Ionic Devices, World Publishing Co.*, 359 (1988)

[38] S. Gottesfeld, *J. Electrochem. Soc.*, **127** (1980) 272.

[39] N.R. Armstrong, A.W.C. Lin, M. Fujihira, T. Kuwana, *Anal. Chem.*, **48** (1976) 741.

[40] E. Avendaño, A. Azens, G.A. Niklasson, C.G. Granqvist, *Mater. Sci. Eng. B* **138** (2007) 112.

[41] S.-H. Lee, S.-K. Joo, *Sol. Energy Mater. Sol. Cells* **39** (1995) 155.

[42] J.H.G. Mathew, S.P. Sapers, M.J. Cumbo, N.A. O'Brien, R.B. Sargent, V.P. Raksha, R.B. Ladaherne, B.P. Hichwa, *J. Non-Cryst. Solids* **218** (1997) 342.

[43] A. Azens, L. Kullman, G. Vaivars, H. Nordborg, C.G. Granqvist, *Solid State Ionics* **113** (1998) 449.

[44] R. Lechner, L.K. Thomas, *Solar Energy Mater. Solar Cells* **54** (1998) 139.

[45] J. Nagai, G.D. McMeeking, Y. Saitoh, *Sol. Energy Mater. Sol. Cells* **56** (1999) 309.

[46] J. Karlsson, A. Roos, *Solar Energy* **68** (2000) 493.

[47] A. Azens, G. Vaivars, M. Veszelei, L. Kullman, C.G. Granqvist, *J. Appl. Phys*. **89** (2001) 7885.

[48] K.-S. Ahn, Y.-C. Nah, Y.-E. Sung, K.-Y. Cho, S.-S. Shin, J.-K. Park, *Appl. Phys. Lett.* **81** (2002) 3930.

[49] K.-S. Ahn, Y.-C. Nah, J.-Y. Park, Y.-E. Sung, K.-Y. Cho, S.-S. Shin, J.-K. Park, *Appl. Phys. Lett.* **82** (2003) 3379.

[50] C. Person, I. Porqueras, M. Vives, C. Corbella, A. Pinyol, E. Bertran, *Solid State Ionics* **165** (2003) 73.

[51] A.-K. Jonsson, M. Furlani, G.A. Niklasson, *Sol. Energy Mater. Sol. Cells* **84** (2004) 361.

[52] A.-L. Larsson, G.A. Niklasson, *Sol. Energy Mater. Sol. Cells* **84** (2004) 351.

[53] A.-L. Larsson, G.A. Niklasson, *Mater. Lett.* **58** (2004) 2517–2520.

[54] A. Azens, G. Gustavsson, R. Karmhag, C.G. Granqvist*, Solid State Ionics* **165** (2003) 1.

[55] A. Azens, E. Avendaño, C.G. Granqvist, *Proc. Soc. Photo-Opt. Instrum. Engr*. **5123** (2003) 185.

[56] M. Rubin, S.-J. Wen, T. Richardson, J. Kerr, K. von Rottkay, J. Slack, *Sol. Energy Mater. Sol. Cells* **54** (1998) 59.

[57] F. Michalak, K. Von Rottkay, T. Richardson, J. Slack, M. Rubin, M. *Electrochim. Acta* **44** (1999) 3085.

[58] A. Urbano, F.F. Ferreira, S.C. deCastro, R. Landers, M.C.A. Fantini, A. Gorenstein, *Electrochim. Acta* **46** (2001) 2269.

[59] M. Rubin, K. Von Rottkay, S.J. Wen, N. Özer, J. Slack, *Sol. Energy Mater. Sol. Cells* **54** (1998) 49.

[60] S. Passerini, B. Scrosati, A. Gorenstein, *J. Electrochem. Soc.* **137** (1990) 3297.

[61] S.-J. Wen, J. Kerr, M. Rubin, J. Slack, K. Von Rottkay, *Sol. Energy Mater. Sol. Cells* **56** (1999) 299.

[62] Y.-I. Kim, B.-W. Kim, J.-H. Choy, G. Campet, N.-G. Park, J. Portier, B. Morel, *J. Korean Chem. Soc.* **41** (1997) 11.

[63] E. Avendano, A. Azens, G.A. Niklasson, C.G. Granqvist, *Sol. Energy Mater. Sol. Cells* **84** (2004) 337.

[64] J.-C. Giron, *Ph.D. Thesis*, l'Universite Paris, 1994.

[65] M. Martini, G.E.S. Brito, M.C.A. Fantini, A.F. Craievich, A. Gorenstein, *Electrochim. Acta* **46** (2001) 2275.

[66] I. Bouessay, A. Rougier, P. Poizot, J. Moscovici, A. Michalowicz, J.-M. Tarascon, *Electrochim. Acta* **50** (2005) 3737.

[67] M. Martini, G.E.S. Brito, M.C.A. Fantini, A.F. Craievich, A. Gorenstein, *Electrochim. Acta* **46** (2001) 2275.

[68] Y. Makimura, A. Rougier, J.-M. Tarascon, *Appl. Surf. Sci.* **252** (2006) 4593.

[69] N. Penin, A. Rougier, L. Laffont, P. Poizot, J.-M. Tarascon, *Sol. Energy Mater. Sol. Cells* **90** (2006) 422.

[70] R.S. Conell, D.A. Cordgan, B.R. Poweii, *Sol. Energy Mater.* **25** (1992) 301.

[71] Y. Ushio, A. Ishikawa, T. Niwa, *Thin Soild Films* **280** (1996) 233.

[72] C.M. Lampert, R.C. Popowich, *Optical Materials Technology for Energy Efficiency and Solar Energy Conversion VIII,* SPIE, (1989) 1149**.**

[73] A. Pennisi, C.M. Lampert, *SPIE,* **1061** (1988) 131.

[74] S. Passerini and B. Scrosati, A. Gorenstein, A.M. Andersson, C.G. Granqvist, *J. Electrochem. Soc.* **136** (1989) 3394.

[75] S. Yamada, T. Yoshioka, M. Miyashita, K. Urabe, M. Kitao, *J. Appl. Phys.* **63** (1988) 2116.

[76] F. Decker, S. Passerini, R. Pileggi, B. Scrosati, *Electrochim. Acta* **37** (1992) 1033.

[77] I. Bouessay, A. Rougier, J.-M. Tarascon, *J. Electrochem. Soc.* **151** (2004) H145.

[78] I. Bouessay, A. Rougier, B. Beaudoin, J.-B. Leriche, *Appl. Surf. Sci.* **186** (2002) 490.

[79] A. Fukazawa, M. Chihiro, *European patent* EPXXDW EP 1434083, 2004.

[80] D. Calloway, *J. Chem. Educ.* **74(7)** (1997) 744.

[81] *http://www.sage-ec.com* (Date accessed: 13 April 2010).

[82] J.S.E.M. Svensson, C.G. Granqvist, *Solar Energy Mater.* **12** (1985) 391.

[83] *http://fr.wikipedia.org/wiki/Nickel* (Date accessed: 13 April 2010).

[84] N. N. Greenwood, A. Earnshaw, *Chemistry of the Elements, Oxford: Pergamon*, (1984) 1336.

[85] K.-S. Lee, H.-J. Koo, K.-H. Ham, W.-S. Ahn, *Bull. Kor. Chem. Soc.*, **16** (1995) 164.

[86] R. Merlin, *Phys. Rev. Lett.*, **54** (1985) 2727.

[87] K. Lascelles, L. G. Morgan, D. Nicholls, D. Beyersmann, *"Nickel Compounds" in Ullmann's Encyclopedia of Industrial Chemistry 2005 Wiley-VCH, Weinheim*, 2005.

[88] U.S. Dept. of Health and Human Services,"*Toxicology and Carcinogenesis Studies of Nickel Oxide*", (07/1996) 451.

[89] P. Oliva, J. Leonardi, J.F. Laurent, C. Delmas, J.J. Braconnier, M. Figlarz, F. Fievet, A.de Guibert, *J. Power Sources*, **8** (1982) 229.

[90] S. Le Bihan, J. Guenot, M. Figlarz, *C.R. Acad. Sci., Ser. C* **270** (1970) 2131.

[91] R. Barnard, C. F. Randell and F. L. Tye, *J. Electroanal. Chem.* **119** (1981) 17.

[92] O. Glemser, J. Einerhand, *2. Anorg. Allg. Chem.* **261** (1950) 26.

[93] H. Bode, K. Dehmelt, J. Witte, *Electrochim. Acta* **11** (1966) 1079.

[94] G. W. D. Briggs, E. Jones, W. F. K. Wynne-Jones, *Trans. Faraday Sot*. **51** (394) (1955) 1433;

[95] G. W. D. Briggs, E. Jones, W. F. K. Wynne-Jones, *Trans. Faraday Sot*. **52** (405) (1956) 1260.

[96] F. P. Kober, *J. Electrochem. Soc*. **112** (1965) 1064.

[97] F. P. Kober, *J. Electrochem. Soc.* **114** (1967) 215.

[98] R. Barnard, G. T. Crickmore, J. A. Lee, F. L. Tye, *J. Appl. Electrochem.* **10** (1980) 61.

[99] N. Yu. Uflyand, A. M. Novakovski, Yu. M. Pozin, S. A. Rozentsveig, *Elektrokhimiya* **2** (1966) 234.

[100] N. Yu. Uflyand, A. M. Novakovski, Yu. M. Pozin, S. A. Rozentsveig, *Elektrokhimiya* **3** (1967) 537.

[101] Fantini, M.C.A., *SPIE Proceedings* **1536** (1991) 81.

[102] J.-Y. Park, K.-S. Ahn, Y.-C Nah, H.-S. Shim, *J. Sol-Gel Sci. Technol.* **31** (2004) 323.

[103] A. Surca, B. Orel, R.C. Korosec, P.Bukovec, B.Philer, *J. Electroanal. Chem.* **443** (1997) 57.

[104] D.D. Ragan, P. Svedlindh, C.G. Granqvist, *Sol. Energy Mater. Sol. Cells* **54** (1998) 247.

[105] M. Martini, *Electrochim. Acta* **46** (2001) 2275.

[106] M.K. Carpenter, R.S. Conell, D.A. Corrigan, *Solar Energy Mater.* **16** (1987) 333.

[107] L. Xu, H. Zhang, E. Wang, A. Wu, Z. Li, *Mater. Chem. Phys*. **77** (2002) 384.

[108] I. Serebrennikova, V.I. Birss, *J. Electrochem. Soc*. **144** (1997) 566.

[109] L. Ottaviano, A. Pennis, F. Simone, *Surf. Interface Anal.* **36** (2004) 1335.

[110] J. Nagai, *Sol. Energy Mater. Sol. Cells* **31** (1993) 291.

[111] L. Ottaviano, A. Pennis, F. Simone, *Surf. Interf. Anal.* **36** (2004) 1335.

[112] M. Fantini, A. Gorenstein, *Sol. Energy Mater. Sol. Cells* **16** (1987) 487.

[113] A. Azens, L. Kullman, G. Vaivars, H. Nordborg and C.G. Granqvist, *Solid State Ionics* **113-115** (1998) 449.

[114] J. Scarminio, W. Estrada, A. Andersson, A. Gorenstein, F. Decker, *J. Electrochem. Soc*. **139** (1992) 1236.

[115] D. B. Chrisey, G. K. Hubler, *John Wiley & Sons* (1994).

[116] *http://en.wikipedia.org/wiki/Pulsed_laser_deposition* (Date accessed: 13 April 2010).

[117] F. Breech, L. Cross, *Appl. Spectrosc.* **16** (1962) 59.

[118] A. Al-Kahlout, S. Heusing, M. A. Aegerter, *J. Sol-Gel Sci. Techn.* **39** (2006) 195.

[119] A. Al-Kahlout, A. Pawlicka, M. A. Aegerter, *Sol. Energy Mater. Sol. Cells* **90** (2006) 3583.

[120] A. Al-Kahlout, *Ph.D. thesis*, Universität des Saarlandes, Germany (2006).

[121] A. Al-Kahlout, M. A. Aegerter, *Sol. Energy Mater. Sol. Cells* **91** (2007) 213.

[122] C. J. Brinker, A. J. Hurd, P. R. Schunk, G. C. Frye, C. S. Ashley, *J. Non-Cryst. Solids* **147** (1992) 424.

[123] *http://en.wikipedia.org/wiki/Dip-coating* (Date accessed: 13 April 2010).

[124] M.N. Rahaman, *Ceramic Processing. Boca Rato*n *CRC Press*. ISBN 0-8493-7285-2, (2007) 242.

[125] L.D. Landau, B.G. Levich, *Acta Physiochim*. **17** (1942) 42.

[126] L.L. Hench, J.K. West, *Chem. Rev.* **90(1)** (1990) 33.

Chapter II

Electrochromic properties of undoped and lithium-doped nickel oxide thin films prepared by Pulsed Laser Deposition (PLD)

1. Introduction; outline of our strategy

Many attempts have been made to apply nickel oxide based thin films with aqueous basic electrolytes as electrode for electrochromic devices [1-10]. According to previous research works, it was found that the addition of Mg, Y, Si, Ce, Al elements could enhance optical properties and durability of NiO based films [3,5,6,11-13]. Recently, A. Rougier et al. have reported better durability for PLD/NiO (PLD/NiO symbolizing NiO thin film deposited by Pulsed Laser Deposition) film by adding elements such as W, Ta, Co [14,15]. It is worth recalling that the mechanism involved in PLD-NiO thin films is a surface phenomenon related to the hydroxide/oxyhydroxide electrochemical reversible reaction due to an initial step associated with the chemical formation of the hydroxide active layer when dipping NiO thin films in KOH electrolyte (Fig. 1) [16].

Careful electrochemical study of NiO thin films, deposited by PLD, showed that their poor electrochemical durability was related to a self-discharge phenomenon associated with the dissolution of the oxidized phase as shown in Fig. 1 [16].

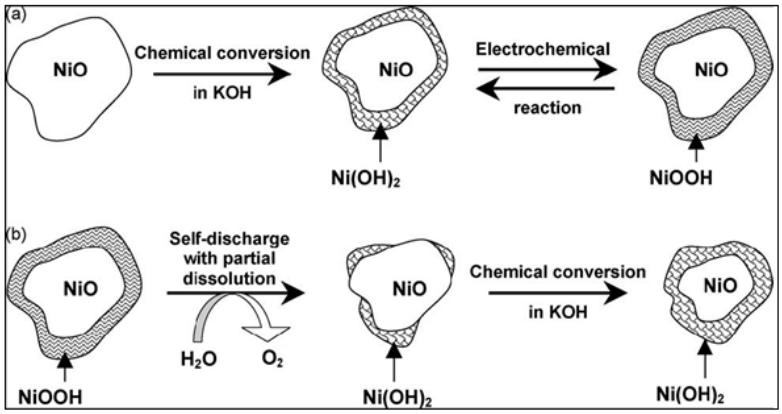

Fig. 1: Scheme of (a) oxidation process of nickel oxide (NiO) and (b) self-discharge phenomenon [16].

The dissolution phenomenon was reduced for the above quoted Ni-M-O thin films (M = W, Ta, Co, Mg, Al, Si, Ce, Y) due to the amorphization of the nickel oxide structure

[3,5,6,11,13,15]. Indeed, according to a previously reported 'electrochemical model' structural disorder inhibits phase transformation [17,18].

This chapter was aimed at investigating if an enhancement of the durability of NiO films could be similarly obtained by the addition of lithium. To our knowledge, lithiated nickel oxide thin films have never been tested in KOH electrolyte for electrochromism even though many research works on lithiated nickel oxide thin films tested in lithium based electrolyte were reported [3,4,19-25].

In the present study, Li-Ni-O thin films were grown from Li-Ni-O target by PLD at room temperature under 10^{-1} mbar oxygen pressure. The latter conditions were previously optimized for NiO based thin film [26]. As quoted above, we have characterized the electrochromic properties of lithiated NiO thin films in 1M KOH aqueous electrolyte for the first time. Physicochemical properties of the thin films were investigated using several tools such as transmission electron microscopy (TEM: *Philips-CM200, 200 kV*), field emission–scanning electron microscopy (FE-SEM: *JEOL JSM-6700F and TESCAN MIRA II LMH - CS microscopes*), X-ray diffraction (XRD: *Philips XRD X'PERT PRO 12 diffractometer with Cu Kα (λ=1.5418 Å)*), inductively coupled plasma (ICP: *Varian ICP-OES 700 series*). Herein, we will discuss the electrochromic properties of PLD/Li-Ni-O thin films in comparison with PLD/NiO ones, grown using the same conditions *(PLD: Lambda Physik, Compex 102, λ = 248 nm)*.

2. Targets of NiO and Li-Ni-O

2-1. NiO target

Stoichiometric $Ni^{II}O$ powder (green color) was pressed under a pressure of 200 kg/cm^{-1} with a typical hand pressing machine and annealed at 800 ^{o}C for 24 hrs under ambient atmosphere. The temperature was elevated by 1.5 ^{o}C per minute up to 800 ^{o}C. And

then the sample was cooled down naturally to room temperature. The surface of the resulting NiO target was smoothed with a piece of sandpaper. The target maintained its original green color after sintering at 800 °C. It indicates that the nickel ions remain stabilized as Ni^{2+}. The XRD pattern corresponds to the expected rock salt cubic structure of nickel oxide (S.G.: Fm-3m) with cell parameter of 4.17 Å (Fig. 2).

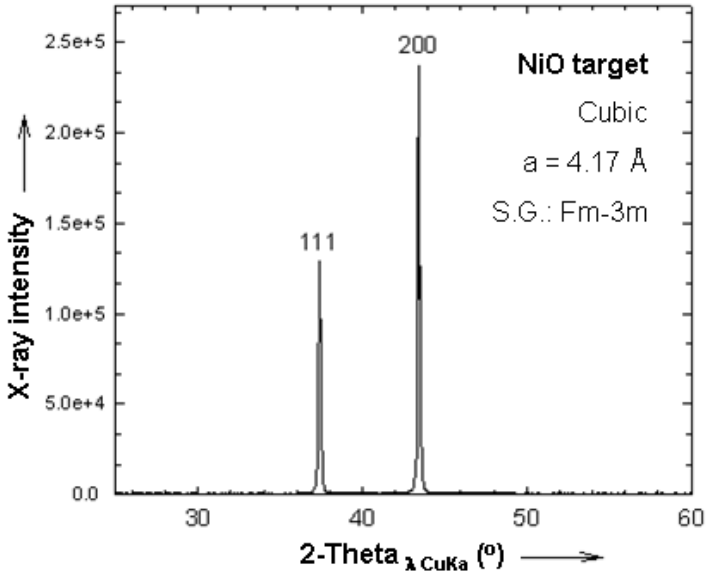

Fig. 2: XRD pattern of NiO target.

The density of the target of 4.43 (65 % of the theoretical density: 6.82 [27-29]) was deduced from its dimensions (0.432 cm thick and 0.910 cm radius measured with a digital vernier caliper) and its weight (4.98 g measured using an analytical balance). This bulk density was also confirmed from mercury displacement method using an AutoPore IIV 9500 mercury porosimeter.

2-2. Li-Ni-O target

Li-Ni-O targets were prepared from powder composition of $Li_{0.68}Ni_{1.32}O_2$ in air. Such composition was prepared by heating a mixture of 0.34 Li_2CO_3 *(+5 % of excess of Li_2CO_3 to compensate lithium loss during heating)* and 1.32 NiO (Fig. 3) [30,31] at 650 ^oC for 10 hrs in

air. The powder was ground, pelletized, and then sintered in the same conditions as for NiO pellet. The XRD pattern of the target corresponds to the rhombohedral structure of nominal $Li_{0.68}Ni_{1.32}O_2$ with the expected cell parameter of a = 2.91 Å and c = 14.23 Å (Fig. 3), (JCPDS 88-1605) [32].

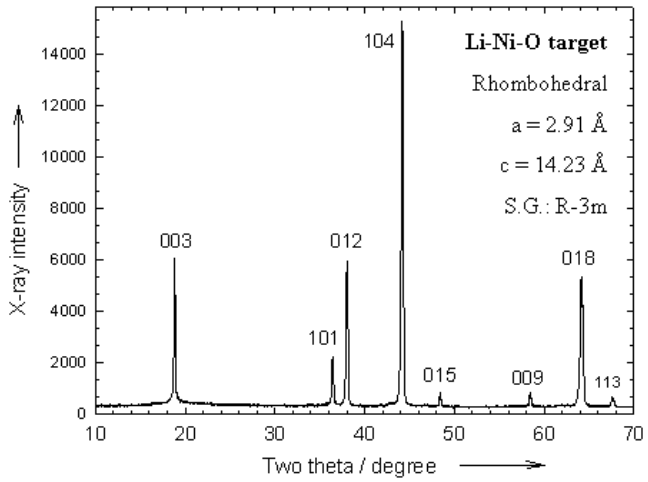

Fig. 3: XRD pattern of $Li_{0.68}Ni_{1.32}O_2$ target.

Li-Ni-O target is black (like the powder). This color accounts for the presence of Ni^{3+} as it could reasonably be expected from its composition: $Li_{0.68}Ni^{II}_{0.64}Ni^{III}_{0.68}O_2$. The density of Li-Ni-O target (0.421 cm thick, 0.895 cm radius, 4.83 g weight) is 4.56 (83 % of the theoretical density: 5.50 [33]). The higher target density observed for the Li-Ni-O target as compared to NiO one might be related to the lithium presence which favors grain percolation.

For sake of simplicity, the corresponding deposited thin films will be later on symbolized as Li-Ni-O.

3. Thin films

3-1. Preparation

The experimental conditions used to deposit the NiO and Li-Ni-O films are similar to those previously optimized by A. Rougier et al. for NiO-thin-film deposition by PLD

[14,16]. A KrF excimer laser beam (Lambda Physik, Compex 102, λ = 248 nm) with a laser fluency of 1- 2 J cm^{-2} was used for film deposition as illustrated in Fig. 4. The substrates (FTO/glass and glass) were firstly cleaned via sonication in ethanol, then washed with distilled water and finally dried with an air blow gun. The cleaned substrate was fixed on the holder of the PLD chamber with double sided tape. The surface of FTO/glass (1 x 2.5 cm^2) was partially covered by a scotch tape leaving approximately 1 x 1 cm^2. The target was fixed on the round shaped holder with silver paste.

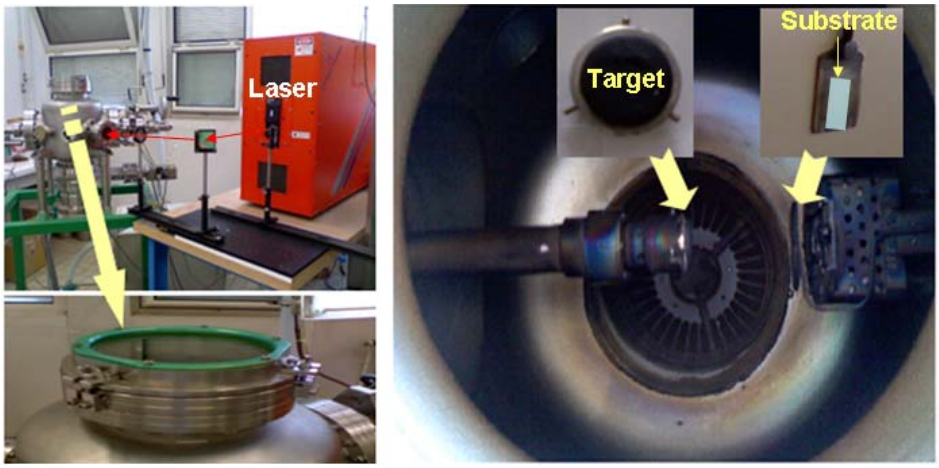

Fig. 4: Illustration of the Pulsed Laser Deposition (PLD) set up (LRCS-CNRS).

The distance between the substrate and target was fixed at 3.7 cm. This distance was determined based on the shape of the plasma plume. The base pressure in the chamber was in the order of 3.10^{-5} mbar. Afterwards oxygen was introduced so as to reach 10^{-1} mbar oxygen pressure in the chamber. The target was rotated while it was being pulsed by a KrF excimer laser beam (λ = 248 nm) at a repetition rate of 5 Hz leading to the film deposition on the substrate. The colors of plasma plume for the NiO and Li-Ni-O targets are blue and pink, respectively (Fig. 5). The shape of the plasma plume was not changed until the deposition was finished, accounting for a uniform deposition with time.

(a) NiO (b) Li-Ni-O

Fig. 5: Plasma plumes during deposition of (a) NiO and (b) Li-Ni-O thin films.

The deposition time was varied from 10 min to 2 hrs. As summarized in Table 1, the films deposited for 1 h and 2 hrs were intended for XRD, ICP, and density characterizations, respectively. The thinner films deposited for 10 min were intended for thickness measurement, surface morphology, and electrochemical and optical characterizations.

	Target			Film							
	Crystal symmetry and compositon	Space group	Density	Crystal symmetry and composition	Space group	Density	Substrate	Deposition duration (min)	Thickness (nm ± 5 %)	Transmittance (% at $T_{\lambda=650\ nm}$)	Purpose
NiO	Cubic NiO	Fm-3m	4.43	cubic NiO	Fm-3m	3.96	SnO_2:F (FTO)	10	~80	~98	SEM, AFM, Electrochemical and Optical measurements
				cubic NiO	Fm-3m	3.96	glass	60	~450	~30	XRD and TEM measurements
				cubic NiO	Fm-3m	3.96	glass	120	~900	< 10	Density measurements
Li-Ni-O	$Li_{0.68}Ni_{1.32}O_2$ Rhombohedral	R-3m	4.56	cubic $Li_{0.21}Ni_{0.79}O$	Fm-3m	4.00	SnO_2:F (FTO)	10	~80	~82	SEM, AFM, Electrochemical and Optical measurements
				cubic $Li_{0.21}Ni_{0.79}O$	Fm-3m	4.00	glass	60	~480	< 5	XRD and TEM measurements
				cubic $Li_{0.21}Ni_{0.79}O$	Fm-3m	4.00	glass	120	~960	< 3	ICP and density measurements

Table 1: Main characteristics of NiO and Li-Ni-O targets and corresponding thin films.

The FTO coated glass substrate was purchased from SOLEMS ($R_{\square}$ = 10 Ω for a 600 nm film thickness). The density of the films was measured using an ultra micro balance. The film composition was deduced by ICP for thickest one and assumed same for thinner ones due to the homogeneous plasma plume during deposition.

3-2. Structural, morphological characterizations, and chemical composition of NiO and Li-Ni-O thin films

3-2-a. Structural characterization

The XRD pattern of Li-Ni-O thin film is displayed in Fig. 6 in comparison with that of NiO thin film, both films being deposited onto glass substrates. Both XRD patterns show (111) preferred orientation of NiO cubic structure (S.G.: Fm-3m). It is known that $Li_xNi_{1-x}O$ with lithium ratio $x > 0.3$ shows hexagonal structure [34-39] whereas for $x < 0.3$ the cubic structure of nickel oxide is maintained [40-42]. It suggests that the lithium content is less than $x = 0.3$ in our $Li_xNi_{1-x}O$ films as it will be confirmed below.

Considering the decrease of intensity of (111) peak and its widening and also the appearance of (200) peak after lithium addition for Li-Ni-O thin film compared to NiO one, it becomes certain that the partial substitution of nickel by lithium in NiO not only decreases the (111) preferred orientation of NiO cubic structure but also creates structural disorder.

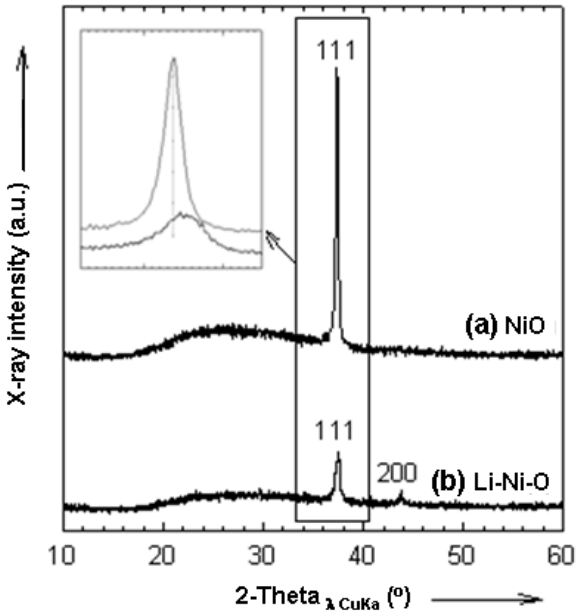

Fig. 6: XRD patterns of (a) NiO and (b) Li-Ni-O thin films.
Inset shows the magnification between 36.2 and 38.5 ° region.

The lattice parameters were estimated from the XRD patterns using a least square fitting analysis. They are reported in Table 2. The calculated cell parameter for NiO thin film is very close to that of stoichiometric bulk NiO (Table 2) as it could be reasonably expected, regarding the high transparency of the deposited thin film, $T_{\lambda=550nm}$ = 98 % (Table 1). A smaller cell parameter is observed for Li-Ni-O thin film (Table 2). It is known that $Li_xNi_{1-x}O$, in which the Li^+ ion occupies substitutional positions, has a smaller lattice parameter than NiO [28,29,43,44]. The cell parameter of 4.136 Å for Li-Ni-O thin film is in good agreement with the phase composition of $Li_{0.21}Ni_{0.79}O$ observed by Li et al. [44] and Antolini et al. (Table 2) [28,29].

Sample	*a* (Å)
Stoichiometric NiO [44]	4.173 (Z. Li et al.)
Our NiO film	4.171
$Li_{0.21}Ni_{0.79}O$ [28,29]	4.137 (E. Antolini et al.)
Our Li-Ni-O film	4.136

Table 2: Lattice parameters of NiO and Li-Ni-O thin films.

Selected area electron diffraction (SAED) was carried out to cross confirm the XRD data. The thin films deposited on glass substrates were removed by scratching the surface for measurements. The SAED patterns shown in Fig. 7 indicate that the NiO and Li-Ni-O thin films crystallize in the bunsenite nickel oxide phase (JCPDS-No 71-1179) of cubic setting [14,45,46]. The distances between Ni atom layers, shown in Fig. 8, were deduced from the lattice fringes obtained from TEM measurements. For (111) and (200) orientations, the distances between Ni atom layers are 0.243 and 0.207 nm for NiO thin film and 0.237 and 0.202 nm for Li-Ni-O thin film. The deduced cell parameters 4.171 Å for NiO and 4.136 Å for Li-Ni-O are close to those reported in the literature (Table 2).

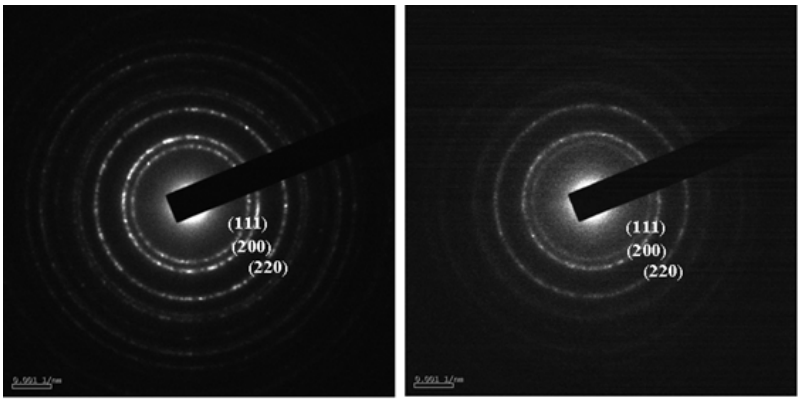

(a) NiO (b) Li-Ni-O

Fig. 7: SAED patterns of (a) PLD/NiO and (b) PLD/Li-Ni-O thin films deposited at room temperature under 10^{-1} mbar of oxygen.

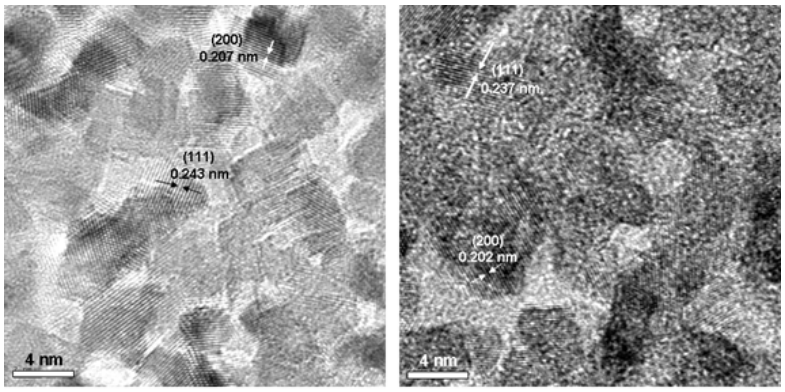

(a) NiO (b) Li-Ni-O

Fig. 8: Lattice fringes of (a) PLD/NiO and (b) PLD/Li-Ni-O thin films deposited at room temperature under 10^{-1} mbar of oxygen

As illustrated in Fig. 7 and 8, less clear SAED pattern and TEM image are observed for Li-Ni-O thin film. It suggests a more disordered phase with lithium addition in agreement with XRD data (Fig. 6).

3-2-b. Morphological characterization

Fig. 9 and 10 show FE-SEM and AFM images of the thin films deposited for 10 min on FTO substrates, respectively. The thin films exhibit different morphologies: indeed, homogeneous surface is observed for NiO thin film as compared to Li-Ni-O one (Fig. 9). This discrepancy explains the larger roughness of the Li-Ni-O thin film determined by

atomic force microscopy (Fig. 10 and 11), resulting in: $R_{a(NiO)} \sim 0.4$ nm < $R_{a(Li\text{-}Ni\text{-}O)} \sim 5.0$ nm.

The thicknesses of the NiO and Li-Ni-O thin films, deduced from Fig. 9 are quite similar (~ 80 nm).

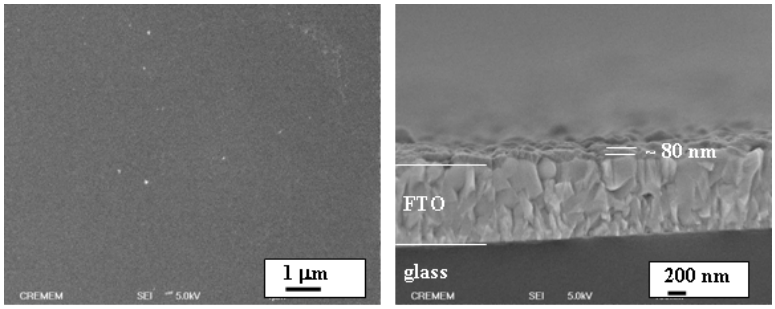

(a) NiO

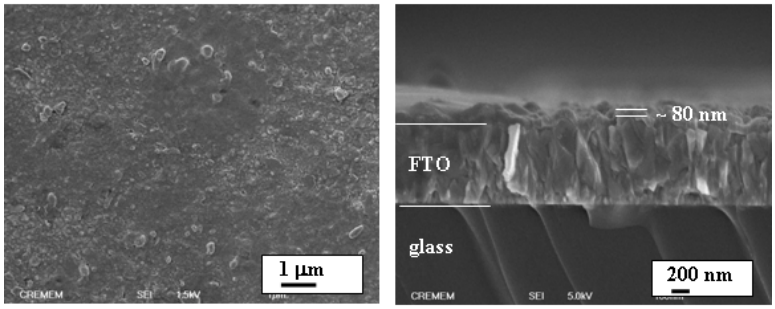

(b) Li-Ni-O

Fig. 9: FE-SEM images of surface and cross section for (a) PLD/NiO and (b) PLD/Li-Ni-O thin films deposited at room temperature under 10^{-1} mbar of oxygen.

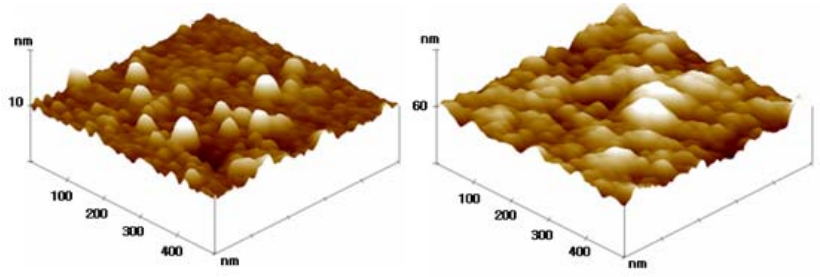

(a) NiO (b) Li-Ni-O

Fig. 10: AFM images for (a) PLD/NiO and (b) PLD/Li-Ni-O thin films deposited at room temperature under 10^{-1} mbar of oxygen. Note the different z-axis scales.

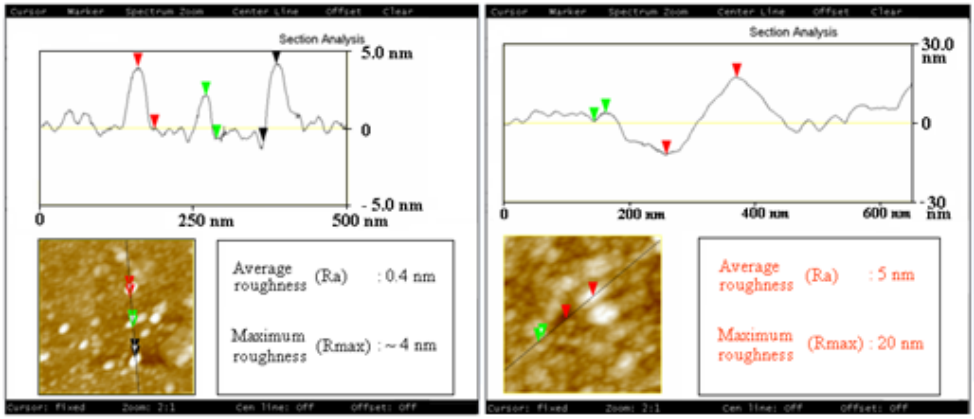

(a) NiO (b) Li-Ni-O

Fig. 11: Section analyses of AFM images for (a) PLD/NiO and (b) PLD/Li-Ni-O thin films deposited at room temperature under 10^{-1} mbar of oxygen allowing the assessment of the thin film roughness.

3-2-c. Chemical composition

The composition of Li-Ni-O film was determined by ICP measurements. The Li-Ni-O films deposited on glass substrates were removed by scratching the surface and then dissolved in diluted hydrochloric acid for measurements. It was found that chemical formula of the deposited thin film is ~ $Li_{0.21}Ni_{0.79}O$ (± 0.01) and is in good agreement with XRD prediction. The lower content of lithium in the thin film compared to that of target (Table 1) can be explained by the high volatility of lithium during film deposition [47,48].

3-3. Wetting characteristics of the film surfaces estimated from contact angle measurements

The contact angle measurement is a well known method to determine the wetting characteristics of film surfaces [49]. The contact angle measurements were performed, at Institut des Sciences Moléculaires (ISM) under the guidance of Prof. Thierry Toupance, using a Krüss DAS 100 apparatus (Drop shap system DAS 10 Mk2) at 20 °C in static mode using H_2O solvent (6 µl). This measurement may be helpful here since the electrochemical tests of the thin films will be performed in aqueous media (§ 2.4); the

wettability of the deposited material and of the substrate should, therefore, be considered. The highest contact angle (107.3 °) value is observed for NiO thin film as compared to FTO (70.1 °) and Li-Ni-O (34.4 °) thin films (Fig. 12). This clearly indicates that NiO thin film has a less hydrophilic character than FTO and Li-Ni-O thin films, the latter film showing a strong hydrophilic character. It is worth reminding that a contact angle lower than 20 ° stands for superhydrophilic character, in between 20 to 90 ° for hydrophilic character, and above 90 ° for hydrophobic character.

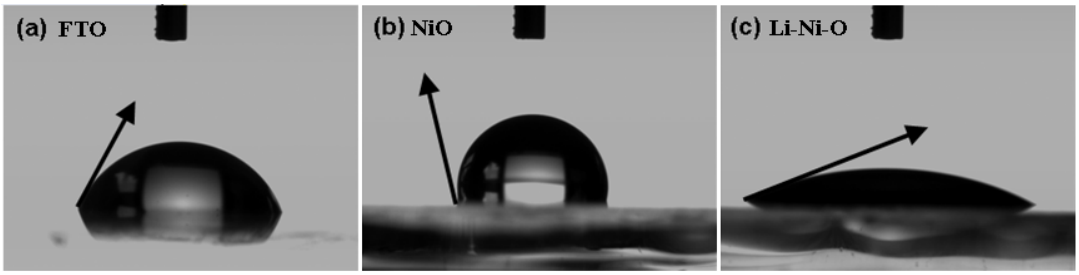

Fig. 12: Contact angles obtained with H_2O solvent on (a) glass/FTO substrate, (b) glass/FTO/PLD-NiO thin film, and (c) glass/FTO/PLD-Li-Ni-O thin film. The PLD thin films were deposited at room temperature under 10^{-1} mbar of oxygen. The accuracy is ± 0.05 °.
(a Krüss DAS 100 apparatus (Drop-shaped system DAS 10 Mk2) was employed to measure contact angles at 20 °C in static mode using H_2O solvent (6 µl). The results correspond to the mean value of at least three measurements.)

3-4. Electrochromic properties of NiO and Li-Ni-O thin films

The electrochemical and optical measurements were performed on the ~ 80 nm-thin-films deposited on FTO substrates.

3-4-a. Electrochemical measurements

Cyclic voltammograms (CVs) and chronoamperometry (CA) were recorded within the -0.10 mV - 0.58 mV potential window versus Hg/HgO. The CVs measured at a scan rate of 10 mV / s in 1M KOH electrolyte after 2, 100, and 1000 cycles are compared in

Fig.13. The appearance of a broad area in the 0.00 V – 0.35 V for the 2nd cycled CV curves of both thin films illustrates a pseudo-capacitive behavior indicating that surface reactions are involved [26]. At higher voltages, redox peaks become clearly visible for NiO thin films whereas a very broad answer is observed for Li-Ni-O thin films, probably due to higher disordered structure. At this early state of cycling, reversible coloration bleaching process is already observed. As shown in Fig. 13, from 2nd to 100th cycle the anodic peaks shift to higher potentials while the cathodic peaks shift to lower potentials in accordance with an increase in polarization. From 100th to 1000th cycle, both anodic and cathodic peaks are shifted to higher potentials as a signature of an overall oxidation of the material (Fig. 13). This point will be discussed below.

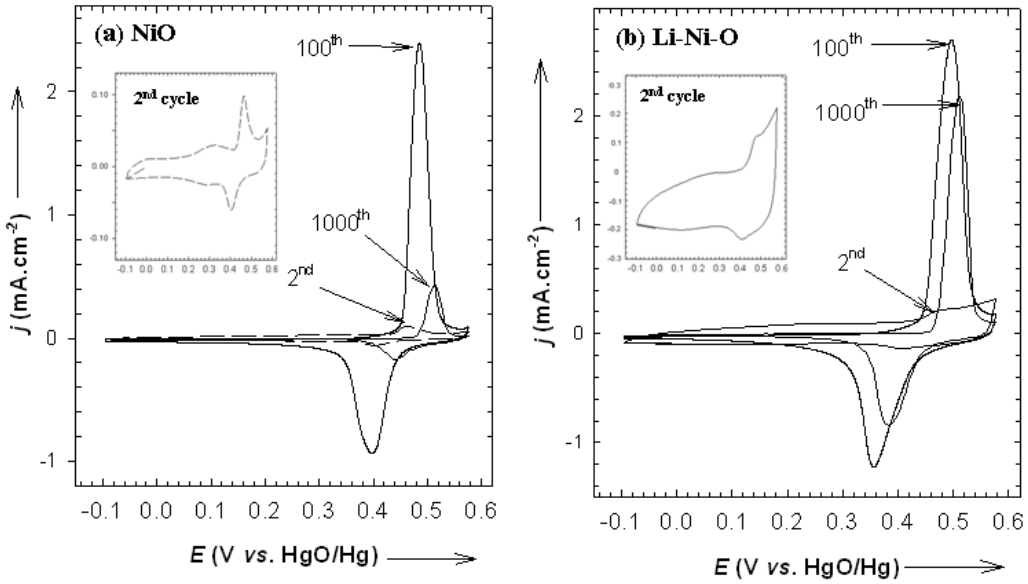

Fig. 13: Cyclic voltammograms of (a) NiO thin film and (b) Li-Ni-O thin film after 2nd, 100th and 1000th cycles. Three-electrode-cell configuration consisting of a working electrode (NiO or Li-Ni-O thin films), a counter electrode (platinum foil), and a reference electrode (Hg/HgO/1M KOH) was employed. All the measurements were carried out at the scan rate of 10 mV / s in 1M KOH electrolyte between -0.10 V and 0.58 V. (Inset figures indicate the magnified CV curve of the 2nd cycle

Fig. 14a shows the evolution of the coulombic capacity of the NiO and Li-Ni-O thin films upon cycling. The Li-Ni-O thin film clearly exhibits higher capacity than that of NiO one, very likely due to its more disordered structure in agreement with literature [17,18].

The cycling life of the thin films follows the previously reported three-step process involving an activation period, a steady state, and a degradation period [45,50]. The activation period occurs from the initial cycle to ~ 100^{th} cycle. It corresponds to the gradual participation of the bulk of the films in the electrochemical process. The steady state lasts only a few cycles (Fig. 14a). A simple calculation by using coulombic capacities, experimental densities, film surface and thickness allowed us to estimate the maximum percentage of Ni ions which contributes to the coloration/bleaching reactions. It was found that ~ 25 % and ~ 30 % of the total nickel atoms participated in the EC reactions for NiO and Li-Ni-O thin films, respectively [51].

Beyond 100^{th} cycle the capacity decreases continuously. However the decrease is much less pronounced for Li-Ni-O thin film. After 1000 cycles, Li-Ni-O thin films maintained 61 % of their initial coulombic capacity whereas it is only of 18 % for NiO thin film (Fig. 14b). Related to this result, cross section images obtained from FE-SEM measurements show a more pronounced peeling-off for NiO thin film as compared to Li-Ni-O thin film after 1000 cycles (Fig. 15a). Therefore, we suggest that the decrease of the capacity is also correlated to the progressive loss of mechanical adhesion of the thin films from the FTO substrates, which is more pronounced for NiO layer. It can be reasonably assumed that there is a relationship between mechanical adhesion and wetting property of the NiO based thin films (Fig. 12 ⇒ higher hydrophilic character for Li-Ni-O thin films). In addition, the formula of the cycled film deduced from ICP can be expressed as ~ $Li_{0.19}Ni_{0.81}O$.

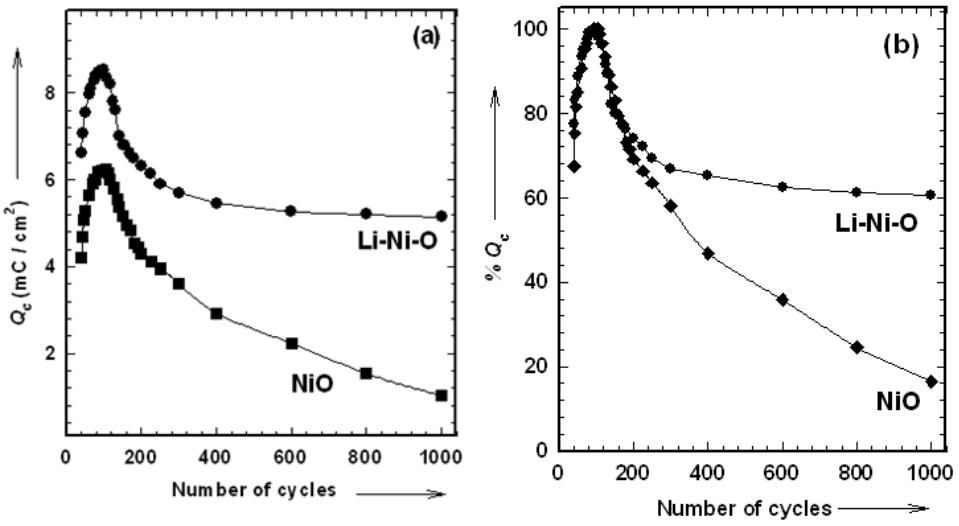

Fig. 14: (a) Coulombic capacity and (b) % coulombic capacity of NiO (Solid square) and Li-Ni-O (Solid circle) thin films upon cycling up to 1000 cycles. The electrochemical test was carried out in 1M KOH electrolyte with three-electrode-cell configuration consisting of a working electrode (NiO or Li-Ni-O thin films), a counter electrode (platinum foil), and a reference electrode (Hg/HgO/1M KOH).

The coulombic capacity was deduced based on cathodic part of chronoamperometry peaks in order to exclude the influence of the oxygen evolution. The applied voltages were -0.10 V and 0.58 V during 30 seconds for cathodic and anodic parts, respectively. Cyclovoltammetry was also performed every 100 cycles.

The FE-SEM images of the cycled film thickness and surface are shown in Fig. 15, respectively. An increase in film thickness from 80 to 120 nm is observed after cycling (see Fig. 9 and 15a), probably due to the formation of hydrated phases. As shown in Fig. 15b, the surfaces of the cycled films exhibit large agglomerates separated by some voids.

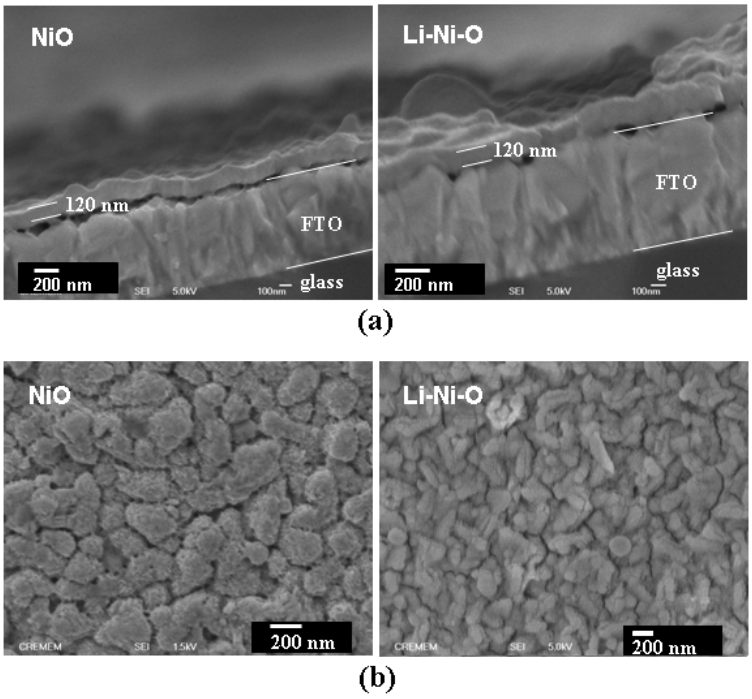

Fig. 15: (a) FE-SEM cross section and FE-SEM images of PLD/NiO and (b) PLD/Li-Ni-O thin films deposited at room temperature under 10^{-1} mbar oxygen pressure showing peeling off after 1000th cycle

3-4-b. Optical measurement

Optical properties of the thin films were measured before and after cycling (Fig. 16). The lower transmittance of the as-prepared Li-Ni-O thin films ($T_{\lambda=550nm}$ ~ 82 %) as compared to the one of NiO ($T_{\lambda=550nm}$ ~ 98 %) is associated with a brownish color due to the presence of trivalent nickel ions in Li-Ni-O thin film according to its $Li^{+}_{0.21}Ni^{2+}_{0.58}Ni^{3+}_{0.21}O$ formula. One deduces the following contrast ratios at 550 nm, expressed as ratio between the transmittance in the bleached state and the transmittance in the colored state:

NiO : 91/63 = 1.44 (100th cycle) // 71/52 = 1.36 (1000th cycle)

Li-Ni-O : 73/37 = 1.97 (100th cycle) // 50/18 = 2.77 (1000th cycle)

A higher contrast ratio accounting for improved electrochromic performances is observed for Li-Ni-O thin film as compared to NiO one.

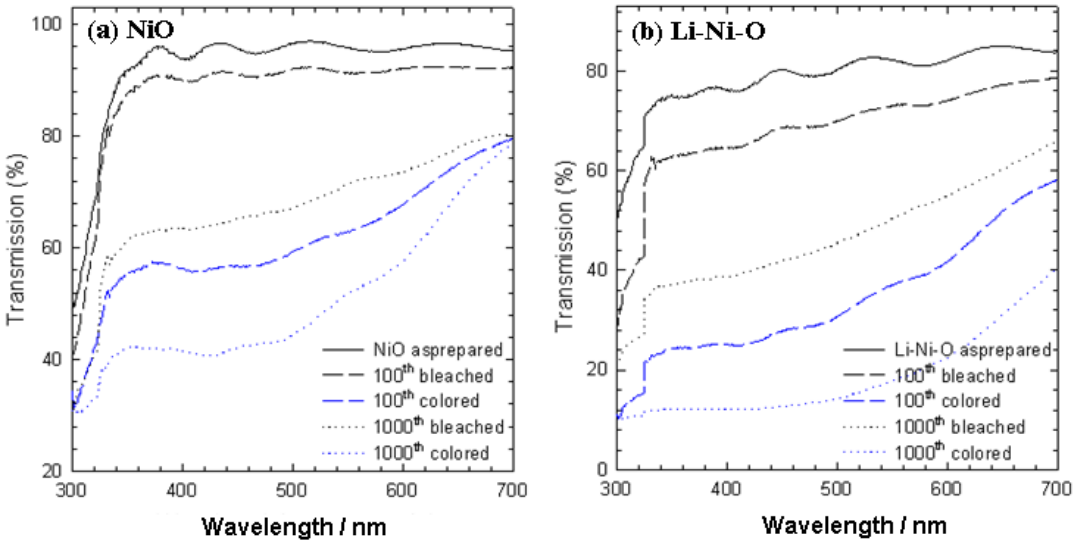

Fig. 16: The value of transmittance (%) of (a) NiO and (b) Li-Ni-O thin films after 100 and 1000 cycles. All transmittance values were measured at 550 nm. The blue curves indicate colored state.

Fig. 17 compares the transmittance between as-deposited and cycled thin films in their bleached states. It clearly shows irreversibility for both films, which is associated with remaining brownish color. This phenomenon is more pronounced for Li-Ni-O thin films. At the present time, the reason for this higher irreversibility is not clearly understood.

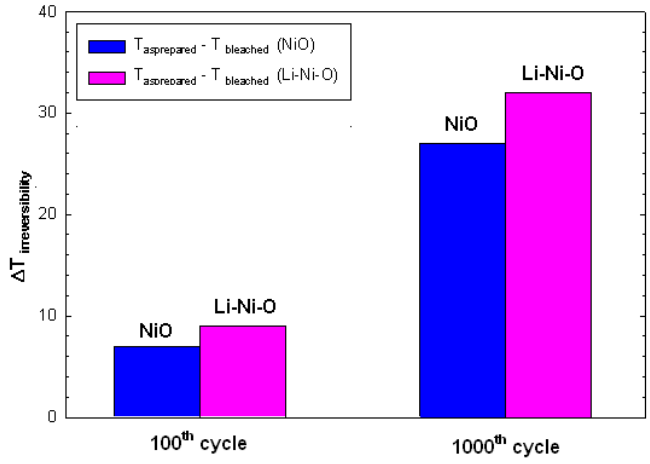

Fig. 17: ΔT value of NiO and Li-Ni-O thin films at 100th and 1000th cycle. All the measurements were carried out using UV-Visible spectrometer between 300 nm and 700 nm.

4. Conclusion

In the present work, cubic structured NiO and $Li_{0.21}Ni_{0.79}O$ (Li-Ni-O) thin films were successfully deposited by the Pulsed Laser Deposition method. From structural analyses, it was found that lithium doping to NiO led to a structural disorder. In agreement with literature [17,18], it is believed that this structural disorder is responsible for the higher coulombic capacity of Li-Ni-O thin films. Simultaneously, Li-Ni-O thin films show better cycling life as a result of stronger mechanical adhesion on FTO substrate (i.e. higer resistance to peeling off). However, the persistence of a brownish coloration upon cycling indicates a more complex mechanism that needs to be further clarified.

In chapter III, another solution dealing with preparation and characterization of composite TiO_2/NiO thin films will be investigated in order to stabilize the electrochromic durability of NiO thin films.

5. References

[1] A. Azens, G.G. Granqvist, *J. Appl. Electrochem.* **7** (2003) 64.

[2] F. Michalak, K. von Rottkay, T. Richardson, J. Slack, M. Rubin, *Electrochim. Acta* **44** (1999) 3085.

[3] E. Avendaño, A. Azens, G.A. Niklasson, C.G. Granqvist, *Sol. Energy Mater. Sol. Cells* **84** (2004) 337.

[4] S.-J. Wen, J. Kerr, M. Rubin, J. Slack, K. von Rottkay, *Energy Mater. Sol. Cells* **56** (1999) 299.

[5] C.G. Granqvist, E. Avendaño, A. Azens, *Thin Solid Films* **442** (2003) 201.

[6] M. Martini, G.E.S. Brito, M.C.A. Fantini, A.F. Craievich, A. Gorenstein, *Electrochim. Acta* **46** (2001) 2275.

[7] *http://www.econtrol-glas.de/* (Date accessed: 13 April 2010).

[8] *http://www.sage-ec.com/* (Date accessed: 13 April 2010).

[9] M. Wigginton, *Glass in Architecture, Phaidon,* London, 1966.

[10] A. Campagno, *Intelligente Galsfassaden/Intelligent Galss FaÇades, 4th Edition*, birkhäuser, Basel, 1999.

[11] X. Lou, X. Zhao, J. Feng, X. Zhou, *Prog. Organic Coatings* **64** (2009) 300.

[12] R.M. Bendert, D.A. Corrigan, *J. Electrochem. Soc.* **136** (1989) 1369.

[13] D.A. Corrigan, R.M. Bendert, *J. Electrochem. Soc.* **136** (1989) 723.

[14] N. Penin, A. Rougier, L. Laffont, P. Poizot, J.-M. Tarascon, *Sol. Energy Mater. Sol. Cells* **90** (2006) 422.

[15] Y. Makimura, A. Rougier, J.-M. Tarascon, *Appl. Surf. Sci.* **252** (2006) 4593.

[16] I. Bouessay, A. Rougier, P. Poizot, J. Moscovici, A. Michalowicz, J.-M. Tarascon, *Electrochim. Acta* **50** (2005) 3737.

[17] N. Treuil, C. Labrugère, M. Menetrier, J. Portier, G. Campet , A. Deshayes, J.-C. Frison, S.-J. Hwang, S.-W. Song J.-H. Choy, *J. Phys. Chem. B* **103** (1999) 2100.

[18] J.-H. Choy, Y.-I. Kim, G. Campet , J. Portier, P. V. Huong, *J. Solid State Chem.* **142**, (1999) 368.

[19] M. Rubin, S.-J. Wen, T. Richardson, J. Kerr, K. von Rottkay, J. Slack, *Sol. Energy Mater. Sol. Cells* **54** (1998) 59.

[20] F. Michalak, K. von Rottkay, T. Richardson, J. Slack, M. Rubin, *Electrochim. Acta* **44** (1999) 3085.

[21] A. Urbano, F.F. Ferreira, S.C. deCastro, R. Landers, M.C.A. Fantini, A. Gorenstein, *Electrochim. Acta* **46** (2001) 2269.

[22] M. Rubin, K. von Rottkay, S.J. Wen, N. Ozer, J. Slack, *Sol. Energy Mater. Sol. Cells* **54** (1998) 49.

[23] S. Passerini, B. Scrosati, A. Gorenstein, *J. Electrochem. Soc.* **137** (1990) 3297.

[24] Y.-I. Kim, B.-W. Kim, J.-H. Choy, G. Campet, N.-G. Park, J. Portier, B. Morel, *J. Korean Chem. Soc.* **41** (1997) 11.

[25] J.-C. Giron, *Ph.D. Thesis, l'Universite Paris*, 1994.

[26] I. Bouessay, A. Rougier, B. Beaudoin, J.-B. Leriche, *Appl. Surf. Sci.* **186** (2002) 490.

[27] E. Antolini, M. Ferretti, *Mater. Lett.* **30** (1997) 59.

[28] E. Antolini, *Phys. Stat. Sol.* **173** (1999) 357.

[29] E. Antolini, L. Giorgi, *Ceram. Int.* **24** (1998) 117.

[30] G. Perentz, E. Horopanitis, I. Samaras, S. Kokku, L. Papadimitriou, *J. Solid State Electrochem.* **8** (2003) 51.

[31] S. Linderoth, A. Smith, N. Bonanos, A. Hagen, L. Mikkelsen, K. Kammer, D. Lybye, P.V. Hendriksen, F.W. Poulsen, M. Mogensen, W.G. Wang, *Proceedings of the 26th Risø Interernational Symposium on Materials Science, Denmark* (2005).

[32] J. Morales, C. Perez-Vicente, J.L. Tirado, *Mater. Res. Bull.* **25** (1990) 623.

[33] JCPDS-No 88 1605-*International centre for diffraction data*.

[34] D. Rahmer, S. Machill, H. Schlröb, K. Siury, M. Kloss, W. Plieth, *J. Solid State Electrochem.* **2** (1998) 78.

[35] A. Rougier, A.V. Chadwick, C. Delmas, *Nucl. Instrum. Methods Phys. Res. B* **97** (1995) 75.

[36] A. Rougier, C. Delmas, A.V. Chadwick, *Solid State Commun.* **94** (1995) 123.

[37] J.N. Reimers, W. Li, J.R. Dahn, *Phys. Rev. B* **47** (1993) 8486.

[38] J.R. Dahn, U. Von Sacken, C.A. Michal, *Solid State Ionics* **44** (1990) 87.

[39] R. Stoyanova, E. Zhecheva, S. Angelov, *Solid State Ionics* **59** (1993) 17.

[40] J. B. Goodenough, D. G. Wickham, W. J. Croft, *J. Phys. Chem. Solids* **5** (1958) 107.

[41] J. B. Goodenough, D. G. Wickham, W. J. Croft, *Physics* **29** (1958) 382.

[42] E. Antolini, *Physica Status Solidi (a)* **173** (1999) 357.

[43] J. Van Elp, H. Eskes, P. Kuiper and G.A. Sawatzky, *Phys. Rev. B* **45** (1992) 1612.

[44] Z. Li, C. Wang, X. Ma, L. Yuan, J. Sun, *Mater. Chem. Phys*. **91** (2005) 36.

[45] I. Bouessay, A. Rougier, J.-M. Tarascon, *J. Electrochem. Soc.* **151** (2004) H145.

[46] H. Bode, K. Dehmelt, J. Witte, *Electrochim. Acta* **11** (1996) 1079.

[47] J. López-Iturbe, M.A. Camacho-López, L. Escobar-Alarcón, E. Camps, *Supericies y Vacío* **18(4)** (2005) 27.

[48] F. K. Shokoohi, J. M. Tarascon, B. J. Wilkens, *Appl. Phys. Lett.* **59** (1991) 1260.

[49] C. Y. Kuan, M. H. Hon, J. M. Chou, I. C. Leu, *J. Electrochem. Soc.* **156** (2009) J32.

[50] F. Decker, S. Passerini, R. Pileggi, B. Scrosati, *Electrochim. Acta* **37** (1992) 1033.

[51] Y. Sato, S. Tamura, K. Murai, *The Electrochem. Soc. Proceedings* **96** (1996) 64.

Chapter III

Effect of Zn addition on the physicochemical properties of electrochromic TiO_2/NiO thin films

1. Introduction; outline of our strategy

As quoted earlier in Chapter II, NiO thin films show rather poor electrochromic performances in basic electrolyte upon cycling [1-8]. Based on the doping idea of NiO [8-15], we established in chapter II that Li substituted NiO films, of $Li_{0.21}Ni_{0.79}O$ composition, showed enhanced durability upon cycling in aqueous KOH electrolyte compared to pure NiO thin films. However, despite this improvement, the $Li_{0.21}Ni_{0.79}O$ films exhibited traces of peeling off after 1000 cycles associated with a decrease of the electrochromic performances. Therefore, there still remains a challenging issue to increase the electrochemical durability of NiO based electrodes in aqueous KOH electrolytes.

There were a few attempts to protect NiO nanoparticles from direct contact with the aqueous KOH electrolyte. The most efficient one consisted of embedding the NiO nanoparticles into a TiO_2 matrix [16-21]. In some cases, the corresponding TiO_2/NiO films have been prepared with sol of $NiCl_2$ and Ti(IV)butoxide in 1-butanol [16], or by mixing nickel nitrate, nickel acetate or, nickel chloride and Ti(IV)alkoxide [17]. These works presented detailed studies of the thermal behavior of xerogels, of the phase structure and morphology of the layers before and after coloration tested in KOH electrolyte. Lately, Al-Kahlout *et al.* have also reported TiO_2/NiO composite films, deposited on FTO substrates in a glove box, using nickel acetate and titanium isopropoxide [18-21]. Their composite films, based on 25 % of TiO_2 and 75 % of NiO (in molar %), showed enhanced electrochromic durability upon cycling in aqueous 1M KOH electrolyte, compared to that of NiO electrodes. However, in spite of this enhancement, Al-Kahlout *et al.* observed a strong decrease of the performances beyond 6000 cycles. We will show below that this decay probably originates from the peeling off of the films from the FTO substrates.

In the present work, in order to enhance even more the cyclability of the composite TiO_2/NiO thin films, we have considered our results in chapter II related to the wettability

of the NiO-based films and their corresponding mechanical adhesion on the FTO substrates. These results led us to adopt the strategy, presented hereafter. We have employed a concept which uses Zn^{2+} as a dopant for TiO_2 in TiO_2/NiO: the objective was to enhance the wettability and, therefore, the mechanical adhesion of the TiO_2 matrix on the FTO substrate by doping TiO_2 with Zn^{2+}, thereby creating neutral oxygen vacancies, □, in the $Ti^{4+}_{1-x}Zn^{2+}_{x}O^{2-}_{2-x}\square_x$ formula. We have, indeed, reasonably considered that the presence of the neutral anionic vacancies, $\square_x$, in $Ti^{4+}_{1-x}Zn^{2+}_{x}O^{2-}_{2-x}\square_x$, would reinforce the hydrophilic character of the film via coulombic attraction between Ti^{4+}-□-Zn^{2+} entities and H_2O according to: Ti^{4+}-□-Zn^{2+} + $H_2O^{\delta-}$ → 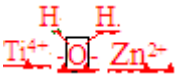 . If it is the case, the electrochemical durability of the composite $Ti^{4+}_{1-x}Zn^{2+}_{x}O^{2-}_{2-x}\square_x$ /NiO films in aqueous 1M KOH electrolyte would be well extended beyond the 6000 cycles reported by Al-Kahlout *et al.* for their TiO_2/NiO thin films [18-21].

Therefore, herein in order to check the validity of this assumption, we will discuss the effect of Zn doping to TiO_2 matrix on the electrochromic properties of TiO_2/NiO films prepared by a dip-coating method from precursor coating solutions presented in the §.2 of this chapter. The following compositions were investigated:

- Composition 1: TiO_2/NiO (20 % of TiO_2 and 80 % of NiO (molar %)).
  (We selected this composition because we found that it showed superior electrochromic contrast ($T_{bleached}/T_{colored}$ = 2.32 (550 nm, 1000th cycle)) compared to the thin films based on 25 % of TiO_2 and 75 % of NiO reported by Al-Kahlout et al. ($T_{bleached}/T_{colored}$ = ~ 2.25 (550 nm, 1000th cycle)) [18-21].)
- Composition 2: $Ti^{4+}_{0.9}Zn^{2+}_{0.1}O^{2-}_{1.9}\square_{0.1}$ /NiO (20 % of $Ti^{4+}_{0.9}Zn^{2+}_{0.1}O^{2-}_{1.9}\square_{0.1}$ and 80 % of NiO (molar %))
- Composition 3*: '$Ti^{4+}_{0.85}Zn^{2+}_{0.15}O^{2-}_{1.85}\square_{0.15}$' /NiO (20 % of '$Ti^{4+}_{0.085}Zn^{2+}_{0.15}O^{2-}_{1.85}\square_{0.15}$' and 80 % of NiO (molar %)).
  *(*We will show in fact that we could not reach the composition $Ti^{4+}_{0.085}Zn^{2+}_{0.15}O^{2-}_{1.85}\square_{0.15}$, but that allowed us to estimate the solubility limit of ZnO into TiO_2 observed under our experimental conditions.)*

2. Precursor coating solutions

2-1. Preparation

The preparation process of the precursor coating solutions, to synthesize the films of the compositions 1-3 listed above, under ambient atmosphere, is illustrated in Fig. 1. Firstly titanium *iso*-propoxide was added to ethanol. And then zinc acetate dihydrate, $Zn(CH_3COO)_2{\cdot}2H_2O$, was added (the order could be reversed). Lastly 0.05 mol nickel acetate tetra hydrate, $Ni(CH_3COO)_2{\cdot}4H_2O$, was added to the solution where zinc acetate dihydrate and titanium *iso*-propoxide (0.0125 total mol) were already dissolved in 100 cm^3 of ethanol. Let us call "titanium *iso*-propoxide" as "TnP" from now on.

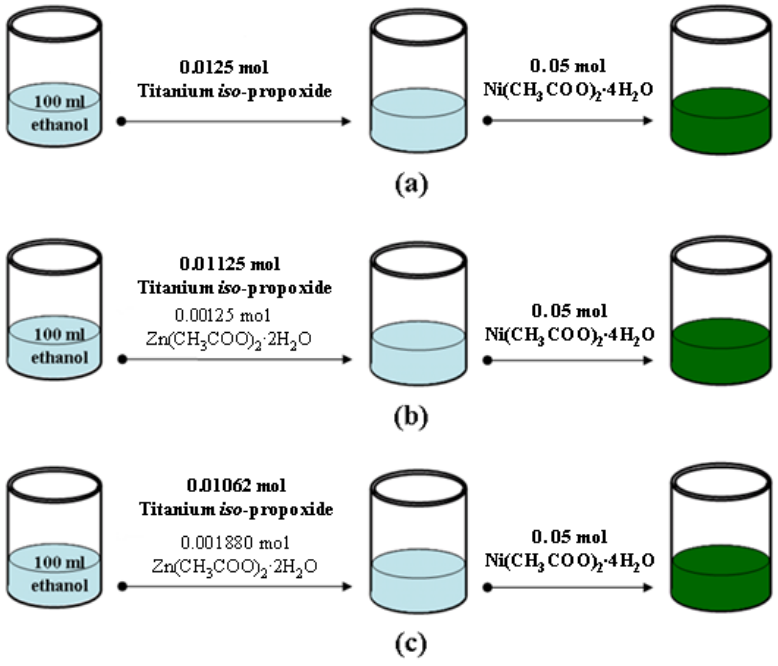

Fig. 1: Illustration of the preparation of the precursor coating solutions for: (a) composition 1 (TiO_2/NiO (20 % of TiO_2 and 80 % of NiO (molar %)), (b) composition 2 ($Ti^{4+}_{0.9}Zn^{2+}_{0.1}O^{2-}_{1.9}\square_{0.1}$ /NiO (20 % of $Ti^{4+}_{0.9}Zn^{2+}_{0.1}O^{2-}_{1.9}\square_{0.1}$ and 80 % of NiO (molar %)), and (c) composition 3 ('$Ti^{4+}_{0.85}Zn^{2+}_{0.15}O^{2-}_{1.85}\square_{0.15}$' /NiO (20 % of '$Ti^{4+}_{0.085}Zn^{2+}_{0.15}O^{2-}_{1.85}\square_{0.15}$' and 80 % of NiO (molar %)).

2-2. Effect of Zn addition on the delayed hydrolysis of titanium *iso*-propoxide (TnP)

We have firstly aged, under ambient atmosphere, a solution containing only 0.0125 mol of TnP in 100 ml of ethanol and confirmed a fast hydrolysis of TnP in 5 min (Fig. 2a). When TnP, $Ti[OCH(CH_3)_2]_4$, and Zn acetate dihydrate, Zn $(CH_3COO)_2 \cdot 2H_2O$ were successively added to 100 ml of ethanol (containing total 0.0125 mol with 10 mol % of Zn over Ti), the solution maintained its transparency even after 24 hrs with no trace of hydrolysis of TnP (Fig. 2b). This remarkable delayed hydrolysis of TnP allowed us to carry out advantageously the coating processes of our $Ti_{1-x}Zn_xO_{2-x}$/NiO films under ambient atmosphere while the inert atmosphere of a glove box was needed by Al-Kahlout *et al.* [18-20] for the preparation of their TiO_2/NiO thin films.

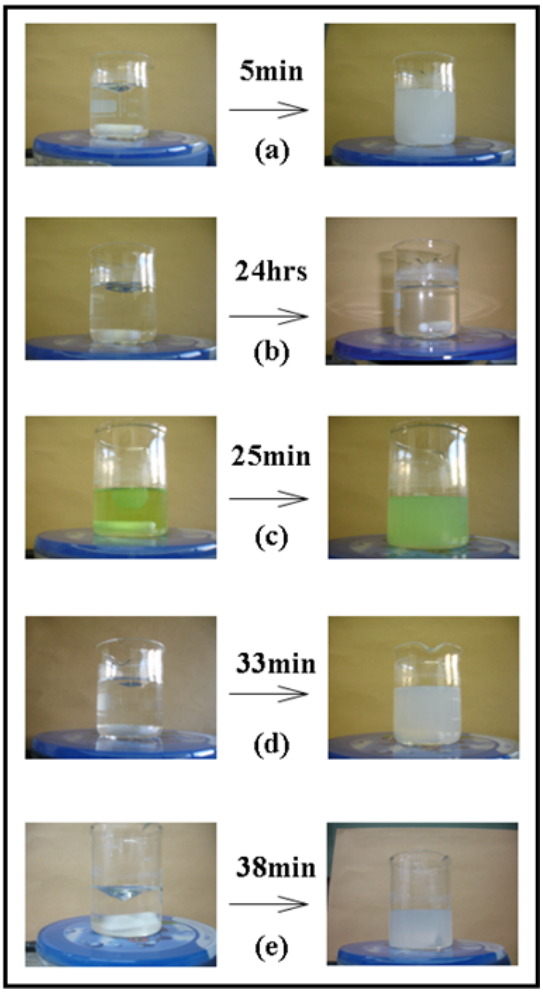

Fig. 2: Ethanol based coating solution containing (a) TnP, (b) TnP with Zn acetate, (c) TnP with Ni acetate, (d) TnP with Zn chloride, and (e) TnP with Mg acetate. (Except solution a, all other solutions contain 90 mol % of TnP and 10 mol % of other compound. All solutions consist of 0.0125 total mol. dissolved in 100ml of ethanol.)

In order to check if mainly Zn acetate would be the driving force of this delay, other compounds were considered (Fig. 2c, d, and e). When Ni or Mg acetate were added to the TnP in ethanol solution, hydrolysis is slightly postponed since it occurred in around 30 min (Fig. 2c and 2e). It would mean that some specific interactions between the components occur. In order to see the effect of different functional groups, Zn chloride was also tried which led to the hydrolyzed TnP in around 30 min (Fig. 2d). Therefore, we see that, among all the compounds tested, uniquely Zn acetate remarkably delays the TnP hydrolysis. That will allow an easy deposition of the Zn-doped films under ambient atmosphere, as said above.

In order to further optimize the sintering conditions of the films that we want free of organic species, the thermal characterization of products, obtained once the precursor coating solutions have been heated at 100 °C, has been carried out and presented below.

3. Thermal characterization of samples obtained from the precursor coating solutions

After heating for 10 hrs at 100 °C the precursor solutions presented above on Fig. 1a and 1b, gels of Ti and Ni species and of Zn added Ti and Ni species were obtained. The weight changes were analyzed from room temperature to 1000 ^{o}C by TG-DTA analysis. As illustrated in Fig. 3, the TG curves (black line) show distinct steps of weight loss upon heating. The weight loss (~ 30 %) from room temperature to 240 ^{o}C would account not only for the loss of physically/chemically absorbed water but also for a departure of organic species. Indeed, the corresponding DTA curves (blue line) show exothermic peak indicating that the departure of organic species is dominant compared to the physically/chemically absorbed water. The weight loss of ~ 30 % between around 240 ^{o}C and 350 ^{o}C, with the DTA curves showing endothermic peak, can be explained by both the

formation of metal-oxygen bonds [33-35] (endothermic reaction) and the decomposition of *iso*-propoxide groups of titanium and acetate groups of nickel and zinc leading to the departure of organic species. No significant weight loss was observed above ~ 350 ^{o}C. The resulting powdered samples consist of TiO_2/NiO and Zn-doped TiO_2/NiO as will be clarified hereafter.

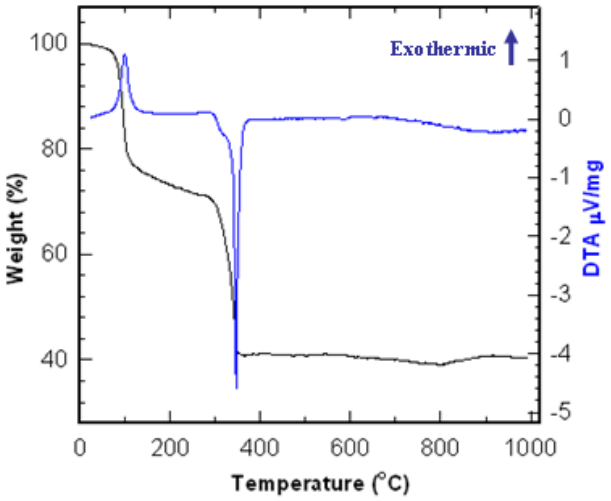

(a) Ti and Ni species

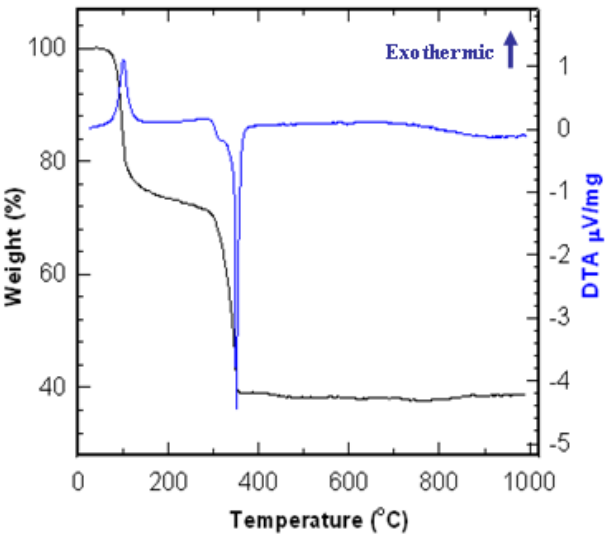

(b) Zn added Ti and Ni species

Fig. 3: TG and DTA curves of gels of (a) Ti and Ni species and of (b) Zn added Ti and Ni species. This thermal study was carried out from room temperature to 1000 ^{o}C under air. The heating temperature was increased by 5 ^{o}C per min.

Taking into account the complete weight loss around 350 ^{o}C, it can be reasonably deduced that the minimum heating temperature for the synthesis of inorganic TiO_2/NiO and of Zn doped TiO_2/NiO films prepared from the precursor coating solutions, should be around 350 ^{o}C. It is also necessary to decide the minimum heating duration. In this regard TG measurements were carried out by heating the gels at 350 ^{o}C for 3 hrs. As shown in Fig. 4, both products show similar evolutions corresponding to two distinct steps of weight loss. The first step (which corresponds to the departure of water and possible organic species) led to around 28 % in weight loss within ~ 37 min and the second step (which corresponds to the departure of the organic species and the formation of metal-oxygen bonds) led to another weight loss of around 32 % within ~ 38 min. The DTA curves show the corresponding exothermic and endothermic peaks.

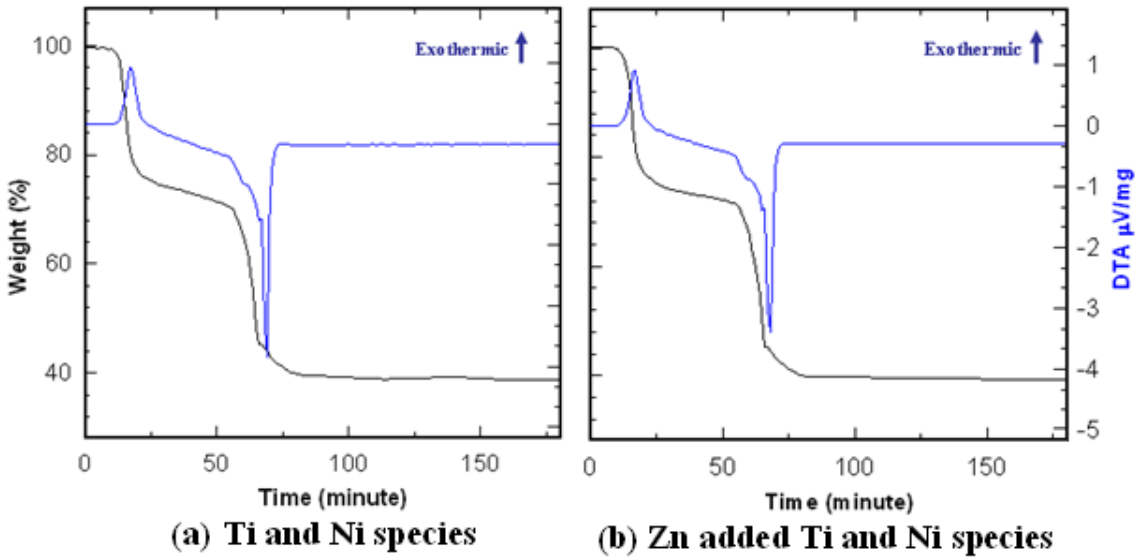

Fig. 4: TG and DTA curves from gels of (a) Ti and Ni species and from (b) Zn added Ti and Ni species. This thermal study was carried out at a fixed temperature of 350 ^{o}C for 3 hrs under air flow.

From these results it can be deduced that the sintering temperature of the films prepared from the precursor solutions can be 350 ^{o}C and the heating duration should be

longer than 75 min. In our case, we employed 2 hrs as a heating duration to make it sure to achieve the deposition of inorganic films free (or quasi free) of organic moieties.

At this stage, a number of key points need to be clarified such as: will zinc be really substituted to titanium and not to nickel in the Zn doped TiO_2/NiO thin films prepared using the above quoted experimental conditions? In order to clarify this important point, we have achieved the following characterizations.

4. Structural characterizations

4-1. Gels from Ti *iso*-propoxide (TnP) and from zinc acetate dihydrate added to TnP and corresponding heated samples

Figs. 5 and 6 show the powder X-ray diffraction (XRD) patterns of as prepared TnP gel and Zn added TnP gel (Zn:Ti = 1:9) and corresponding heated samples at 350 ^oC and 500 ^oC for 2 hrs.

As could reasonably be expected, the gels are X-ray amorphous (Fig. 5 and 6 (the bottom pattern)). Once heated at 350 ^oC TnP led to TiO_2 anatase (JCPDS No. 73-1764), (Fig. 5). Most interestingly, no XRD peaks were visible for the Zn added sample after similar heating process (T = 350 ^oC), (Fig. 6: the middle XRD pattern). It indicates that Zn addition inhibits the crystallization of titanium dioxide. Both samples heated at 500 ^oC were crystallized into TiO_2 anatase.

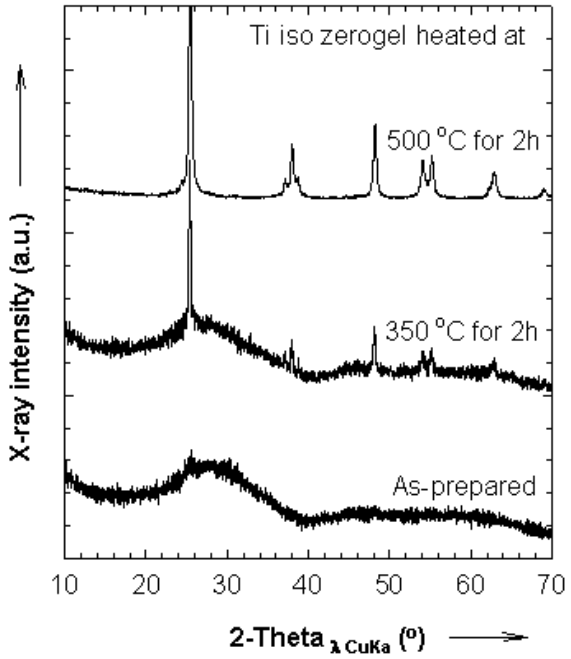

Fig. 5: XRD patterns for the gels of titanium *iso*-propoxide (TnP) and of annealed samples at 350 and 500 °C for 2 hrs.

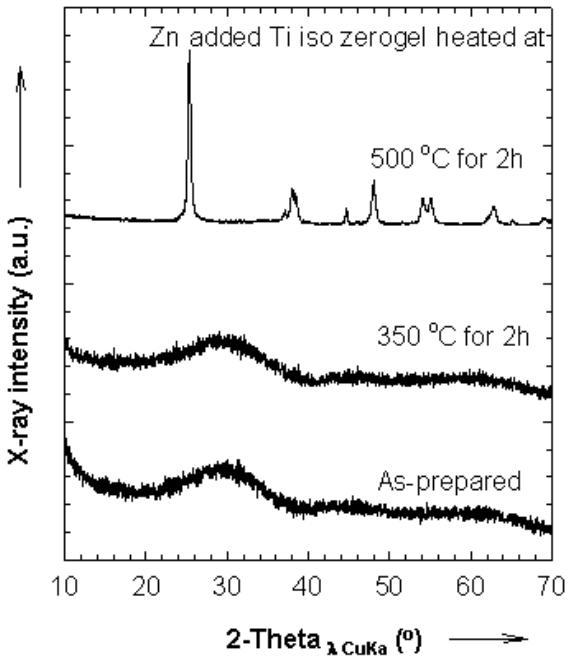

Fig. 6: Powder XRD patterns for Zn acetated dihydrate added gel of titanium *iso*-propoxide (TnP) and of annealed samples at 350 and 500 °C for 2 hrs.

For the Zn added sample, the shift towards lower 2-theta values illustrates the successful partial substitution of Ti^{4+} (r_{Ti4+} = 0.605 Å) ions with larger Zn^{2+} (r_{Zn2+} = 0.740 Å) ions [36]. Therefore, neutral oxygen vacancies will be created according to the $Ti_{1-x}Zn_xO_{2-x}\square_x$ formula.

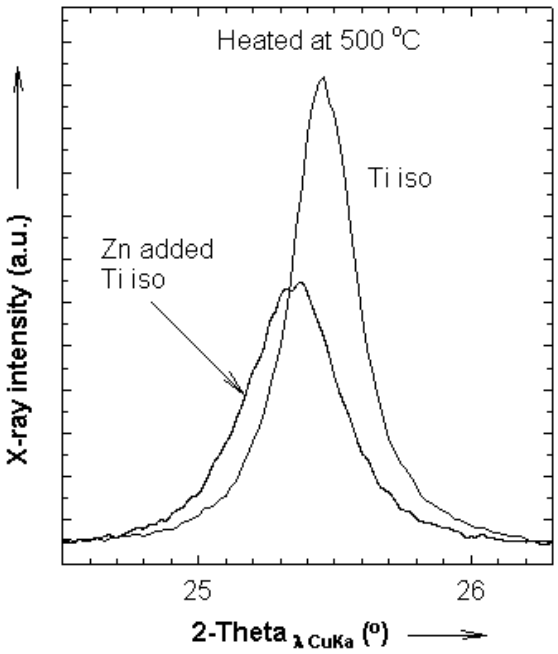

Fig. 7: Magnification of the XRD patterns in the 24.5 and 26.3 degree two theta value of TiO_2 and Zn-doped TiO_2 powders (Fig. 5 and 6). Ti iso indicates Ti *iso*-propoxide.

It was established before [32, 37] that the presence of neutral oxygen vacancies favors grain percolation. In the present case such enhanced grain percolation occurred also for a sintering temperature of 350 °C (Fig. 8). It gives an indirect evidence of the occurrence of the neutral oxygen vacancies in the sample heated at 350 °C.

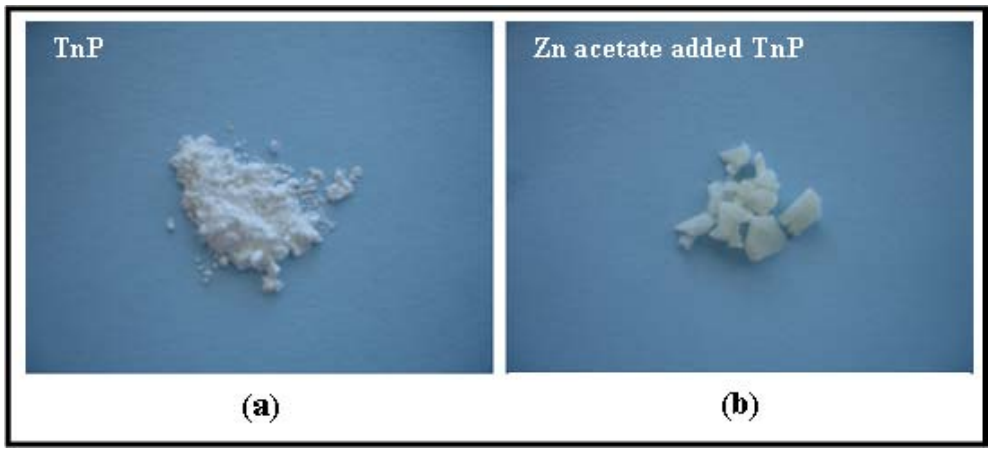

Fig. 8: Photos of samples obtained from heating a) Titanium *iso*-propoxide (TnP) and b) Zn acetate·$2H_2O$ added to TnP at 350 °C for 2 hrs under ambient atmosphere.

4-2. Gels from nickel acetate tetrahydrate mixed with zinc acetate dihydrate and corresponding heated samples

We have also performed XRD measurement of the gel arising from the solution where Ni acetate tetrahydrate and Zn acetate dihydrate are dissolved and of the corresponding heated sample in order to investigate any possibility of substitution between Zn and Ni under our working conditions. The XRD patterns in Fig. 9a correspond to the sample for which the ratio, Zn:Ni=0.00125:0.05, is that of the coating solution (b) listed on Fig.1. Even though the amount of zinc oxide is very low, considering the above ratio, we can see the three distinct peaks, with obviously low intensities, originating from typical ZnO phase (JCPDS No. 5-0664) [38]. Also we could confirm no shift of NiO peaks of Zn added Ni sample (Fig. 9b). The above findings indicate that zinc is not substituted to Ni in the employed heating condition (350 °C, which will be the sintering temperature of our films).

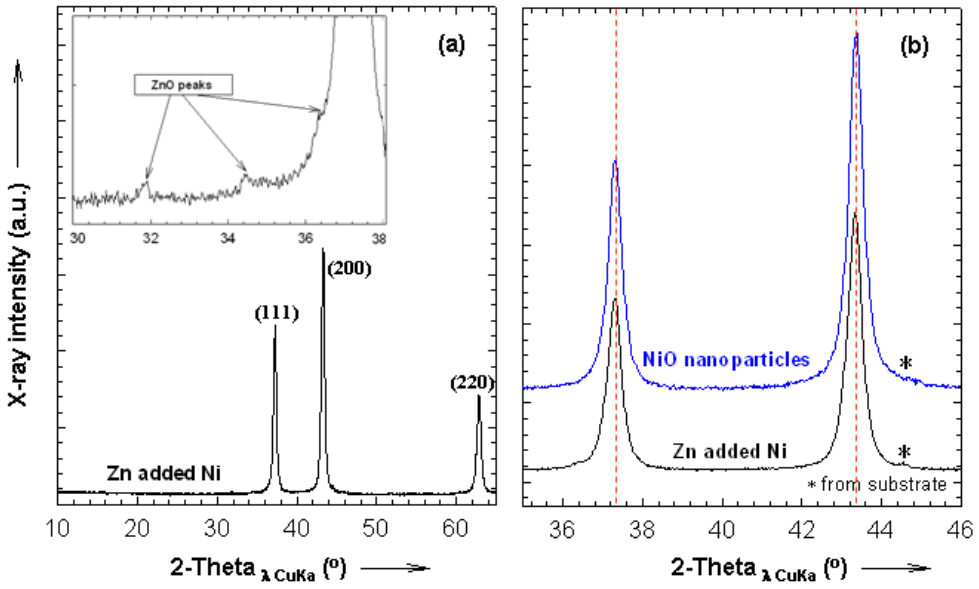

Fig. 9: XRD patterns for (a) the powdered sample resulting from heating at 350 °C for 2 hrs the gel arising from the solution of Ni acetate tetrahydrate and Zn acetate dihydrate in ethanol and (b) NiO nanoparticles compared to (a)

(The Zn/Ni = 0.025 ratio considered here is identical to that of solution of composition (b) (Fig. 1))

4-3. Gels from TnP and zinc acetate dihydrate mixed with nickel acetate tetrahydrate and corresponding heated samples

In this section we tried to approach the maximum amount of Zn which can be substituted to Ti in the TiO_2 matrix in which nickel oxide nanoparticles are embedded in. Therefore, the gels considered here arise from the coating solutions (b) and (c) in Fig. 1. They were obtained by heating the solutions at 100 °C for 10 hrs. As expected, they are X-ray amorphous. After heating the gels at 350 °C for 2 hrs, powders are obtained. If all Zn ions introduced are substituted for Ti ions, the powders will have the composition 2 and 3, defined above in § 1 and reported again hereafter for sake of clarity:

- Composition 2: $Ti^{4+}_{0.9}Zn^{2+}_{0.1}O^{2-}_{1.9}\square_{0.1}$/NiO (20 % of $Ti^{4+}_{0.9}Zn^{2+}_{0.1}O^{2-}_{1.9}\square_{0.1}$ and 80 % of NiO (molar %))
- Composition 3: '$Ti^{4+}_{0.85}Zn^{2+}_{0.15}O^{2-}_{1.85}\square_{0.15}$'/NiO (20 % of '$Ti^{4+}_{0.85}Zn^{2+}_{0.15}O^{2-}_{1.85}\square_{0.15}$' and 80 % of NiO (molar %)).

As shown in Fig. 10a and 10b, both, powders show XRD peaks at 37.3, 43.5, and 63.2 degree in two theta value which is a good match with cubic phased NiO structure. It indicates that Zn-doped TiO_2 in the composite powders are X-ray amorphous, as will be confirmed later for the corresponding films. It is important to note that a trace of ZnO [38] can be observed for composition 3 around 31.7, 34.5, and 36 degree (Fig. 10b). It means that the 15 mol % of Zn over Ti exceeded the substitution limit of Zn over Ti in the present synthetic condition. This point will be confirmed below (§ 5.4).

In case of the composition 2, no observation of additional peaks between 30 and 38 degree in two theta value was found as can be seen in Fig. 10a (bottom panel).

Consequently, the limit of substitution of Zn to Ti sites is around 10 mol % over Ti in the employed synthetic condition. The main peaks in the diffraction patterns of Fig. 10 are indexed as NiO (JCPDS 4-0835) [39].

Consequently, the films obtained from the coating solution (b), (Fig. 1), will be considered in the following; they will consist of crystallized NiO nanoparticles (80 % molar) embedded in an X-ray amorphous $Ti^{4+}_{0.9}Zn^{2+}_{0.1}O^{2-}_{1.9}\square_{0.1}$ matrix (20 % molar).

Let us quote that a similar XRD pattern, not reported here for sake of clarity, is obtained for the TiO_2/NiO powder (composition 1). It means that, here as well, NiO nanoparticles are embedded in a X-ray amorphous TiO_2 matrix, as could be expected [18,20].

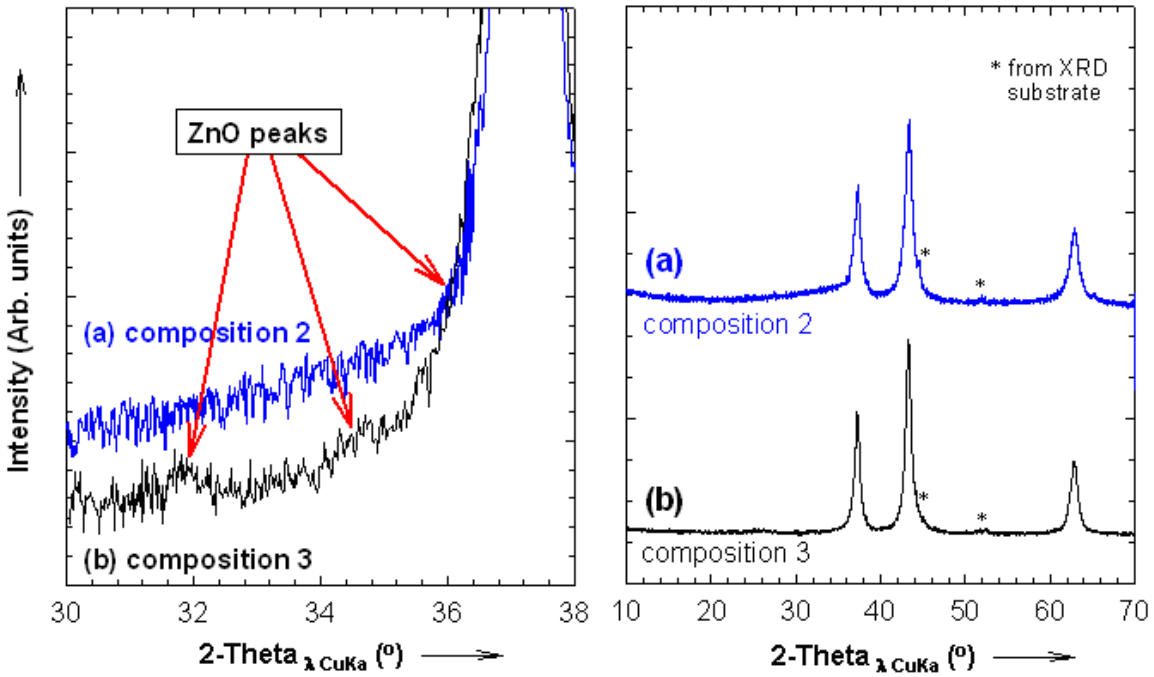

Fig. 10: Powder XRD patterns for a) composition 2 and b) composition 3 synthesized at 350 °C for 2 hrs in air. (The upper panel indicates the magnified patterns of the bottom panel between 30 and 38 degree in two theta value.)

Composition 2: $Ti^{4+}_{0.9}Zn^{2+}_{0.1}O^{2-}_{1.9}\square_{0.1}$/NiO (20 % of $Ti^{4+}_{0.9}Zn^{2+}_{0.1}O^{2-}_{1.9}\square_{0.1}$ and 80 % of NiO (molar %))

Composition 3: '$Ti^{4+}_{0.85}Zn^{2+}_{0.15}O^{2-}_{1.85}\square_{0.15}$'/NiO (20 % of '$Ti^{4+}_{0.85}Zn^{2+}_{0.15}O^{2-}_{1.85}\square_{0.15}$' and 80 % of NiO (molar %)).

4-4. XRD patterns of TiO_2/NiO (composition 1) and Zn doped TiO_2/NiO (composition 2) powders

Fig. 12 shows XRD patterns of the TiO_2/NiO and Zn doped TiO_2/NiO powders obtained from the coating solutions (a) and (b) which will be used for film deposition. The powders were obtained using the synthetic conditions defined above (conclusion of § 3): heating at 350 ^oC for 2 hrs in air with heating rate of 5 ^oC per min. These conditions will be used to sinter films. There is no distinct difference between the two XRD patterns.

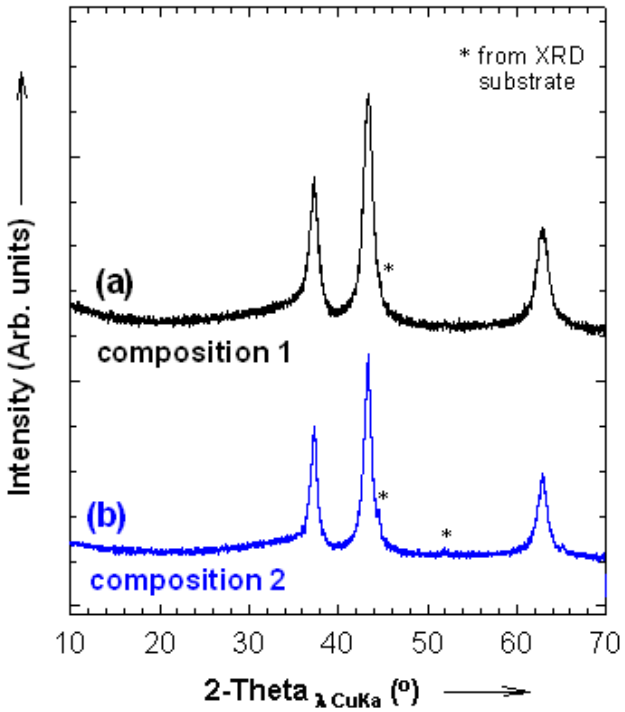

Fig. 11: Powder XRD patterns of a) composition 1 and b) composition 2 synthesized at 350 ^oC for 2 hrs in air.

Composition 1: TiO_2/NiO (20 % of TiO_2 and 80 % of NiO (molar %)).

Composition 2: $Ti^{4+}_{0.9}Zn^{2+}_{0.1}O^{2-}_{1.9}\square_{0.1}$/NiO (20 % of $Ti^{4+}_{0.9}Zn^{2+}_{0.1}O^{2-}_{1.9}\square_{0.1}$ and 80 % of NiO (molar %))

5. Thin films

5-1. Preparation of thin films

As quoted above, FTO/glass was used as conductive substrates for the thin films deposition. Before used, the substrates went through the cleaning steps defined in chapter

II. The non conductive side (glass part) of the FTO substrate was covered by a scotch tape to avoid any possible coating of the films on the back side.

In this present work a dip-coating method was employed (Fig. 11). We have prepared TiO_2/NiO thin films (composition 1 in § 1) and the Zn doped TiO_2/NiO thin films (composition 2 in §.1) using the following optimized* identical condition *(*by 'optimized', we mean homogeneous films showing a high transparency in the bleached state; in addition, we will see below that the films thickness is close to that reported in chapter 2 for NiO-based thin films deposited by PLD, allowing comparative capacity)*. The films were first dip-coated on FTO substrates with a withdrawing speed of 2 mm/s under ambient atmosphere. The dipping duration was 10 min. After the dip-coating process the coated films were left in ambient atmosphere for 10 hrs. Afterwards, following the sintering procedure defined above, the films were progressively heated in ambient atmosphere from room temperature to 350 °C with a temperature increase of 5 ^{o}C per min. After heating at 350 ^{o}C for 2 hrs, the films were ready for characterizations.

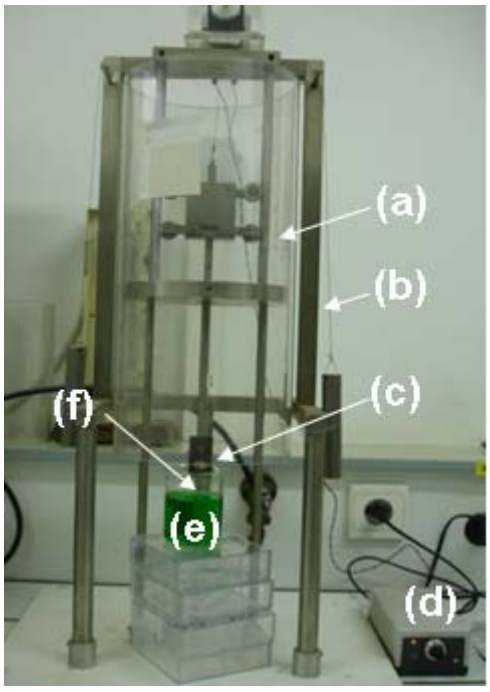

Fig. 11: Illustration of the employed dip-coating tool consisted by (a) a cover, (b) a main body, (c) a film holder, and (d) a speed controller. (e) and (f) indicate a coating solution and FTO substrate, respectively.

5-2. Structural characterizations and chemical composition

5-2-a. Structural characterizations

Selected area electron diffraction (SAED) patterns of the thin films, obtained from TEM measurements, are shown in Fig. 12. For both films, the distance between nickel atom layers was measured resulting in 0.24 and 0.21 nm for (111) and (200), respectively, which accounts for NiO structure. The less clear SAED pattern in Fig. 12b is not an indication of a lower crystallinity for Zn doped TiO_2/NiO, according to Fig. 11. It may be due to the denser Zn doped TiO_2 matrix, compared to TiO_2 one, which interferes with the diffracted electrons. More investigation is under process to clarify this point.

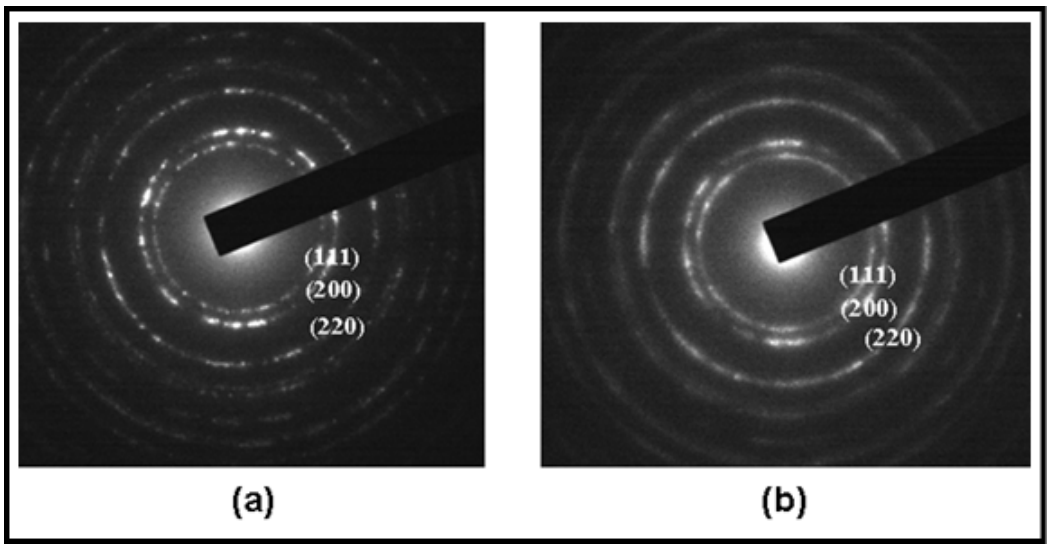

Fig.12: SAED patterns of (a) TiO_2/NiO and (b) Zn doped TiO_2/NiO thin films.

5-2-b. Chemical composition

We have performed energy dispersive spectroscopy (EDS) and EDS mapping analyses to confirm the existence of the elements (Ni, Ti, and Zn) and their homogeneous distribution [40]. The films were scratched for these measurements. As shown with EDS images in Fig. 13a, we could confirm that the TiO_2/NiO film contains titanium and nickel, as obviously expected. The additionally detected elements such as Si and Cu originated

from FTO substrate and cupper TEM grid. In case of Zn doped TiO_2/NiO thin film the presence of zinc was confirmed even though the intensity of the peak is quite small.

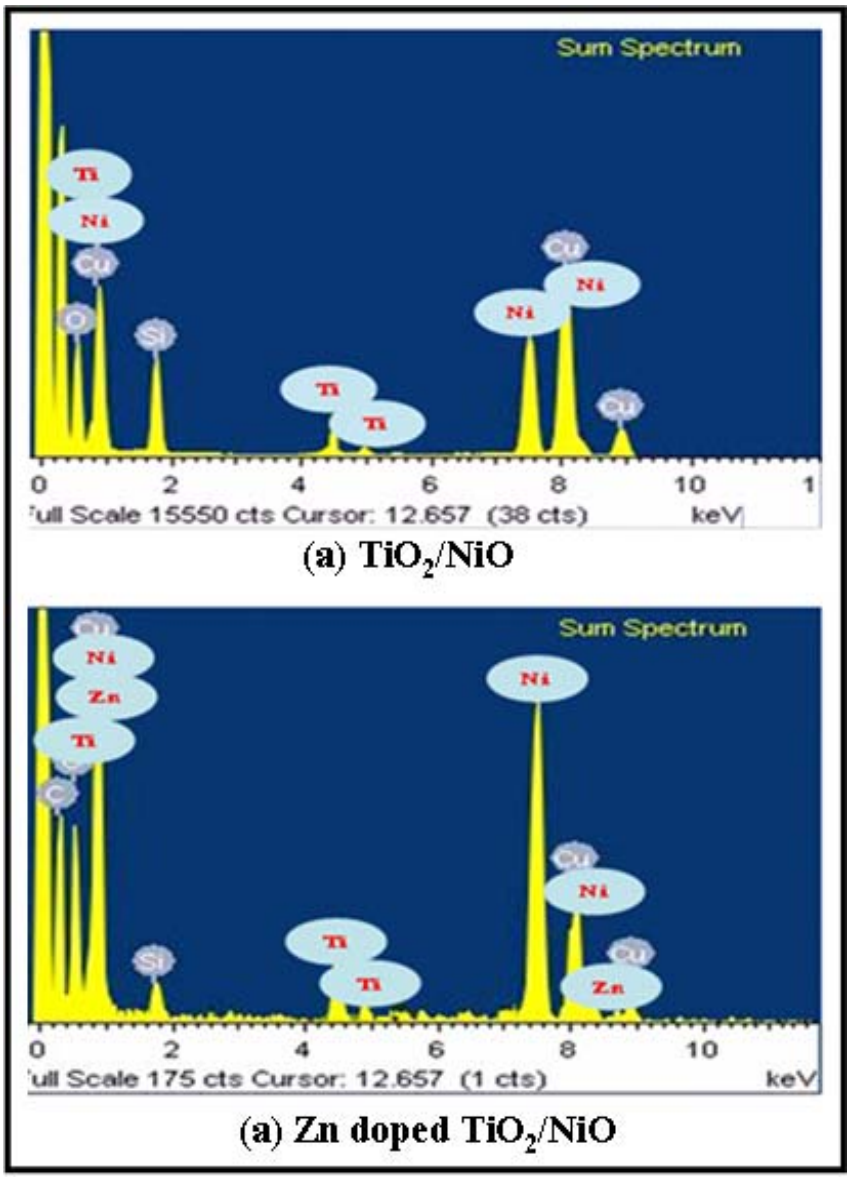

Fig.13: EDS images of (a) TiO_2/NiO and (b) Zn doped TiO_2/NiO thin films. This result was obtained by TEM/EDS measurement.

EDS mapping measurement was carried out to check element distribution over the whole area [40]. STEM image in Fig. 14 corresponds to the area where all the mapping images were obtained. All the obtained mapping images with different color depending on different element exhibit a homogeneous distribution of Ti and Ni.

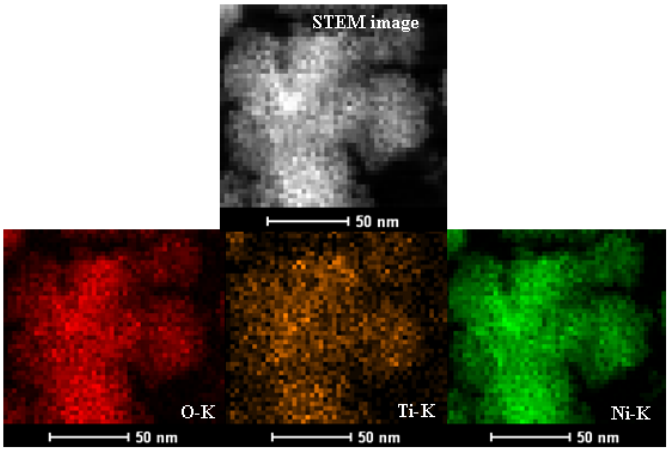

Fig.14: EDS mapping images of TiO_2/NiO thin film.

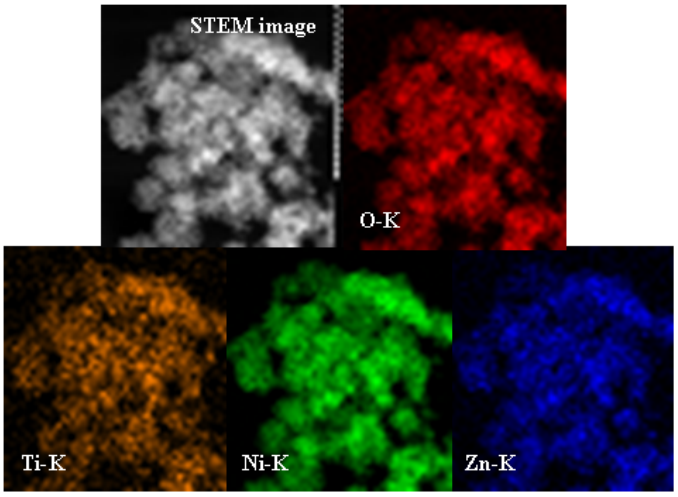

Fig. 15: EDS mapping images of Zn doped TiO_2/NiO thin film.

In case of Zn doped thin film, the obtained Zn mapping data is consistent with STEM image indicative of homogeneous substitution of Zn over the whole area of the film (Fig. 15). These results would mean that the expected film compositions, composition 1 (TiO_2/NiO (20 % of TiO_2 and 80 % of NiO (molar %)) and composition 2 ($Ti^{4+}_{0.9}Zn^{2+}_{0.1}O^{2-}_{1.9}\square_{0.1}$/NiO (20 % of $Ti^{4+}_{0.9}Zn^{2+}_{0.1}O^{2-}_{1.9}\square_{0.1}$ and 80 % of NiO (molar %)), occur all over the surface. In fact, the film composition has been checked using inductively coupled plasma (ICP) analysis as shown hereafter.

The formula of TiO_2/NiO and Zn doped thin films, $Ti_{1-x}Zn_xO_{2-x}\square_x$/NiO, was determined into TiO_2 (~ 20 % molar)/NiO (~ 80 % molar) and $Ti_{0.91}Zn_{0.09}O_{1.91}\square_{0.09}$ (~ 20

% molar)/NiO (~ 80 % molar) respectively. These formulae are in good agreement with the compositions 1 and 2.

5-3. Morphological characterizations

5-3-a. FE-SEM measurement

As can be seen in Fig. 16a regular cracks exist over the whole surface for TiO_2/NiO thin film whereas no cracks were visible for the Zn doped thin film. We do believe that this evolution is attributed to the presence of the neutral oxygen vacancies, in agreement with the Zn^{2+} substitution to Ti^{4+} sites according to: $Ti^{4+}_{0.9}Zn^{2+}_{0.1}O_{1.9}\square_{0.1}$. Indeed, previous work at the ICMCB-CNRS and University of Rome has evidenced that the neutral oxygen vacancies with unstable energy level lead to grain percolation [32,42] and, thereby inhibit cracking.

The thin films show, more or less, the same thickness as shown in Fig. 16b. It is also observable that the films are homogeneously coated over the whole area and show their uniform thickness as well.

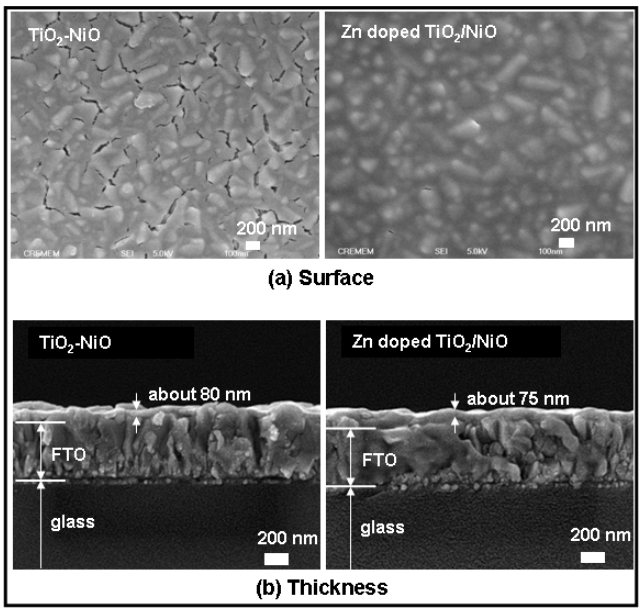

Fig. 16: SEM images for (a) surface and (b) thickness of as-prepared TiO_2/NiO and Zn doped TiO_2/NiO thin films.

5-3-b. HR-TEM measurement

As can be seen in Fig. 17, there is no difference on lattice distance for both thin films, in agreement with above reported Fig. 12.

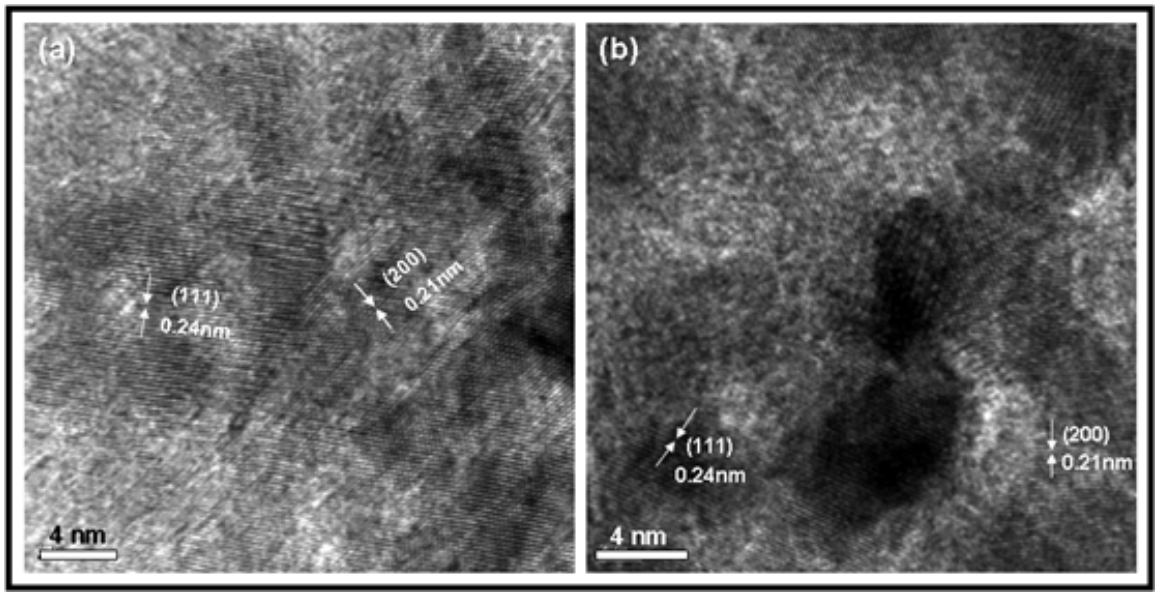

Fig. 17: TEM images with lattice fringe of (a) TiO_2/NiO and (b) Zn doped TIO_2/NiO thin films. (The arrows indicate lattice distance.)

The less clear lattice images in Fig. 17b are not, as we discussed above (Fig. 12), an indication of a lower crystallinity for Zn doped TiO_2/NiO.

The TEM images were also obtained via cross section method as shown in Fig. 18. The nano-sized nickel oxide particles are linked one another. It is believed that the links between nickel oxide nanoparticles are due to the amorphous titanium oxide matrix where nickel oxide particles are embedded in.

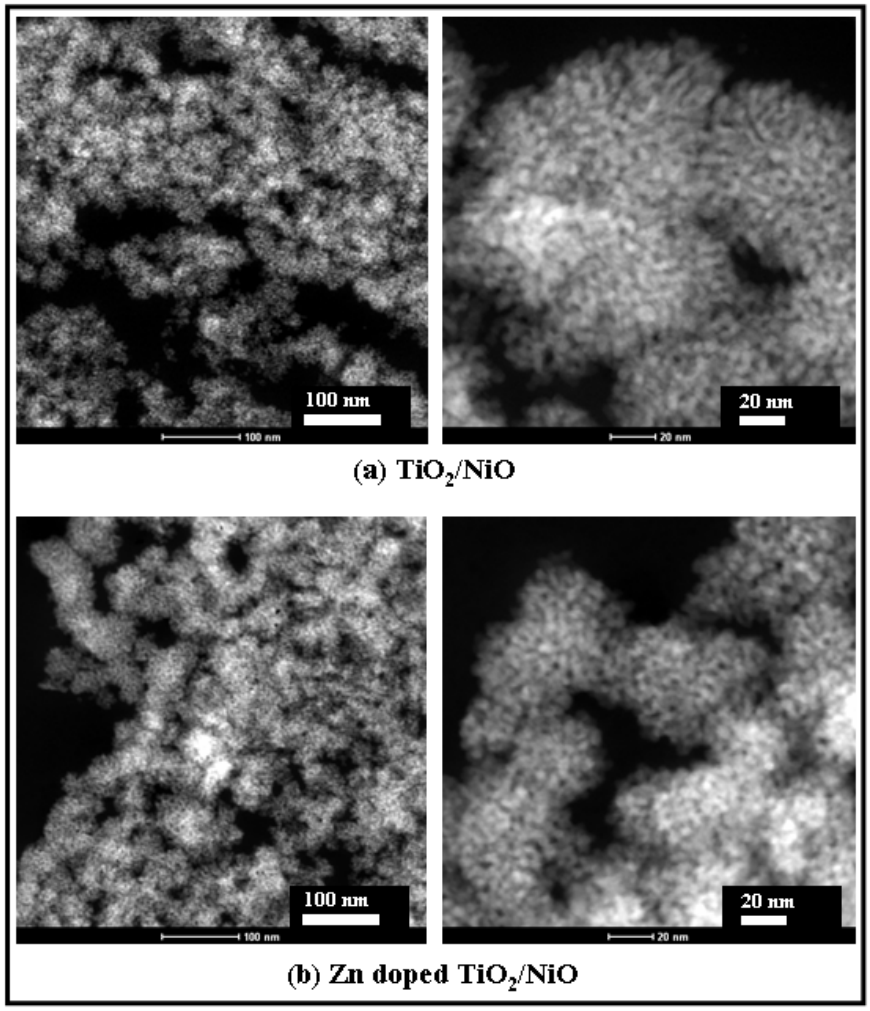

Fig. 18: TEM images of (a) TiO_2/NiO (composition 1 in §. 1) and (b) Zn doped TiO_2/NiO (composition 2 in §. 1) thin films obtained from cross section measurements. (Right panel indicates the magnification.)

(The preparation method of the samples for cross section: the scratched films were blended with acrylic resin (methyl methacrylate: n-butyl methacrylate 4:6, 1.5 % benzoyl peroxide) in a polyethylene capsule and the sample was then sliced using the ultra-microtome with a diamond knife.)

5-4. Wetting characteristics of the film surfaces estimated from contact angle measurements

In this chapter contact angles of the films were also measured with H_2O to monitor the wettability of the films depending on the presence of zinc in TiO_2 matrix, and therefore, of the presence of neutral oxygen vacancies as illustrated by $Ti^{4+}_{0.9}Zn^{2+}_{0.1}O^{2-}$

$_{1.9}\square_{0.1}$/NiO. The composite TiO_2/NiO shows smaller contact angle (76.8 °, Fig. 19b) than NiO (107.3 °, Fig. 19a) indicative of enhanced hydrophilicity due to the presence of TiO_2. This trend is emphasized for Zn doped thin films, likely due to the presence of neutral oxygen vacancy. However, increasing Zn content from 10 to 15 % over Ti leads to an increase of contact angles from 51.2 ° to 59.0 ° (Fig. 19a,19b). Knowing that ZnO itself is less hydrophilic than TiO_2 [42], we conclude that 15 % of Zn over Ti in composition 3 exceeded the substitution limit of Zn over Ti, as quoted in § 4.3.

The influence of the increase of the wettability on the electrochromic properties of the composite thin films will be investigated below.

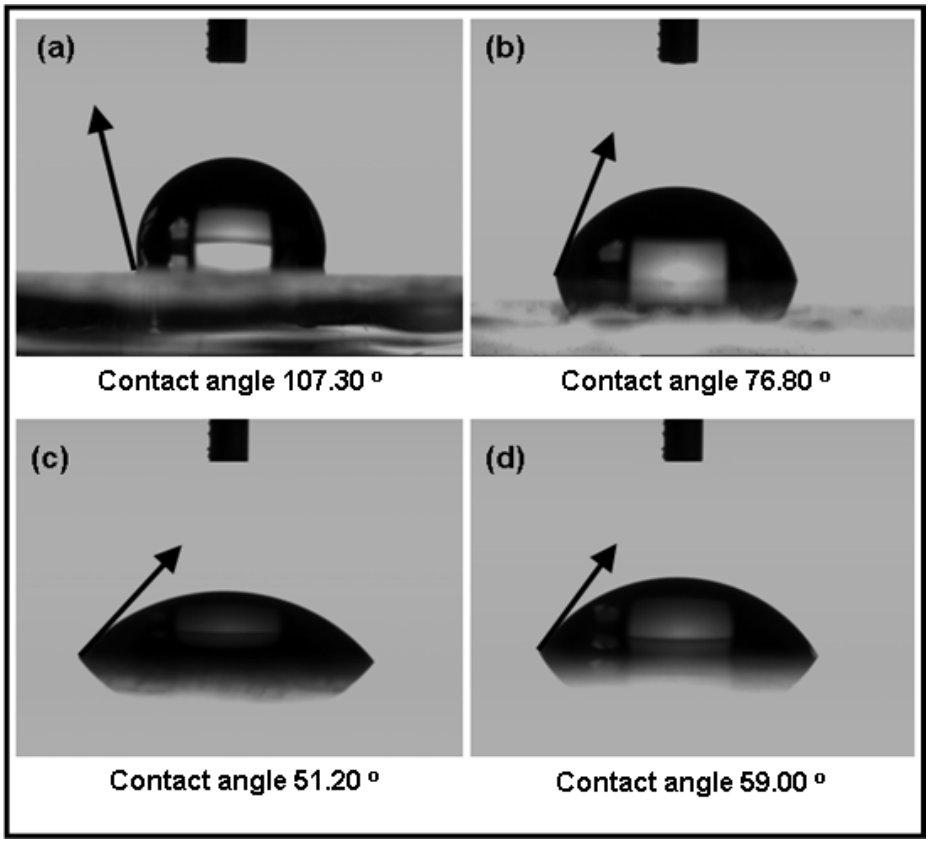

Fig. 19: Contact angles obtained with H_2O solvent of (a) NiO, (b) TiO_2/NiO, (c) Zn (10 mol % over Ti) doped TiO_2/NiO, and (d) Zn (15 mol % over Ti) doped TiO_2/NiO thin films. The accuracy is ± 0.05.

5-5. Electrochromic properties of TiO_2/NiO and Zn doped TiO_2/NiO thin films

5-5-a. Electrochemical measurements

Cyclic voltammograms (CVs) and chronoamperometry (CA) of TiO_2/NiO and $Ti^{4+}_{0.9}Zn^{2+}_{0.1}O^{2-}_{1.9}\square_{0.1}$/NiO films were performed within the 0 V ~ 0.55 V potential windows versus Hg/HgO. The CVs performed at a scan rate of 10 mV/s in 1M KOH electrolyte. for TiO_2/NiO and $Ti^{4+}_{0.9}Zn^{2+}_{0.1}O_{1.9}\square_{0.1}$/NiO thin films are compared in Fig. 20 at 1st, 1000th, 3000th, and 6000th cycle. Upon cycling, for TiO_2/NiO thin films, there is a continuous evolution towards higher potential of the anodic peak. It shifted from 0.40 V to 0.47 V from 1000th to 6000th cycle. Concomitantly, a slight shift towards lower potential is observed upon reduction (0.14 V → 0.12 V). In contrast, between 1000th cycle and 6000th cycle Zn doped thin film shows negligible change in oxidation potential (~ 0.40 V) whereas reduction potential increases upon cycling (0.14 V → 0.18 V, Fig. 20b).

The change in the shape of the CV curves tends to indicate that the electrochemical hydroxide/oxyhydroxide active phases slightly differ in nature upon cycling.

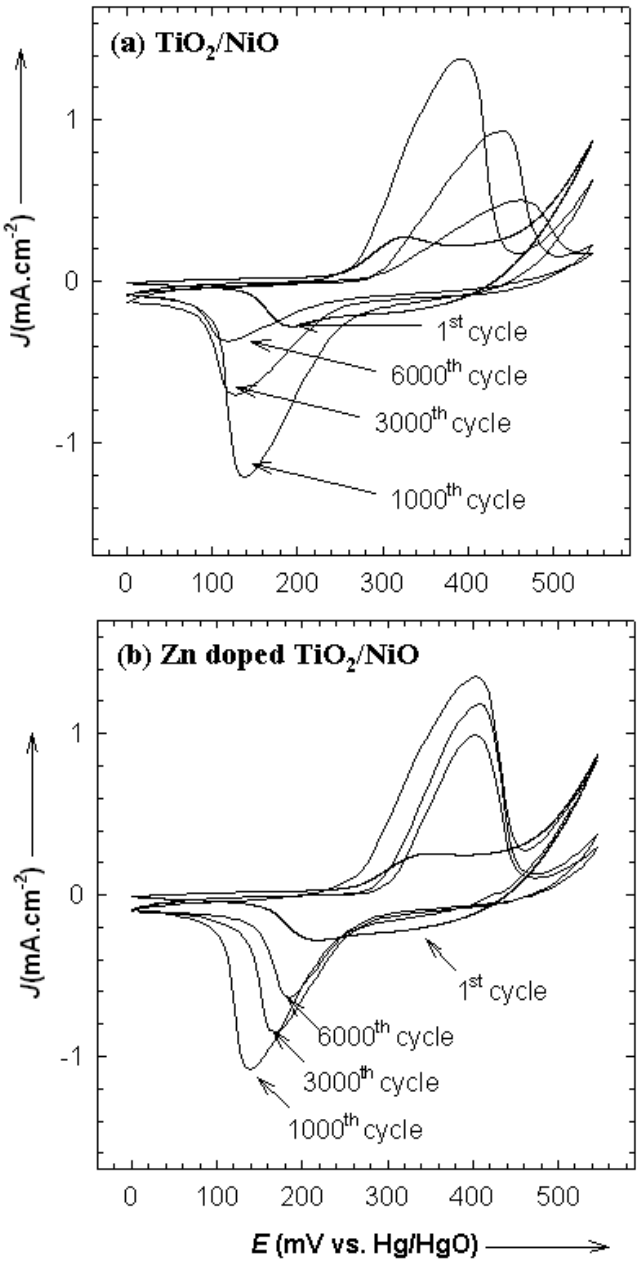

Fig. 20: Cyclic voltammograms of TiO_2/NiO and Zn doped TiO_2/NiO thin films at 1st, 1000th, 3000th, and 6000th cycle. Three-electrode-cell configuration consists of a working electrode (the prepared films), a counter electrode (platinum foil), and a reference electrode (Hg/HgO/1M KOH). All the measurements were carried out at a scam rate of 10 mV/s in 1M KOH electrolyte between 0 V and 0.55 V.

The coulombic capacities, Q_c, for the TiO_2/NiO and Zn doped TiO_2/NiO thin films upon cycling are compared in Fig. 21. The cycling life of the thin films follow the previously reported three-step process consisting of an activation period, a steady state, and

a degradation period [4,43]. The activation period occurs from the initial cycle to ~1000 cycles for TiO_2/NiO and Zn doped TiO_2/NiO thin films. The steady state occurs during a few cycles only (Fig. 21). It can be clearly seen that both films experience a continuous decrease of Q_c during degradation period (Fig. 21a). However the decrease is much more pronounced for TiO_2/NiO thin film. In other word, the Zn doped TiO_2/NiO thin films show much more enhanced durability upon cycling. 61 % of the maximum capacity is retained after 8000^{th} cycle, whereas the capacity retention is only of 36 % after 6000^{th} cycle for TiO_2/NiO thin films. The higher cyclability of the Zn doped thin films can be reasonably correlated to enhanced mechanical adhesion.

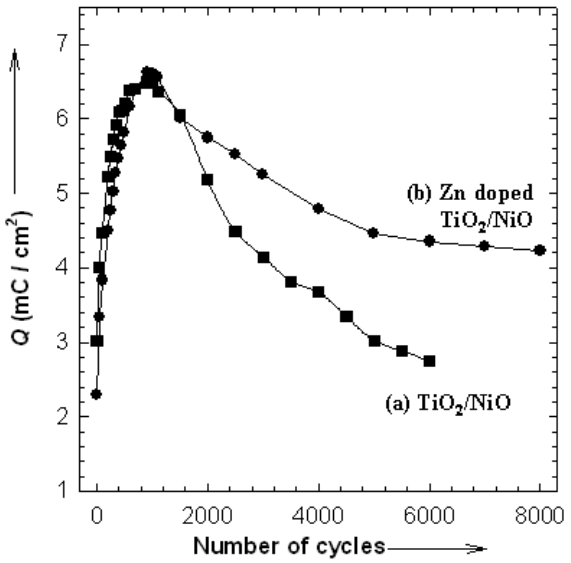

Fig. 21: Coulombic capacity of (a) TiO_2/NiO and (b) Zn (10 mol % over Ti) doped TiO_2/NiO thin films. The electrochemical test was carried out in 1M KOH electrolyte with three-electrode-cell configuration consisting of a working electrode (TiO_2/NiO or Zn doped TiO_2/NiO films), a counter electrode (platinum foil), and a reference electrode (Hg/HgO/1M KOH).

The coulombic capacity was deduced based on the cathodic part of chronoamperometry peaks in order to exclude the influence of the oxygen evolution. The voltages applied for 30 seconds were 0.00 V and 0.55 V for cathodic and anodic parts, respectively. Cyclovoltammetry was also performed every 100 cycles to cross confirm the evolution of capacity.

Such trend was confirmed by FE-SEM measurements. Clear peeling off from the FTO substrate (see the surface, Fig. 22a image) after 8000 cycles is observed for TiO_2/NiO thin film. Numerous brownish pieces were clearly detected in the used electrolyte as shown in Fig. 22b (the upper panel).

On the contrary, the Zn doped TiO_2/NiO thin films did not show any degradation (Fig. 22a,22b). Nevertheless, a careful observation of the thin film' substrate interface indicates an early beginning of loss of adhesion (Fig. 22c, down panel).

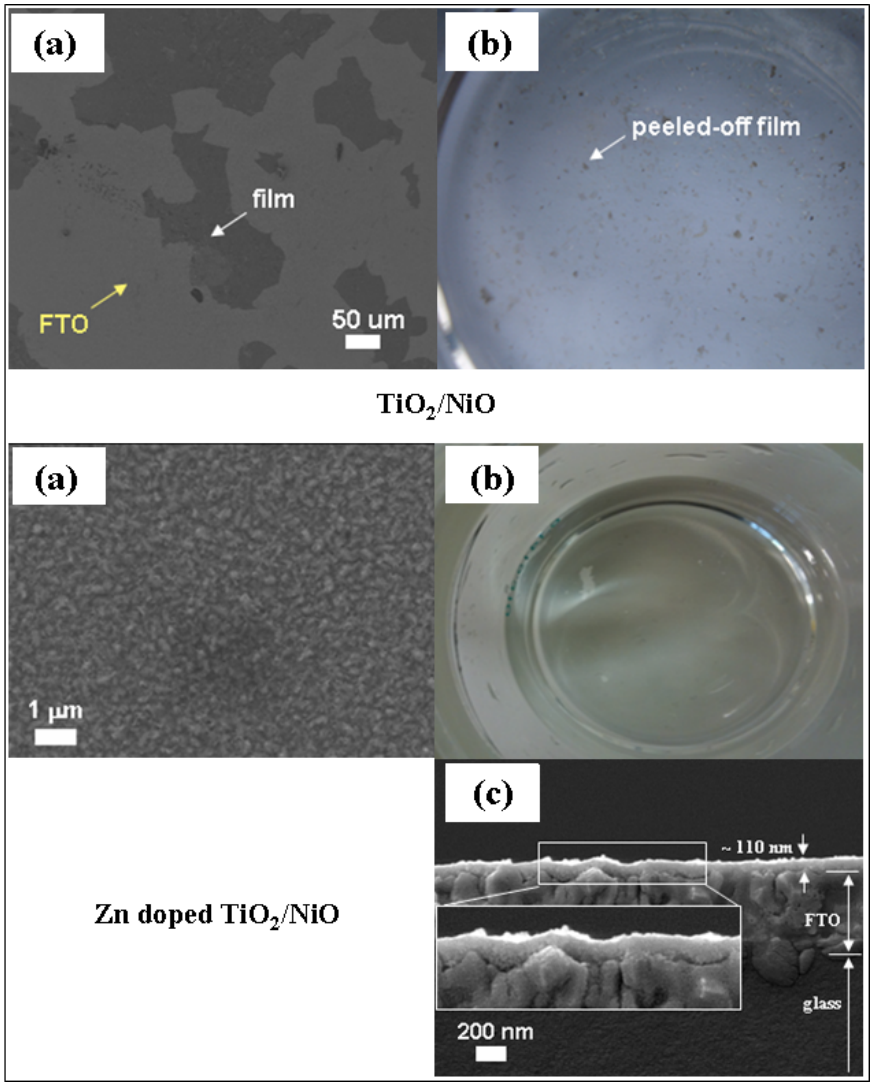

Fig. 22: FE-SEM images of (a) surface and (b) used electrolyte images for TiO_2/NiO (upper panel) and Zn doped TiO_2/NiO (lower panel) thin films after 8000th cycle, respectively. (c) is cross-section image of Zn doped TiO_2/NiO thin film.

5-5-b. Optical properties

Optical properties of the thin films were measured upon cycling in transmittance mode at the wavelength of 550 nm. The transmittances of the as-prepared TiO_2/NiO ($T_{\lambda=550nm}$ ~ 98 %) and Zn doped TiO_2/NiO ($T_{\lambda=550nm}$ ~ 99 %) thin films are similar to one another as shown in Fig.23. TiO_2/NiO thin film at the 1000th cycle exhibits transmittances of 67.5 % in the 'bleached state' and of 37.5 % in the colored state (Fig. 23a), corresponding to a contrast ratio of 1.8. Higher contrast ratio of 2.0 was recorded for Zn doped thin film. Interestingly it remains stable up to 6000 cycles whereas it was impossible to measure it for TiO_2/NiO thin film due to very low film quality as a result of poor mechanical adhesion. On the contrary, Zn doped thin film show significant electrochromic effect even after 8000th cycle. After 8000 cycles, the contrast is rather low mainly due to low transmittance in the bleached state. The later illustrates high irreversibility (i.e. persistence of a brownish color).

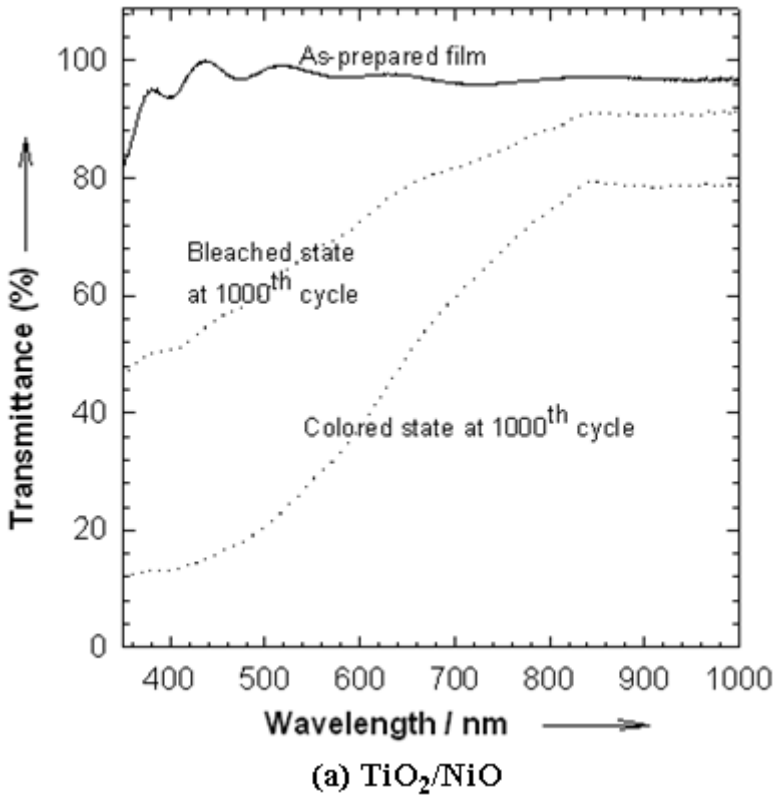

(a) TiO_2/NiO

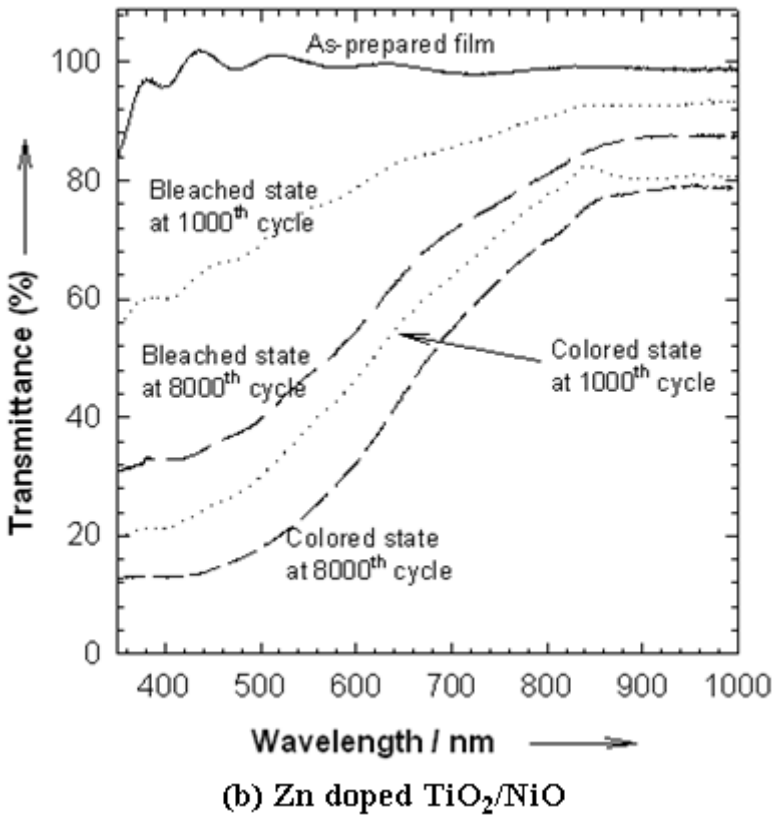

Fig. 23: Transmittance (%) of TiO_2/NiO thin films at 0 and 1000thcycle and Zn doped TiO_2/NiO thin films at 0, 1000th, 8000th cycle. (All the measurements were carried out by UV-Visible Spectrometry between 350 nm and 1000nm and the range of transmittance is from 100 % to 1 %). The voltages applied were 0.00 V and 0.55 V for bleached and colored states, respectively.

6. Conclusion

Owing to the remarkable delay of the hydrolysis of titanium *iso*-propoxide (TnP) in the coating solution after adding Zn acetate dihydrate, the coating processes of the Zn doped thin films could be advantageously carried out under ambient atmosphere. Using this precursor coating solution, in this chapter we have successfully synthesized via a dip coating method $Ti^{4+}_{0.91}Zn^{2+}_{0.09}O^{2-}_{1.91}\square_{0.09}$/NiO composite thin films consisting of X-ray amorphous $Ti^{4+}_{0.91}Zn^{2+}_{0.09}O^{2-}_{1.91}\square_{0.09}$ matrix where nanocrystalline NiO particles are embedded in. The occurrence of the neutral oxygen vacancies induced grain percolation resulting in smooth and homogeneous surface of the thin films with no cracks, contrarily to

undoped TiO_2/NiO films. According to the results of electrochromic performances, it was clearly demonstrated that Zn doping to TiO_2/NiO thin film is effective in enhancing the electrochromic durability. This enhancement can be explained by the enhanced mechanical adhesion of the thin film on FTO substrate. In chapter II, we assumed a relationship between mechanical adhesion and wettability of the films. Here also we established that the wettability of Zn doped thin film ($Ti^{4+}_{0.91}Zn^{2+}_{0.09}O^{2-}_{1.91}\square_{0.09}$/NiO) is superior to that of TiO_2/NiO thin film resulting in better electrochromic durability upon cycling in 1M KOH electrolyte.

In the following chapter, we will present NiO thin film prepared by sol gel method (useful for industrial application) which are advantageously superhydrophilic.

7. References

[1] Y. Ushio, A. Ishikawa, T. Niwa, *Thin Soild Films* **280** (1996) 233.

[2] A. Fukazawa, M. Chihiro, *European Patent* EPXXDW EP 1434083.

[3] I. Bouessay, A. Rougier, P. Poizot, J. Moscovici, A. Michalowicz, J.-M. Tarascon, *Electrochim. Acta* **50** (2005) 3737.

[4] I. Bouessay, A. Rougier, J.-M. Tarascon, *J. Electrochem. Soc.* **151** (2004) H145.

[5] C.M. Lampert, R.C. Popowich, *Optical Materials Technology for Energy Efficiency and Solar Energy Conversion VIII,* SPIE, (1989) 1149.

[6] A. Pennisi, C.M. Lampert, *SPIE,* **1061** (1988) 131.

[7] S. Passerini and B. Scrosati, A. Gorenstein, A.M. Andersson, C.G. Granqvist, *J. Electrochem. Soc.* **136** (1989) 3394.

[8] X. Lou, X. Zhao, J. Feng, X. Zhou, *Prog. Org. Coat.* **64** (2009) 300.

[9] Y. Makimura, A. Rougier, J.-M. Tarascon, *Appl. Surf. Sci.* **252** (2006) 4593.

[10] N. Penin, A. Rougier, L. Laffont, P. Poizot, J.-M. Tarascon, *Sol. Energy Mater. Sol. Cells* **90** (2006) 422.

[11] E. Avendaño, A. Azens, G.A. Niklasson, C.G. Granqvist, *Sol. Energy Mater. Sol. Cells* **84** (2004) 337.

[12] C.G. Granqvist, E. Avendaño, A. Azens, *Thin Solid Films* **442** (2003) 201.

[13] M. Martini, G.E.S. Brito, M.C.A. Fantini, A.F. Craievich, A. Gorenstein, *Electrochim. Acta* **46** (2001) 2275.

[14] R.M. Bendert, D.A. Corrigan, *J. Electrochem. Soc.* **136** (1989) 1369.

[15] D.A. Corrigan, R.M. Bendert, *J. Electrochem. Soc.* **136** (1989) 723.

[16] D.S. Lopez, *Ph.D. thesis*, Leibniz-Institut für Neue Materialien, Saarbruecken, Germany (2003).

[17] M. Martin, G.E.S. Brito, M.C.A. Fantini, A.F. Craievich, A. Gorenstein, *Electrochem. Acta* **46** (2001) 2275.

[18] A. Al-Kahlout, S. Heusing, M. A. Aegerter, *J. Sol-Gel Sci. Techn.* **39** (2006) 195.

[19] A. Al-Kahlout, A. Pawlicka, M. A. Aegerter, *Sol. Energy Mater. Sol. Cells* **90** (2006) 3583.

[20] A. Al-Kahlout, *Ph.D. thesis*, Universität des Saarlandes, Germany (2006).

[21] A. Al-Kahlout, M. A. Aegerter, *Sol. Energy Mater. Sol. Cells* **91** (2007) 213.

[22] Y. Masuda, K. Kato, *J. Cryst. Growth* **311** (2009) 512.

[23] B.-K. Koo, D.-Y. Lee, H.-J. Kim, W.-J. Lee, J.-S. Song, H.-J. Kim, *J. Electroceram.* **17** (2006) 79.

[24] T.-J. Chen, P. Shen, *J. Phys. Chem. C* **113 (1)** (2009) 328.

[25] L. Jing, B. Xin, F. Yuan, L. Xue, B. Wang, H. Fu, *J. Phys. Chem. B* **110** (2006) 17860.

[26] W. Zhanga, S. Zhub, Y. Lib, F. Wang, *Vacuum* **82** (2008) 328.

[27] K. Oyoshi, N. Sumi, I. Umezu, R. Souda, A. Yamazaki, H. Haneda, T. Mitsuhashi, *Nuclear Instruments and Methods in Physics Research Section B* **168** (2000) 221.

[28] Z. S. Wang, C. H. Huang, Y. Y. Huang, Y. J. Hou, P. H. Xie, B. W. Zhang, H. M. Cheng, *Chem. Mater*. **13** (2001) 678.

[29] R. L. Willis, C. Olson, B. O'Regan, T. Lutz, J. Nelson, J. R. Durrant, *J. Phys. Chem. B* **106** (2002) 7605.

[30] R. D. Sun, A. Nakajima, A. Fujishima, T. Watanabe, K. Hashimoto, *J. Phys. Chem. B* **105** (2001) 1984.

[31] V. Kandavelu, H. Kastien, K. Thampi, K. Ravindranathan, *Appl. Catal. B* **48** (2004) 101.

[32] I. Saadeddin, *Ph.D. thesis*, Université Bordeaux 1, France (2007).

[33] H. Arai, S. Okada, Y. Sakurai, J.-I. Yamaki, *Solid State Ionics* **109** (1998) 295.

[34] M.G.S.R. Thomas, W.I.F. David, J.B. Goodenough, *Mat. Res. Bull.* **20** (1985) 1137.

[35] R. Kanno, H. Kubo, Y. Kawamoto, T. Kamiyama, F. Izumi, Y. Takeda, M. Takano, *J. Solid State Chem.* **110** (1994) 216.

[36] R. D. Shannon, *Acta Crystallogr. A* **32** (1976) 751.

[37] G. Campet, I. Saadeddin, K. Zaghib, *International patent* PCT/CA2007/00081, 2007.

[38] B. S. Barros, R. Barbosa, N. R. dos Santos, T. S. Barros, M. A. Souza*, Inorg. Mater.* **42** (2006) 1348.

[39] H. Qiao, Z. Wei, H. Yang, L. Zhu, X. Yan, *J. Nanomater.* **2009** (2009) 5.

[40] F. Amaral, L.C. Costa, M.A. Valente, F. Henry, *J. Non-Cryst. Solids* **355** (2009) 2160.

[41] P. Varshney, M. Deepa, N. Sharma, S.A. Agnihotry, *Solid State Ionics* **152** (2002) 877.

[42] F. Decker, S. Passerini, R. Pileggi, B. Scrosati, *Electrochim. Acta* **37** (1992) 1033.

Chapter IV

Highly stabilized electrochromic performances of sol-gel deposited nickel oxide thin films

1. Introduction; choice of the appropriate sol-gel method to prepare nickel oxide-based thin films

In chapter III, we have shown that we could remarkably enhance the cycling durability of NiO-based thin films in aqueous KOH electrolyte by substituting Ti with Zn in TiO_2 matrix where nano-sized NiO particles are embedded in. The Zn substitution to Ti enhanced the hydrophilic character of the matrix leading to an improvement of the mechanical adhesion of the corresponding films on FTO substrates. However, there still remains a challenging issue to increase even more the cycling durability for an industrial application because the mechanical adhesion of the Zn doped TiO_2/NiO thin films from FTO substrate started to decrease beyond 8000 cycles.

In the frame of our present cooperative research between Ewha Womens University (Seoul) and ICMCB-CNRS based on a general investigation of the hydrophobic and hydrophilic behavior of semiconductors (NiO, TiO_2, ZnO etc.), we could successfully deposit highly hydrophilic NiO-based thin films on FTO/glass substrates using an original sol-gel process presented hereafter.

NiO thin films synthesized using sol-gel routes have been investigated [1-20]. However, one has to find the most appropriate low-cost precursors for the sol-gel deposition of homogeneous nickel oxide films. Nickel alkoxides $[Ni(OR)_2]_n$ and nickel β-diketonatoalkoxides such as $[Ni_4(OMe)_4(\beta\text{-dik})_4(MeOH)_4]$ were first considered by us here but finally disregarded because they are insoluble in the non toxic solvents we selected, such as alcohols [14,15]. On the other hand, donor alkoxide groups, such as dimethylamino-isopropoxide $[OCH(Me)CH_2NMe_2]$ are soluble in ethanol [16]. Therefore precursors like $[Ni(OCH(Me)CH_2NMe_2)_2]$ and $[Li(PriOH)Ni(OCH(Me)CH_2NMe_2)Cl]_2$ were tested in ethanol solution. However, the deposited films on FTO substrates were non

homogeneous. We observed the same lack of homogeneity for films deposited from nickel nitrate, $[Ni(NO_3)_2(H_2O)_6]$ in ethanol solution [17]. Williams *et al.* successfully synthesized a $[Ni(acac)_2(dmaeH)]$ solution starting from a solution of Ni(II)–acetate and Ni(II) acetylacetonatecomplexes into which was added N,N-dimethylaminoethanol (dmaeH) [18-20]. The same authors also found that the addition of dmaeH to nickel acetate tetrahydrate $[Ni(CH_3CO_2)_2(H_2O)_4]$ gives a monomeric Ni(II) complex, $[Ni(CH_3CO_2)_2\text{-}(dmaeH)_2]$ [19,20]. They confirmed the solubility of $[Ni(acac)_2(dmaeH)]$ and $[Ni(CH_3CO_2)_2\text{-}(dmaeH)_2]$, not only in special alcohols such as dmaeH, but also in other ordinary alcohols such as MeOH and EtOH [18-20]. Therefore they were able to report the use of $[Ni(acac)_2(dmaeH)]$ and $[Ni(CH_3CO_2)_2\text{-}(dmaeH)_2]$ as precursors for the sol-gel deposition of homogeneous NiO thin films using alcoholic solutions. However the preparation of these coating solutions required complicated steps such as reflux, repeated heating and cooling processes, use of inert atmosphere, etc. [18-20]. For industrial application, these steps should be avoided since they demand additional costs to set up the required equipment.

In this chapter, we aim at overcoming these issues by synthesizing homogeneous NiO thin films under ambient atmosphere from a coating solution prepared using the following new and easy process. We first prepared a gel-type coating solution by adding $Ni(CH_3COO)_2$ tetrahydrate to a solution of deionized water and dmaeH in ambient atmosphere. Afterwards, in order to make the appropriate coating solutions for thin film deposition, we decreased the viscosity of the gel-type solution by adding small amounts of 2-aminoethanol.

2. Preparation of the coating solutions

First, we prepared three beakers containing both 20 ml of N,N-dimethylaminoethanol (dmaeH) and 20 ml of deionized water. 4.97 g of $Ni(CH_3COO)_2 \cdot 4H_2O$ (F.W. 248.71 g/mol) was then added to each of the three beakers. Afterwards, 0.2 ml, 1.8 ml, and 5.0 ml of 2- aminoethanol were added to the three beakers individually as illustrated in Fig. 1. For convenience, as written in Fig. 1, the coating solutions with 0.2, 1.8, and 5.0 ml of 2- aminoethanol will be called solution (1), solution (2), and solution (3), respectively.

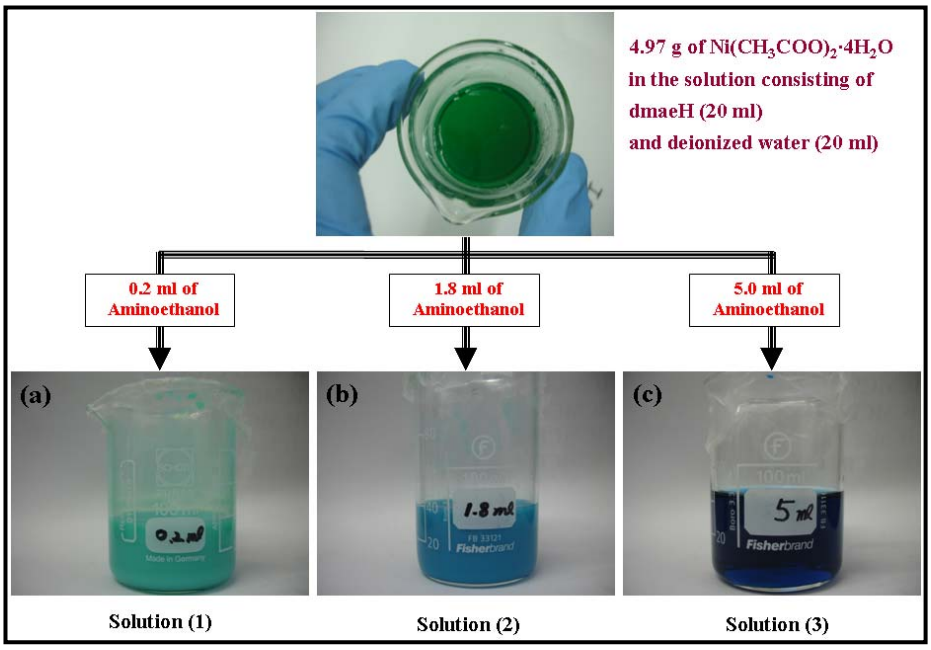

Fig. 1: Coating solutions consisting of dmaeH (20 ml) and deionized water (20 ml) where 4.97 g of nickel acetate tetrahydrate is dissolved together with (a) 0.2 ml (solution 1), (b) 1.8 ml (solution 2), and (c) 5.0 ml (solution 3) of 2-aminoethanol .

The viscosities (η_v) of the three solutions are reported in Fig. 2. η_v decreases from 8 to «0» as the 2-aminoethanol quantity increases.

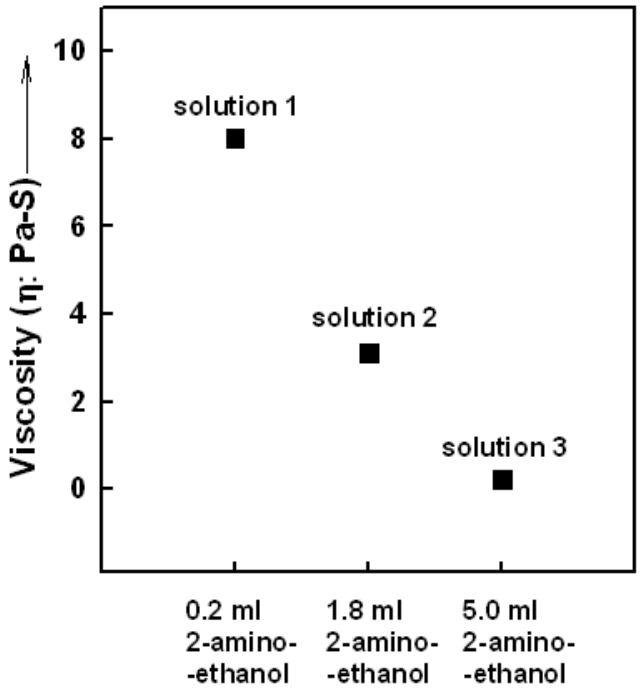

Fig. 2: Evolution of the viscosity of the coating solutions as a function of 2-aminoethanol added.
(TA Instruments AR2000 was used, courtesy to E. Laurichesse in CRPP-CNRS.)

Below are reported the physicochemical properties of powdered samples obtained after heating the coating solutions at different temperatures.

3. Characterization of powders obtained after heating the coating solutions

The powders issued from the coating solutions 1, 2 and 3, heated in air at 300, 400, and 500 ^{o}C, for 4 hrs show similar XRD patterns regardless of the amount of the added 2-aminoethanol. As an example, Fig. 3 reports the evolution of the XRD patterns with heating temperature for powders obtained from solution (2).

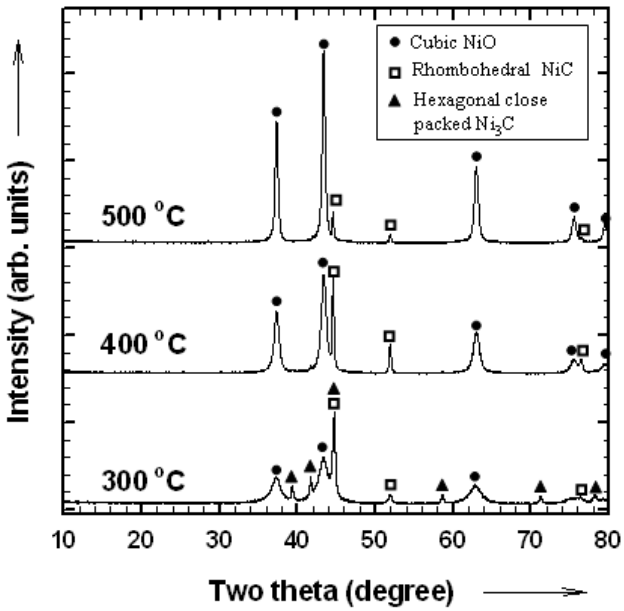

Fig. 3: XRD patterns for powders obtained either from the solutions 1, or 2, or 3. The powders were heated in ambient atmosphere at 300, 400, and 500 ^{o}C, respectively for 4 hrs. Solid circles, open squares, and solid triangles indicate cubic NiO, rhombohedral NiC, and hexagonal closed packed (hcp) Ni_3C, respectively.

. For the samples heated at 300 °C, cubic structured NiO (JCPDS 4-0835) at 37.34, 43.38, and 63.12 ^{o} in two theta value indicated by solid circles was observed together with two clearly observable impurity phases. The latter corresponds to hcp Ni_3C (open squares at 44.5, 52.0, and 76.5 ^{o} in two theta value) [21-28] and rhombohedral NiC (solid triangles at 39.32, 41.64, 58.66, 71.14, and 78.18 ^{o} in two theta value) [29-31]. Carbon- Hydrogen-Nitrogen-Sulphur (CHNS) measurements support the existence of carbon in the samples (Table 1).

	Sol gel powders of solution 2 (1.8 ml 2-aminoethanol)
300 °C for 4 hrs	2.1 wt.%
400 °C for 4 hrs	1.4 wt.%
500 °C for 4 hrs	0.6 wt.%

Table 1: Carbon content obtained from CHNS measurements for the powders obtained after heating solution 2. Similar results, not reported here for sake of simplicity, were observed for powders issued from solutions 1 and 3)

The decrease of carbon content upon heating in air from 300 °C to 400 °C (Table 1) probably results from the decrease of the nickel carbide Ni_3C impurity phase (Fig. 3), which decomposes above 300 °C into Ni metal and amorphous C [32]; above 400 °C Ni and C capture oxygen forming NiO, CO and CO_2 [33]. However, the powders heated at 500 °C still exhibit traces of NiC (Fig. 3).

The particle (crystallite) sizes of the samples, deduced from Fig. 3 using Scherrer equation [34], are listed in Table 2. As expected, the particle size increases as the annealing temperature increases, resulting in ~ 7 nm (for 300 °C), ~ 11 nm (for 400 °C), and ~ 20 nm (for 500 °C) in diameter.

	Sol gel powders of solution 1, 2, and 3
300 °C	~ 7 nm
400 °C	~ 11 nm
500 °C	~ 20 nm

Table 2: Calculated particle sizes of the samples using Scherrer equation.

From now on, we will discuss the properties of the powders obtained after heating the coating solution 2 because the most homogeneous thin films were deposited from this solution. For sake of clarity, we will simplify the names of the heated samples as follows,

- Composition 1: the powder obtained after heating solution 2 at 300 ^{o}C for 4 hrs under air condition.
- Composition 2: the powder obtained after heating solution 2 at 400 ^{o}C for 4 hrs under air condition.
- Composition 3: the powder obtained after heating solution 2 at 500 ^{o}C for 4 hrs under air condition.

TG measurement was carried out for the composition 1. As shown in Fig. 4, the TG graph shows 2.9 % weight loss between room temperature and 300 ^{o}C which probably originates from the evaporation of physisorbed and chemisorbed water molecules.

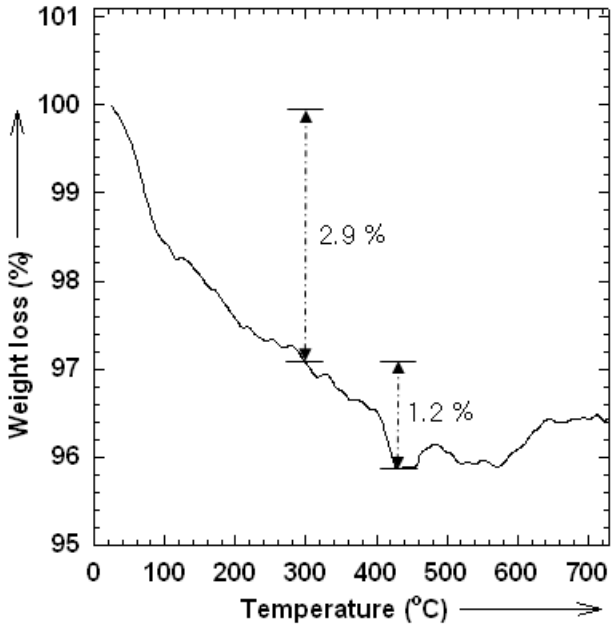

Fig. 4: TG curve of composition 1. **(**The operating temperature was elevated with a heating rate of 5 ^{o}C per minute from room temperature (25 ^{o}C) up to 700 ^{o}C; experiment was carried out under air atmosphere.)

Between 300 ^{o}C and 440 ^{o}C, a 1.2 % weight loss was observed (Fig. 4); This is presumably due to the departure of carbon, probably in the form of CO or CO_2. Let us recall that carbon was probably associated to nickel forming Ni_3C and NiC phases (Fig. 3) and that Ni_3C decomposes above 300 °C [32, 33].

4. Thin films

4-1. Preparation of thin films

We followed the steps described in chapter II to clean the FTO substrates (5 × 2 cm^2 area) onto which the thin films were deposited.

As quoted above, the films were deposited from solution 2 (§ 2). A spin coating method was employed (Fig. 5). Firstly, the cleaned FTO substrate, -which was partially covered by a scotch tape leaving an active area of 2 x 2 cm^2 for film deposition-, was put on the rotated support, and then the coating solution 2 was dropped until it covered the whole active FTO surface. Afterwards, the as coated FTO substrate was aged for 5 minutes in ambient atmosphere and then was continuously rotated at 500 rpm for 5 seconds and at 2000 rpm for 20 seconds (optimized conditions). A continuous blowing of nitrogen is directed toward the substrate during spinning. During spinning, the FTO substrate was held by a vacuum pump. The finally obtained film was dried at room temperature for 10 hrs in air.

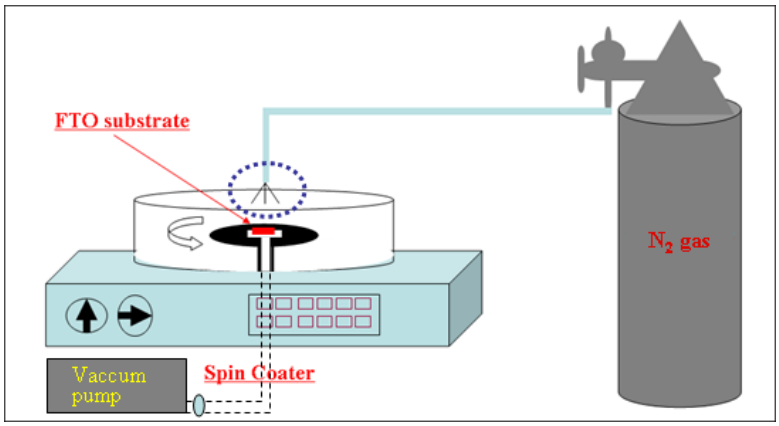

Fig. 5: The illustration of the used spin coating apparatus. *(G3P-8 spin-coater manufactured by Pi-Kem Ldt was used.)*

After drying at room temperature, the films were subjected to similar heat-treatment in air as composition 2 (§ 3), namely 300, 400, and 500 ^oC for 4 hrs; the heating rate was 4 ^oC per minute. Therefore, we can reasonably assume that carbon content in the sintered thin films is the same as that of composition 2 heated at 300 °C (2.1 wt.% of carbon), 400 °C (1.4 wt.% of carbon), 500 °C (0.6 wt.% of carbon), as quoted in § 3.

From now on, for sake of clarity, we will classify the annealed films depending on their different carbon content as follows,

- C-NiO_{300} : symbolizes the thin film heated at 300 ^{o}C for 4 hrs under air condition and having 2.1 wt.% carbon content.
- C-NiO_{400} : symbolizes thin film heated at 400 ^{o}C for 4 hrs under air condition and having 1.4 wt.% carbon content.
- C-NiO_{500} : symbolizes thin film heated at 500 ^{o}C for 4 hrs under air condition and having 0.6 wt.% carbon content.

4-2. Morphological characterizations

Fig. 6a-c show FE-SEM images of surfaces and thicknesses for C-NiO_{300}, C-NiO_{400}, and C-NiO_{500} thin films. The thin films have more or less the same thickness (~ 130 nm) (Fig. 6d). Regarding the homogeneity of the surface, we observe that voids, randomly distributed, become more distinguishable at higher heating temperature.

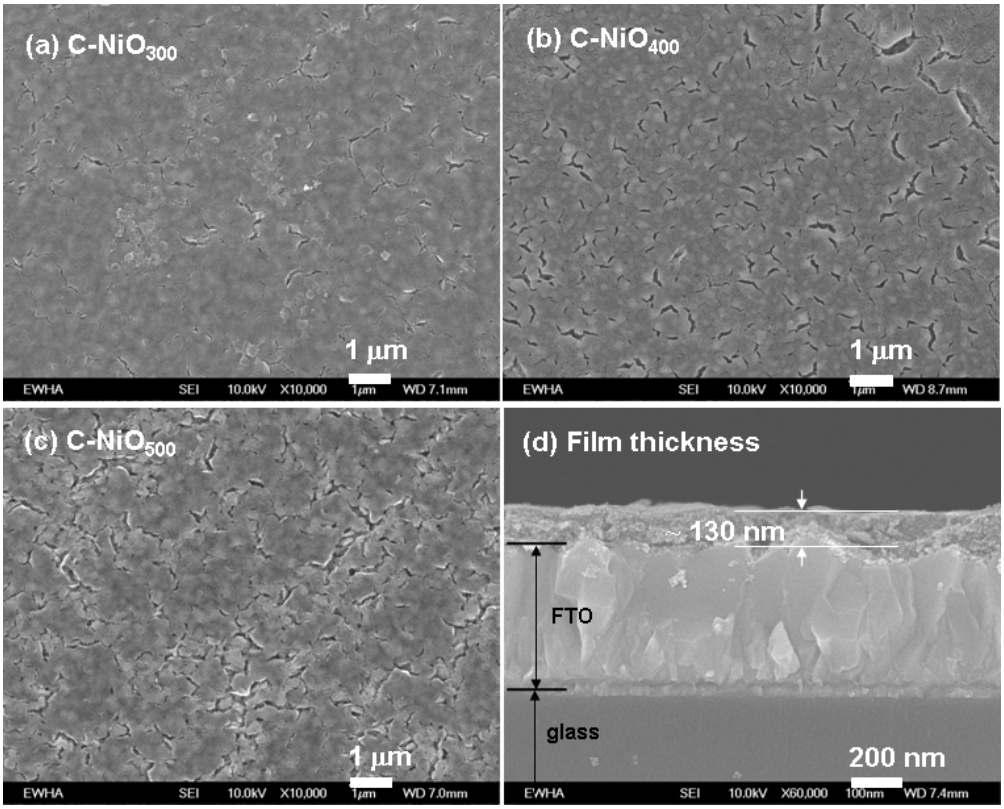

Fig. 6: FE-SEM surface images of (a) C-NiO_{300}, (b) C-NiO_{400}, and (c) C-NiO_{500} thin films and (d) cross section image of C-NiO_{500} thin film (similar thickness was observed from C-NiO_{300} and C-NiO_{400} thin films).

Fig. 7 shows highly magnified FE-SEM, enabling us to visualize the particle growth as the sintering temperature increases from 300 °C to 500 °C. The evolution of particle growth was already confirmed for the powdered samples (§ 3, Table 2).

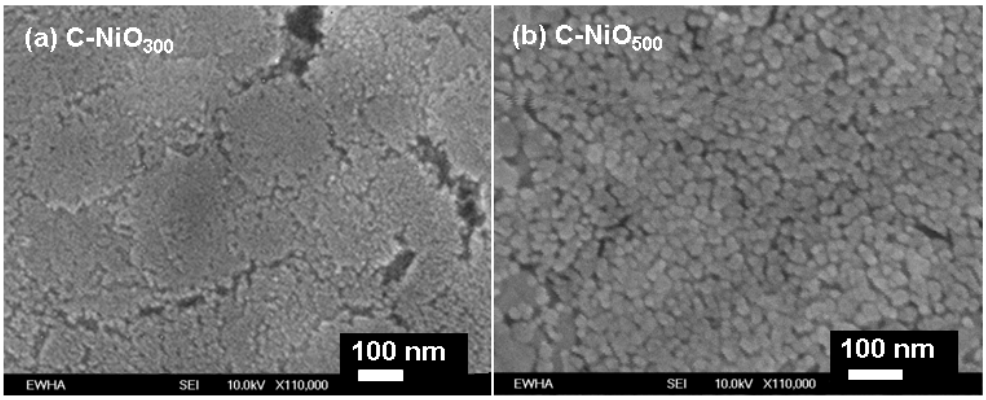

Fig. 7: Highly magnified FE-SEM images for (a) C-NiO_{300} and (b) C-NiO_{500} thin films.

4-3. Wetting characteristics of the film surfaces estimated from contact angle measurements

The contact angles are 15.2, 18.2 and 20.5 ^{o} for C-$NiO_{300,}$ C-NiO_{400}, and C-NiO_{500} thin films, respectively (Fig. 8). These low values account for highly hydrophilic films. The values are far smaller than those observed for PLD deposited NiO films, being 107.3 °. (Chapter II). Here, the C-$NiO_{300,}$ C-NiO_{400}, and C-NiO_{500} thin films contain carbon. If we reasonably assume that we have the same amount of carbon in thin films as we have in powders (films and powders were heated under same conditions), we can deduce, according to table 1, that the contact angle increases as the amount of carbon in the thin film decreases.

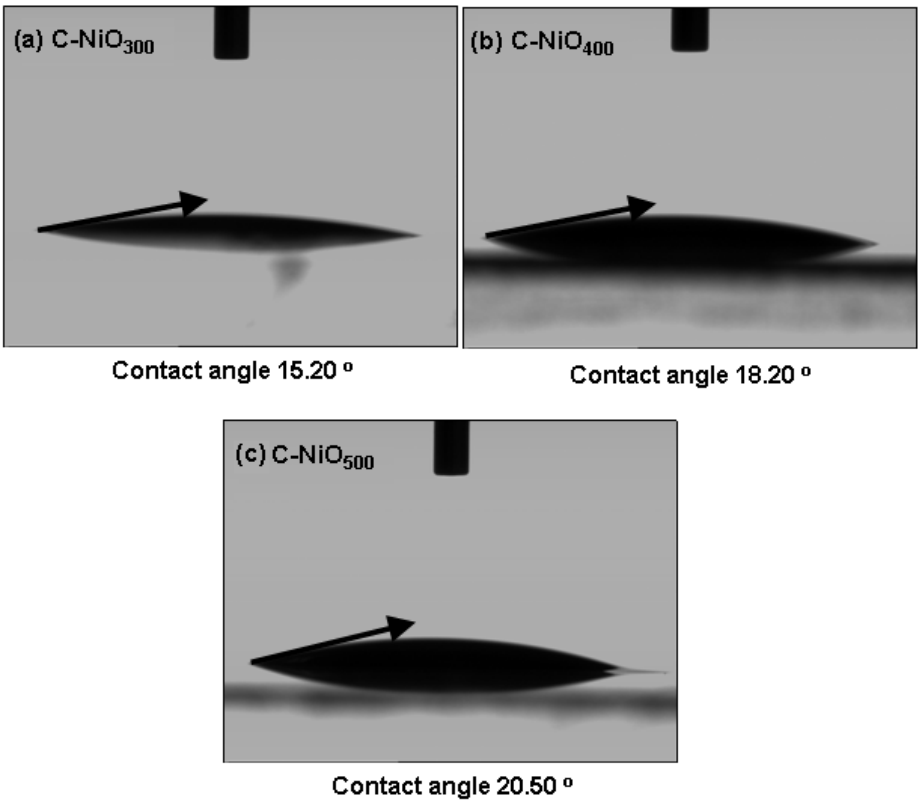

Fig. 8: Contact angles obtained with H_2O for (a) C-NiO_{300}, (b) C-NiO_{400}, and (c) C-NiO_{500} thin films. The accuracy is ± 0.05 °.

4-4. Electrochromic properties of C-NiO thin films

4-4-a. Electrochemical measurements

Cyclic voltammograms (CVs) of C-NiO_{300}, C-NiO_{400}, and C-NiO_{500} thin films were performed within the 0 V ~ 0.60 V potential window versus Hg/HgO at a scan rate of 10 mV / s in 1 M KOH electrolyte. Fig. 9 presents the CV curves of all films at 1st, 400th, 1200th, and 2500th cycle. The inset figures indicate the magnified CV curves of the 1st cycle. The appearance of a broad area in the 0.0 V – 0.35 V for the 1st CV curves of C-NiO_{300} and C-NiO_{400} thin films illustrates a pseudo-capacitive behavior indicating that surface reactions are involved [35]. However, C-NiO_{500} thin film, which is well crystallized (Fig. 7), does not show a pseudo-capacitive behavior.

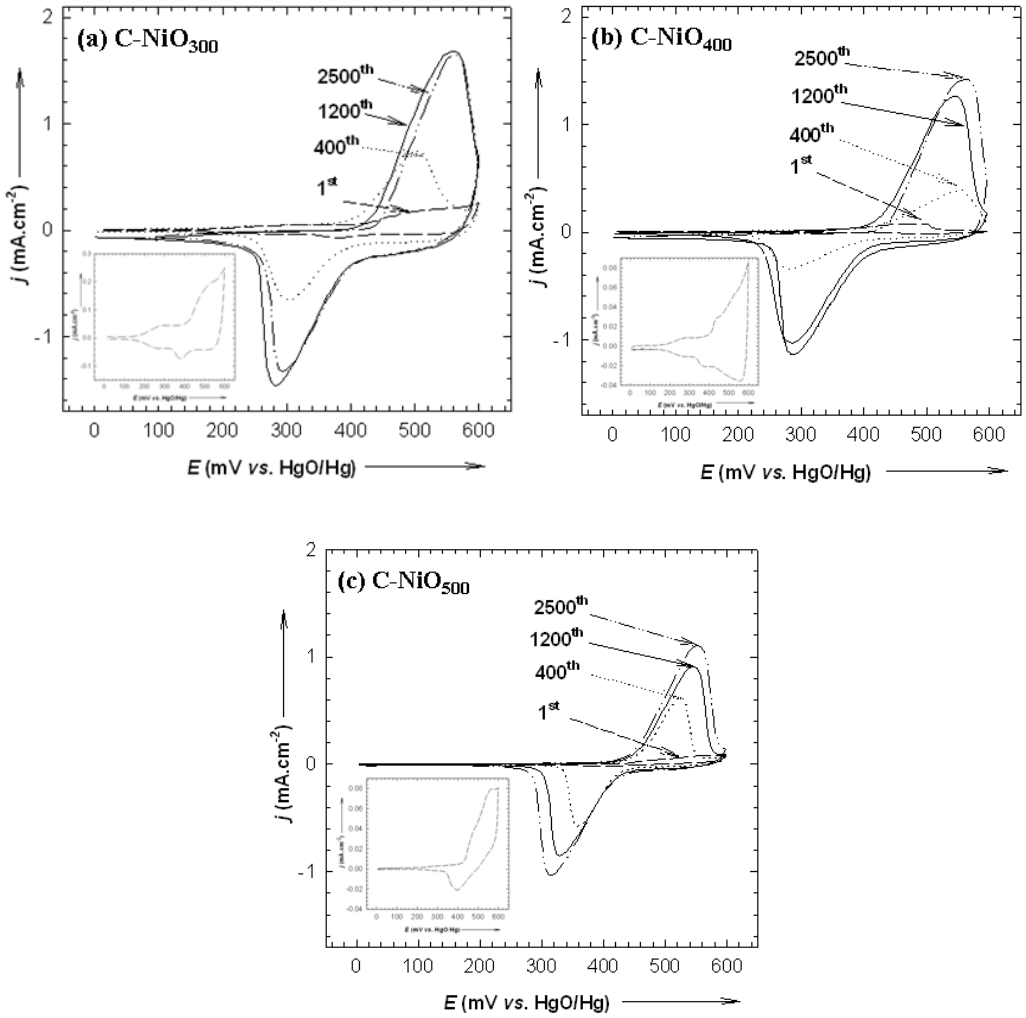

Fig. 9: Cyclic voltammograms of (a) C-NiO_{300}, (b) C-NiO_{400}, and (c) C-NiO_{500} thin films at 1st (long dash line), 400th (dotted line), 1200th (solid line), and 2500th (dash-dot-dot line) cycle. Three-electrode-cell configuration consisting of a working electrode (the C-NiO thin films), a counter electrode (platinum foil), and a reference electrode (Hg/HgO) was used. All the measurements were carried out at a scan rate of 10 mV / s in 1M KOH electrolyte between 0 V and 0.60 V. The inset indicates the magnified curve of 1st cycle.

.

On the contrary to the behaviors previously reported in chapter II (PLD/Li-Ni-O thin film) and chapter III (TiO_2/NiO thin films), C-NiO thin films showed no shrinkage of coulombic capacity beyond their maximum capacity values at ~ 1200th cycle (Fig. 10). This stabilization is most likely due to the enhanced mechanical adhesion of the

hydrophilic films on FTO substrates. Besides C-NiO_{500} thin film showed a slightly gradual increase of coulombic capacity beyond ~ 1200^{th} cycle up to 2500^{th} cycle. Lower coulombic capacities of C-NiO_{500} thin film can be accounted for smaller surface area of nickel oxide particles in the C-NiO_{500} thin film as compared to the ones in the C-NiO_{300} and C-NiO_{400} thin films.

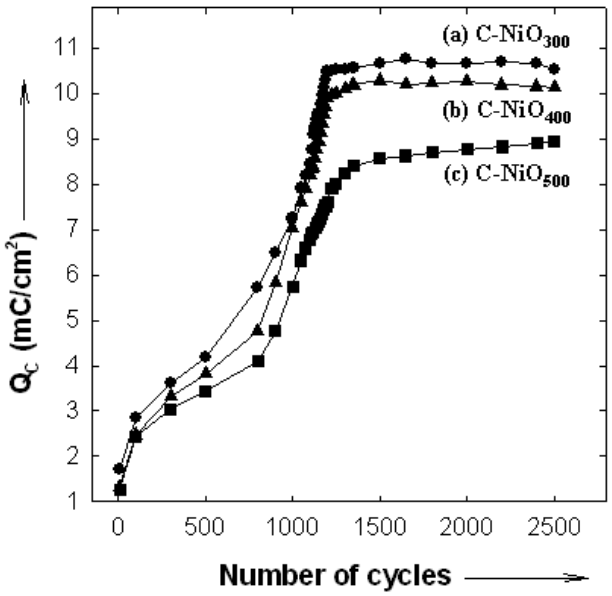

Fig. 10: Coulombic capacity of (a) C-NiO_{300} (circle), (b) C-NiO_{400} (triangle), and (c) C-NiO_{500} (square) thin films. The electrochemical test was carried out in 1M KOH electrolyte with three-electrode-cell configuration consisting of a working electrode (C-NiO thin films), a counter electrode (platinum foil), and a reference electrode (Hg/HgO). All the measurements were carried out at a scan rate of 10 mV/s in 1M KOH electrolyte between 0 V and 0.60 V.

As illustrated in Fig. 10, the films experienced activation and steady state periods, already observed for NiO thin films [36]. Here, the activation period occurs from the initial cycle to ~ 1200 cycles.

Fig. 11a-c show the surface of the thin films after 2500th cycle. The thin films show a homogeneous surface. Most interestingly no trace peeling-off phenomena is evidenced (Fig. 11d).

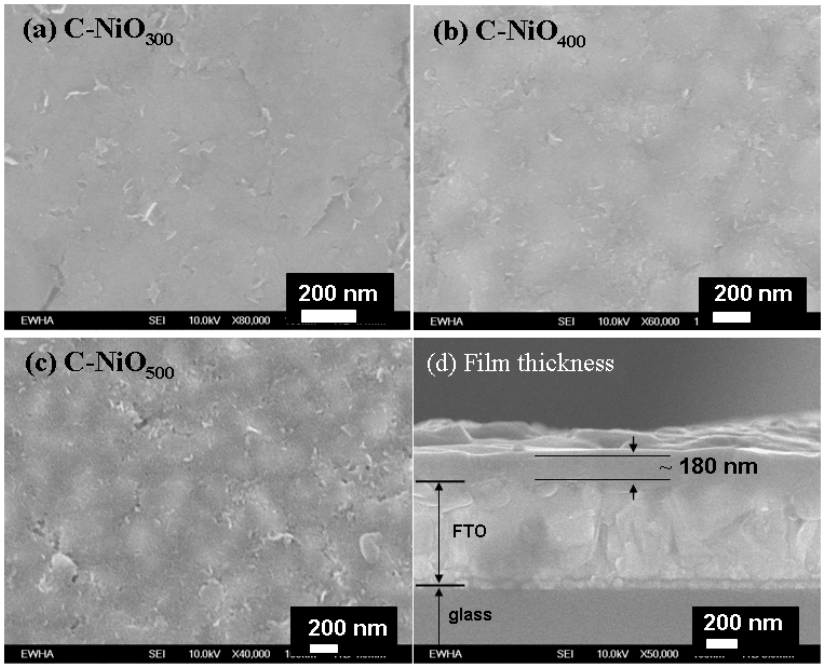

Fig. 11: SEM surface images of the (a) C-NiO_{300}, (b) C-NiO_{400}, and (c) C-NiO_{500} thin films at 2500th cycle and (d) cross section image of C-NiO_{500} thin film at 2500th cycle (similar thickness was observed from C-NiO_{300} and C-NiO_{400} thin films).

4-4-b. Optical properties

In chapter II and III, we could observe a gradual remaining brownish color of the films upon cycling. In this regard, we also investigated the evolution of transmittance upon cycling of the C-NiO thin films at the wavelength of 550 nm. The transmittances of as-prepared C-NiO_{300} ($T_{\lambda=550nm}$ ~ 90 %), C-NiO_{400} ($T_{\lambda=550nm}$ ~ 94 %), and C-NiO_{500} ($T_{\lambda=550nm}$ ~ 94 %) thin films are shown in Fig. 12. At the 1200th cycle, the transmittances of C-NiO_{300} thin film are 83.0 % and 16.5 % for bleached and colored state, respectively (Fig. 12a). C-NiO_{400} thin film exhibits relatively higher transmittance value for the bleached (80.0 %) state and the colored state is 26.0 %, (Fig. 12b). In case of C-NiO_{500} thin film, it

exhibits the highest transmittances for both the bleached (88.0 %) and colored (32.5 %) states (Fig. 12c). It corresponds to a contrast ratio of 2.7. Most interestingly, the optical properties of C-NiO_{500} thin film at bleached state is highly stabilized upon further cycling as compared to C-NiO_{300} and C-NiO_{400} (Fig. 12d). Indeed at the 2500th cycle, its transmittance values at 550 nm are 80 % and 28 % for bleached and colored states, respectively, leading to a contrast ratio of 2.8.

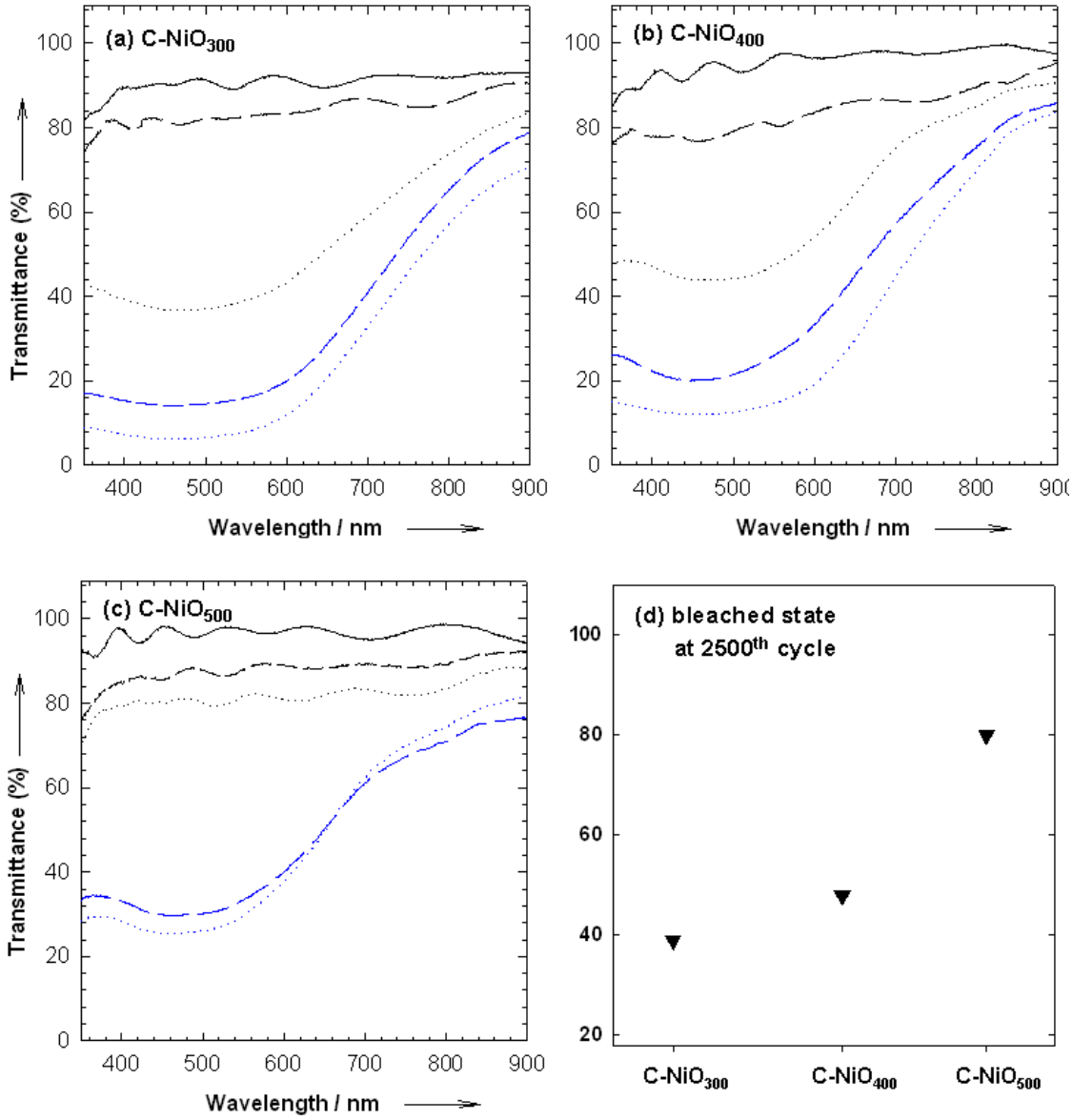

Fig. 12: Transmittances (%) of (a) C-NiO_{300}, (b) C-NiO_{400}, and (c) C-NiO_{500} thin films at 0 (solid line), 1200th (dash line), and 2500th (dotted line) cycle and (d) all the transmittance values in the bleached state at 2500th cycle. The blue lines indicate colored state. All the transmittance values were deduced at the wavelength of 550 nm. (All the

measurements were carried out using UV-Visible Spectrometer between 350 nm and 900nm and the range of transmittance is from 100 % to 1 %)

(The voltages applied for 30 seconds were 0 mV and 600 mV for bleached and colored state, respectively.)

Considering the highest optical performances obtained for C-NiO_{500} thin films, from now on we will discuss their very long-term electrochromic performances.

4-4-c. Long-term electrochromic properties of C-NiO_{500} thin films

Fig. 13 shows CV curves at 2500th (solid line), 8000th (dotted line), 15000th (dash-dot line), and 25000th (dash-dot-dot line). Most interestingly, nearly no decrease of the capacity is observed. The deduced coulombic capacities (Q_c) based on cathodic peaks are 9.73, 9.49, and 9.33 mC/cm^2 for 8000th, 15000th, and 25000th cycles demonstrating the high durability for C-NiO_{500} thin film.

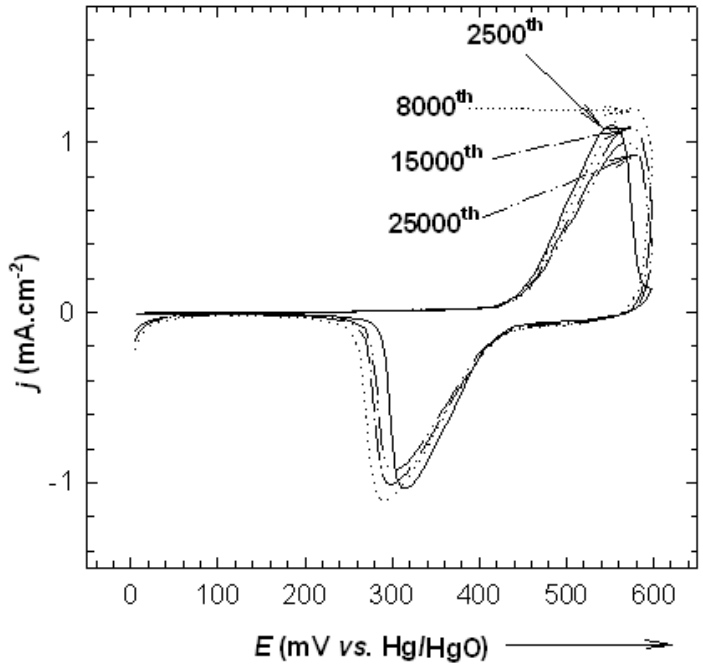

Fig. 13: CV curves of the C-NiO_{500} thin film at 2500th (solid line), 8000th (dotted line), 15000th (dash-dot line), and 25000th (dash-dot-dot line) cycle. The electrochemical test was carried out in 1M KOH electrolyte with three-electrode-cell configuration consisting of a working electrode(C-NiO_{500} thin film), a counter electrode (platinum foil), and a reference electrode (Hg/HgO). All the measurements were carried out at a scan rate of 10 mV / s in 1M KOH electrolyte between 0 V and 0.60 V.

Equally interesting, the transmittances of the C-NiO_{500} thin film after 25000 cycles are 73 % and 27 % for bleached and colored states, respectively as shown in Fig. 14. It corresponds to a contrast ratio of ~ 2.8; this value is the same as that observed for 2500th cycle. However the UV-visible spectrum of bleached state at 25000th cycle moved to lower transmittance as compared to the spectrum (Fig. 12c) at 2500th cycle, indicating a slightly brownish color at bleached state.

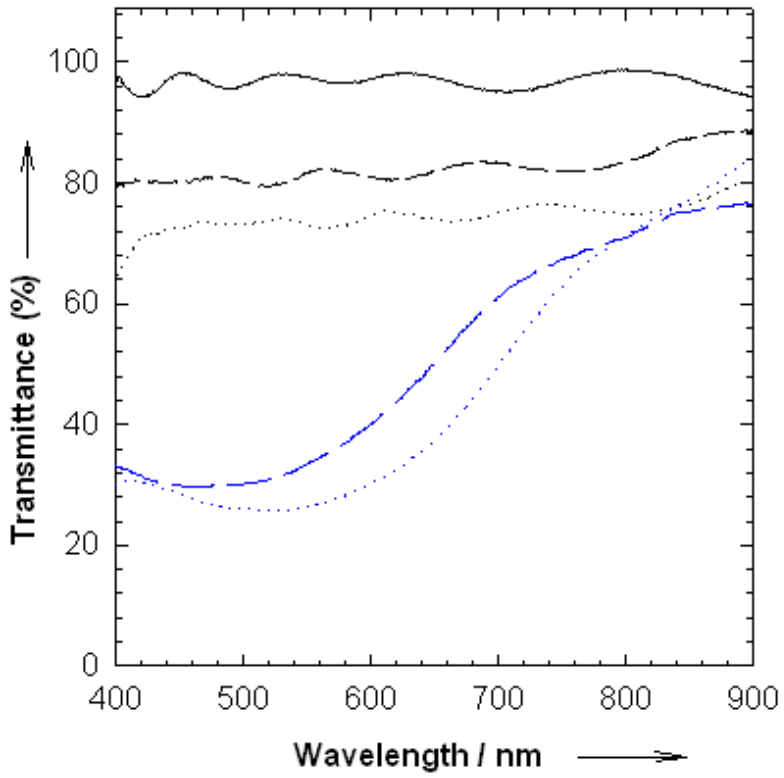

Fig. 14: Transmittance of the C-NiO_{500} thin film at 0 (solid line), 2500th (dash line), and 25000th (dotted line). The blue lines indicate colored state.
The voltages applied for 30 seconds were 0.00 V and 0.60 V for bleached and colored state, respectively.

Fig. 15 shows the surface and cross-section of C-NiO_{500} film at 0, 2500th, 25000th cycles. Some voids are clearly observable for the as-prepared thin film (Fig. 15a taken from Fig. 6). However, a homogeneous surface with no voids is observed after 2500th cycle (Fig. 15b). The origin of this surface modification remains to be clarified. At 25000th cycle,

we can observe a homogeneous film with more but some voids. This phenomenon may be related to the slight decrease of coulombic capacity observed between 8000th and 25000th cycle (Fig 13).

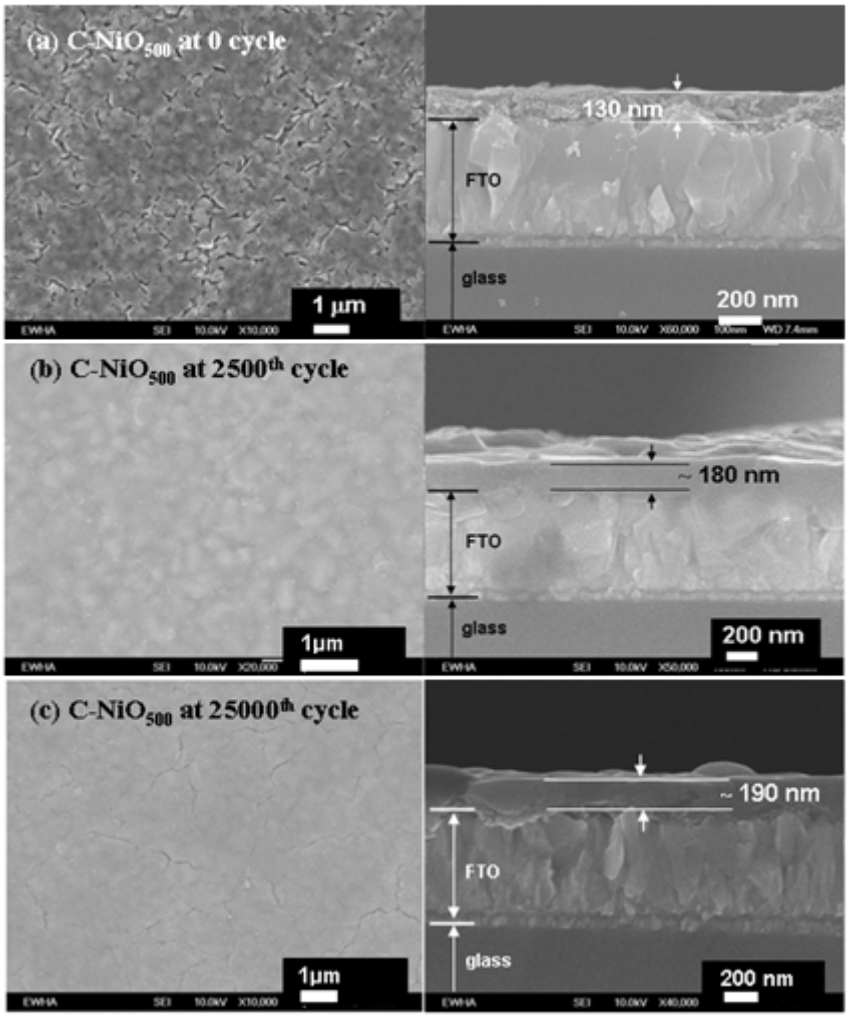

Fig. 15: FE-SEM surface and cross section images for C-NiO_{500} thin film at (a) 0, (b) 2500th, and (c) 25000th cycle.

5. Conclusion

We have proposed an original sol-gel route to prepare carbon contained NiO thin films under ambient atmosphere The viscosity of the gel-type precursor coating solution, based on water, nickel acetate tetrahydrate and N,N-dimethylaminoethanol (dmaeH), was adjusted owing to the addition of 2-aminoethanol, which allowed us to prepare

homogeneous films, C-NiO_{500}, with high electrochromic performances suitable for industrial application. Such high performances were related to the carbon residue in the films (enhancing their hydrophilicity) and the sintering temperature (~ 500 °C). Such C-NiO thin film maintains a very high transparency upon cycling with significant electrochromic properties.

6. References

[1] Y. Ozaki, S. Saito, *Advanced Ceramics, ed. Oxford University Press, ch. 9*, 1988..

[2] F.H. Moser, N.R. Lynam, *US patent* 4959247, 1987.

[3] F.H. Moser, N.R. Lynam, *US patent* 4855161, 1989.

[4] A. Šurca, B. Orel, B. Pihlar, P. Bukovec, *J. Electroanal. Chem.* **408** (1996) 83.

[5] A. Šurca, B. Orel, R. Cerc-Korosãc, P. Bukovec, B. Pihlar, *J. Electroanal. Chem.* **433** (1997) 57.

[6] J. Washo, *US patent* 4347265, 1980.

[7] M. Martini, G.E.S. Brito, M.C.A. Fantini, A.F. Craievich, A. Gorenstein, *Electrochim. Acta* **46** (2001) 2275.

[8] J.L. Garcia-Miquel, Q. Zhang, S.J. Allen, A. Rougier, A. Blyr, H.O. Davies, A.C. Jones, T.J. Leedham, P.A. Williams , S.A. Impey, *Thin Solid Films* **424** (2003) 165.

[9] A. Šurca, B. Orel, B. Pihlar, *J. Sol–Gel Sci. Technol.* **8** (1997) 743.

[10] P.K. Sharma, M.C.A. Fantini, A. Gorenstein, *Solid State Ionics* **113** (1998) 457.

[11] L. Wang, Z. Zhang, Y. Cao, *J. Ceram. Soc . Jpn.* **101** (1993) 227.

[12] R. Cerc Korošec and P. Bukovec, *Acta Chim. Slov.* **53** (2006) 136.

[13] R. Cerc Korošec, P. Bukovec, *Thermochim. Acta* **410** (2004) 65.

[14] R. C. Mehrotra, *Adv. Inorg. Chem. Radiochem.* **26** (1989) 269.

[15] M.A. Halrow, J.S. Sun, J.C. Huffman, G. Christou, *Inorg. Chem.* **34** (1995) 4167.

[16] L.G. Hubert-Pfalzgraf, V.G. Kessler, J. Vaissermann, *Polyhedron* **16** (1997) 4197.

[17] F. H. Moser, N. R. Lynam, *US Patent* 4959247, 1990.

[18] P. A. Williams, A. C. Jones, J. F. Bickley, A. Steiner, H. O. Davies, T. J. Leedham, S. A. Impey, J. Garcia, S. Allen, A. Rougier, A. Blyrd, *J. Mater. Chem.* **11** (2001) 2329.

[19] N. Ya Turova, M. I. Yanovskaya, *Metal alkoxides: precursors for ferroelectric materialst part in Ferroelectric Thin Films: Synthesis and Properties, ed.,* 1996.

[20] C. Paz de Araujo, J. C. Scott, G. W. Taylor, *Gordon and Breach, Amsterdam, ch. 8*, 1996.

[21] Y. H. Leng, H.Y. Shao, Y. T. Wang, M. Suzuki, X. G. Li, *J. Nanosci. Nanotech.* **6** (2006)1.

[22] L.L.-P. Diandra, X.Q. Zhang, S.H. Kim, M. Bonder, R.D. Rieke, *Chem. Mater.* **10** (1998) 164.

[23] L. He, W. Z. Zheng, W. Zhou, H. L. Du, C. P. Chen, L. Guo, *J. Phys. Condens. Matter*. **19** (2007) 036216.

[24] W. Zhou, K. Zheng, L. He, R. M. Wang, L. Guo, C. P. Chen, X. D. Han, Z. Zhang, *Nano Lett*. **8** (2008) 1147.

[25] C. P. Chen, L. He, Y. H. Leng, X. G. Li, *J. Appl. Phys.* **105** (2009) 123923.

[26] L. P.Yue, R. Sabiryanov, E. M. Kirkpatrick, D. L. Leslie-Pelecky, *Phys. Rev. B* **62** (2000) 8969.

[27] P. Hooker, B. J. Tan, K. J. Klabunde, S. Suib, *Chem. Mater.* **3** (1991)974.

[28] M. J. Bonder, E. M. Kirkpatrick, T. Martin, S. -J. Kim, R. D. Rieke, D. L. Leslie-Pelecky, *J. Magn. Magn. Mater.* **220** (2000) 70.

[29] A. I. Reyes de la Torre, J.A. Melo Banda, R. Garcia Alamilla, G. Sandoval Robles, E. Terrés Rojas, A. López Ortega, J. M. Domínguez, *J. Phys. Condens. Matter.* **16** (2004) S2329.

[30] G. Xie, J. Zhang, Y. Lu, K. Wang, X. Mo, P. Lin, *Mater. Sci. Eng. A* **460** (2007) 351.

[31] N. Deb, *J. Therm. Anal. Calorim.* **81** (2005) 61.

[32] Y. Leng, L. Xie, F. Liao, J. Zheng, X. Li, *Thermochim. Acta* **473** (2008) 14.

[33] S. Shimada, *Solid State Ionics* **141** (2001) 99.

[34] P. Scherrer, *Gött. Nachr*. **2** (1918) 98.

[35] F. Decker, S. Passerini, R. Pileggi, B. Scrosati, *Electrochim. Acta* **37** (1992) 1033.

[36] I. Bouessay, A. Rougier, J.-M. Tarascon, *J. Electrochem. Soc.* **151** (2004) H145.

General conclusion and perspectives

Nickel oxide thin films are promising candidates for electrochromic devices due to their optical switch, from a transparent to a brownish state on oxidation, which is advantageously complementary to the blue coloration of cathodic tungsten oxide active electrode. Thus, this combination of nickel and tungsten oxides leads to color neutrality devices. However, limited durability impedes the commercial development of the NiO based counter electrode. Therefore, this work aimed at suggesting solutions to improve the electrochromic performances of NiO based thin films. Among various approaches, main focus was devoted to the preparation of doped NiO thin films, in correlation with enhanced disorder, using various techniques of deposition, namely the Pulsed Laser Deposition (PLD) technique, and the sol-gel one. Interestingly, general trends were successfully concluded from the characterization of the different systems, and in particular a strong enhancement of the durability could be demonstrated from tailoring the hydrophilic character of the NiO based thin films leading to a significant improvement of the substrate/film interface quality.

In chapter II, cubic structured NiO and $Li_{0.21}Ni_{0.79}O$ (Li-Ni-O) thin films were successfully deposited by the PLD method. We could induce structural disorder by lithium addition to NiO, thereby enhancing the film electrochemical-capacity. Moreover, the Li-Ni-O thin films have better adhesion on FTO substrates than NiO ones, leading to higher electrochemical cyclability.

In chapter III, we could remarkably enhance the electrochromic durability of the composite TiO_2/NiO thin films, reported by previous authors, by embedding NiO particles into a Zn^{2+}-doped TiO_2 matrix, leading to a new composite $Ti_{1-x}Zn_xO_{2-x}\square_x$/NiO thin film. The neutral vacancies, $\square_x$, enhance the wettability of the composite film and therefore its mechanical adhesion on FTO substrate. We successfully postponed, for the first time, the hydrolysis of titanium *iso*-propoxide (TnP) based coating solution owing to the addition of

Zn acetate dihydrate. Therefore the Zn doped TiO_2/NiO thin films could be advantageously deposited under ambient atmosphere.

In chapter IV, we developed a new sol-gel method allowing us to synthesize carbon doped NiO thin films having remarkable electrochromic performances, never shown before, suitable for industrial application. Further study is needed to fully understand the origin of their enhanced electrochromic properties. In particular, the synthesis of C-NiO thin films with no impurities such as Ni_3C or NiC need to be investigated. We will also monitor structure and structural changes of the thin films upon cycling using in-situ Extended X-ray Absorption Fine Structure (EXAFS) measurements in collaboration with Ewah Womans Univeristy, Seoul.